Study on Fatigue Behavior of La and Nd Substituted $Bi_4Ti_3O_{12}$ Ferroelectric Thin Films

(LaおよびNd置換した$Bi_4Ti_3O_{12}$強誘電体薄膜の分極反転疲労挙動に関する研究)

Ni ZHONG

Information Device Science

Graduate School of Materials Science

Nara Institute of Science and Technology

Advisor: Prof. Tadashi SHIOSAKI

September 2007

Abstract

Ferroelectric films have attracted extensive interest in the last ten years because of their potential application for nonvolatile ferroelectric random access memory (NvFeRAM). Due to their high polarization, low processing temperature, and excellent fatigue properties, $Bi_4Ti_3O_{12}$ (BiT)-based ferroelectric thin films have been considered as one of the most promising candidate materials for NvFeRAM application. However, there are still some obstacles for NvFeRAM application of ferroelectric films. One of the important problems is the fatigue phenomenon, which is the decrease of switchable polarization with the increase of switching cycles in ferroelectric thin films. To eliminate the fatigue phenomenon, it is necessary to identify the mechanism of fatigue behavior in ferroelectric films. Therefore, investigation of the fatigue mechanism has attracted a lot of attention. The work here involves dielectric and ferroelectric measurements have been carried out for several BiT-based films: $Bi_{3.25}La_{0.75}Ti_3O_{12}$, $Bi_{4-x}Nd_xTi_3O_{12}$ (x=0.2, 0.4, 0.6, 0.8, and 1.0), and $Bi_{4-x}La_xTi_3O_{12}$ (x=0.2, 0.4, 0.6, and 0.8) to clarify the origin of the fatigue behavior in BiT-based ferroelectric thin films,

So far, several mechanisms have been proposed to explain fatigue-free behavior of BiT-based ferroelectric thin films, such as domain pinning and unpinning; stability of oxygen perovskite layers and space compensated by self-regulating $[Bi_2O_2]^{2+}$ layers. However, the dominant mechanism is still ambiguous. Previously proposed fatigue mechanisms are related to defects. It was previously reported that a reduction of oxygen was found near the electrode after fatigue and the fatigue properties of PZT/RuO_x were improved with an increase of oxygen content in RuO_x electrode etc. This suggests that defects, especially oxygen vacancies play a role on the fatigue behavior of ferroelectric thin films.

As is well known, dielectric relaxation is an efficient method to investigate defects such as space charge electrons and oxygen vacancies; therefore, dielectric relaxation is employed here to clarify the existence and the type of the defects in $Bi_{3.25}La_{0.75}Ti_3O_{12}$ ferroelectric thin films. From room temperature to 600 ^oC, both dielectric permittivity (ε_r) and tangent loss (tanδ) were measured on $Bi_{3.25}La_{0.75}Ti_3O_{12}$ films at frequencies from 100 Hz to 1 MHz. In addition to a dielectric peak at 483 ^oC attributed to the paraferroelectric phase transition, three dielectric relaxations were found at about 250 ^oC, 400 ^oC and 500 ^oC, respectively. The dielectric relaxation (～400 ^oC) can be eliminated by a higher sintering temperature and oxygen post-annealing, and it can be induced again by a subsequent nitrogen post-annealing process. The activation energy of dielectric relaxation of this mode is estimated to be 1.89 eV, according to Arrhenius

law. The dielectric relaxation (～500 °C) is not influenced by sintering temperature but is by the post-annealing process. The intensity of this anomaly decreases after oxygen annealing and then increases after nitrogen annealing. The relaxation behavior of this dielectric relaxation is not in accordance with Arrhenius law but is in accordance with Vögel-Fulcher law, and the activation energy is calculated as 0.31eV. It is proposed that the relaxation (～250 °C) is related to both oxygen vacancies and bismuth vacancies; the relaxation (～400 °C) is attributed to single-ionized oxygen vacancies $V_O^{\bullet}$; and the relaxation (～500 °C) is attributed to space change which come from double-ionized oxygen vacancies $V_O^{\bullet\bullet}$. In a word, there are several types of defects in BiT-based ferroelectric thin films, and this is the first time to clarify the existence and type of defects in BiT-based ferroelectric thin films by dielectric relaxation in detail.

Because of the influence of substitution concentration on defect concentration in BiT-based ferroelectrics, $Bi_{4-x}R_xTi_3O_{12}$ (R=La or Nd, x=0.2, 0.4, 0.6, 0.8 and 1.0) films were investigated in detail here for their fatigue behavior. The behavior of dielectric permittivity (ε_r), remnant polarization (P_r), and coercive field (E_c) as a function of switching cycles was analyzed. It was found that with the increase of La or Nd substitutes, fatigue resistance increased. $Bi_{3.2}La_{0.8}Ti_3O_{12}$ and $Bi_{3.2}Nd_{0.8}Ti_3O_{12}$ exhibit fatigue-free behavior from 1 to 10^9 cycles. The fatigue behavior of $Bi_{4-x}R_xTi_3O_{12}$ films could be divided into two parts: 1) an increase of polarization from 1 to 10^6 cycles; 2) a decrease of polarization from 10^6 to 10^9 cycles. For $Bi_{4-x}R_xTi_3O_{12}$ (x=0.2 and 0.4) films, an increase of polarization with switch cycling is found from 1 to 10^6 cycles, whereas, this behavior is weak in $Bi_{4-x}R_xTi_3O_{12}$ (x=0.6 and 0.8) films. This increase of polarization not only relates to concentration of the substitute but also to the annealing temperature. The lower concentration of the substitute, the more pronounced the increase of polarization is. A continuous decrease of dielectric permittivity with switch cycling is found in all $Bi_{4-x}R_xTi_3O_{12}$ films. This decrease of dielectric permittivity of $Bi_{4-x}R_xTi_3O_{12}$ (x=0.2) films is much more pronounced than that of $Bi_{4-x}R_xTi_3O_{12}$ (x=0.8). For the application of nonvolatile ferroelectric random access memory (NvFeRAM), $Bi_{3.4}La_{0.6}Ti_3O_{12}$ and $Bi_{3.4}Nd_{0.6}Ti_3O_{12}$ are considered as optimum compositions, due to their high polarization and good fatigue properties.

A model is proposed to explain all the observed results in this work. A growth of a low-dielectric layer model is used in the current proposed model. All the fatigue behaviors of $Bi_{4-x}R_xTi_3O_{12}$ films could be attributed to the redistribution of the pre-existing defects in $Bi_{4-x}R_xTi_3O_{12}$ films. The domain pinning and unpinning effect and the growth of a low-dielectric layer model are in competition during the fatigue process. During the initial period of the fatigue process (1-10^6 cycles), the defects in the

bulk films are trapped in the interface between the bulk films and the electrodes due to the applied voltage and result in the pre-pinned domain released. Therefore, the polarization increases with switching cycles. However, further movement of the defects from the bulk films to the interface contributes to the extensive growth of a low-dielectric layer. As a result, the field applied to the bulk films decreases, which could explain the decrease of polarization during 10^6-10^9 cycles. On the basis of the proposed model, the growth of the low-dielectric layer and remnant polarization (P_r) of films fatigued various cycles were estimated. The estimated remnant polarization (P_r) is in good agreement with experimental results, suggesting the correctness of the proposed defect-redistribution model. BiT-based films annealed in oxygen atmosphere exhibit relatively stable dielectric permittivity (ε_r) and remnant polarization (P_r) during the fatigue process; therefore, the proposed model shows that oxygen vacancies are the major defects.

TABLE OF CONTENTS

ABSTRACT……………………………………………………………………………..….i
TABLE OF CONTENS……………………………………………………...……….iv

CHAPTER 1 INTRODUCTION……………………………………………...……1

1.1 Foundational knowledge of ferroelectrics……………………………...……………1
1.1.1 Basic definition of ferroelectric and polarization…………………………...….1
1.1.2 The perovskite structure……………………………………………………….1
1.1.3 Domain, polarization and hysteresis loop……………………………………..3
1.1.4 Curie point…………………………………………………………………….4
1.2 Application of ferroelectric film (Non-volatile ferroelectric random access memories, NVFeRAM)………………………………………………………..........6
1.2.1 Basic operation of NVFeRAM………………………………………………..8
1.2.2 Polarization fatigue…………………………………………………………..9
1.2.3 Fatigue mechanisms…………………………………………………………10
1.2.4 Potential materials for NVFeRAM application………………………………12
1.2.5 Bismuth titanate ($Bi_4Ti_3O_{12}$)…………………………………………...13
1.3 Dielectric relaxation……………………………………………………………...15
1.3.1 Base knowledge……………………………………………………………..15
1.3.2 Review of previous investigation using dielectric relaxation………………17
1.4 Fabrication of ferroelectric films………………………………………….......19
1.5 Objectives…………………………………………………………………...…20
References……………………………………………………………………………21

CHAPTER 2 EXPERMENT……………………………………………………..25

2.1 Precursor solution……………………………………………………………..25
2.1.1 Precursor Solution 1# (Toshima Co., Japan)……………………………...25
2.1.2 Precursor Solution 2# (Prepared in Laboratory)……………………………28
2.2 Fabrication of top electrode………..………………………..………………...33
2.3 Phase and structure characteristics………………………………………….34
2.4 Characterization of electric properties……………………………………34
2.4.1 Dielectric properties…………………………………………………………34
2.4.2 Ferroelectric measurement………………………………………………….35

2.4.2.1 Dynamics hysteresis measurement (DHM)…………………………...36
2.4.2.2 Fatigue measurement……………………………………………….37
References……………………………………………………………………….39

CHAPTER 3 FABRICATION AND CHARACTERIZATION OF $Bi_{3.27}La_{0.75}Ti_3O_{12}$ FILMS……………………………………………………………...40

3.1 Introduction………………………………………………………………….40
3.2 Fabrication and measurement of $Bi_{3.25}La_{0.75}Ti_3O_{12}$ (BLT)……………………….41
3.3 Phase characteristics and morphology of BLT films……………………………..41
3.3.1 X-ray diffractioin (XRD) results……………………………………………41
3.3.2 Surface morphology………………………………………………………42
3.4 Electric properties…………………………………………………………..43
3.4.1 Hysteresis loop……………………………………………………………43
3.4.2 Dielectric relaxation………………………………………………………44
3.4.2.1 Dielectric behavior in temperature range of 25 °C-600 °C……………44
3.4.2.2 Influence of annealing on dielectric behavior…………………………50
3.4.2.3 Ac electric conductivity properties……………………………………52
3.4.2.4 Discussion of the mechanisms…………………………………………52
3.4.2.5 Summary……………………………………………………………59
3.5 Conclusion and summary……………………………………………………..60
References……………………………………………………………………….61

CHAPTER 4 FERROELECTRIC BEHAVIOR OF $Bi_{4-x}Nd_xTi_3O_{12}$ THIN FILMS……………………………………………………………...62

4.1 Introduction………………………………………………………………….62
4.2 Experiment…………………………………………………………………..63
4.2.1 Preparation of precursor solution…………………………………………63
4.2.2 Fabrication of $Bi_{4-x}Nd_xTi_3O_{12}$ films……………………………………………63
4.2.3 Characterization…………………………………………………………..65
4.3 Results and Discussion……………………………………………………...65
4.3.1 Crystalline phase and morphology…………………………………………65
4.3.2 Ferroelectric characteristics………………………………………………68
4.3.2.1 Remnant polarization and coercive field………………………………68
4.3.2.2 Fatigue characteristics…………………………………………………73

4.4 Conclusions……………………………………………………………………77
References………………………………………………………………………....79

CHAPTER 5 FERROELECTRIC BEHAVIOR OF $Bi_{4-x}La_xTi_3O_{12}$ THIN FILMS…………………………………………………………………...80

5.1 Introduction……………………………………………………………………80
5.2 Experiment……………………………………………………………………..81
5.3 Results ………………………………………………………………………….82
5.3.1 Crystalline phase and morphology……………………………………………83
5.3.2 Ferroelectric characteristics……………………………………………………85
5.3.2.1 Remnant polarization and coercive field………………………………85
5.3.2.2 Fatigue characteristics…………………………………………………85
5.4 Discussion…………………………………………………………………….....90
5.5 Conclusions……………………………………………………………………92
References………………………………………………………………………93

CHAPTER 6 PROPOSED MODEL FOR FATIGUE BEHAVIOR IN $Bi_{4-x}R_xTi_3O_{12}$………………..…………………………………..….95

6.1 Low-dielectric layer model……………………………………………………95
6.2 Domain pinning and unpinning model………………………………………96
6.3 Fatigue behavior in current work……………………………………………98
6.3.1 The dependence of polarization on cycles……………………………………98
6.3.1.1 An increase of polarization (1-10^6 cycles)……………………………98
6.3.1.2 A decrease of polarization (10^6-10^9 cycles)……………………………99
6.3.2 The dependence of dielectric permittivity and tangent loss on cycles…………99
6.3.2.1 Measurement process…………………………………………………100
6.3.2.2 Influence of composition on dielectric properties……………………100
6.3.2.3 Influence of fatigue frequency on dielectric properties………………102
6.3.3 Fatigue and dielectric behavior of films prepared at O_2 atmosphere…………103
6.3.3.1 X-ray diffraction (XRD)……………………………………………...103
6.3.3.2 The dependence of polarization on cycles……………………………104
6.4 A new model for fatigue behavior of $Bi_{4-x}R_xTi_3O_2$ ferroelectric films: defect-redistribution model…………………………………………...……105
6.4.1 Introduction of defect-redistribution model…….……………………………105

6.4.2 Explanation of the results by the defect-redistribution model……………….107
6.4.2.1 The dependence of fatigue behavior on La and Nd concentration…...107
6.4.2.2 The dependence of fatigue behavior on annealing temperature……...108
6.4.2.3 The dependence of dielectric permittivity on switching cycles………108
6.4.2.4 The influence of fatigue measurement frequency on polarization and dielectric variation…………………………………………………109
6.4.3 Estimation of growth of low-dielectric layer…………………………………109
6.4.4 Estimation of polarization of bulk BLT film…………………………………111
6.5 Conclusions……………………………………………………………………...113
References………………………………………………………………………...115

CHAPTER 7 MAJOR CONCLUSIONS AND SUGGESTIONS FOR FUTURE WORK…………………………………………………………….....117

7.1 Major conclusions……………………………………………………………117
7.2 Suggestions for future work…………..……………………………………119

ACKNOWLEDGEMENTS……………………………………………………..…120
LIST OF PUBLICATIONS…………….……………………………………...121

Chapter 1

Introduction

In this chapter, a brief description of ferroelectrics is introduced. Focusing on its application of nonvolatile memory, the advantage and disadvantage of the most investigated ferroelectric systems are discussed. One of the most important problems, decrease of switchable polarization (polarization fatigue), is paid attention. A review of the previous fatigue studies is provided, and the proposed mechanisms responsible for polarization fatigue are clarified. Moreover, dielectric relaxation has also been introduced since its role on defining defects in ferroelectric. The fabrication method has been addressed. Finally, the objective of this dissertation is outlined, and a brief description of the contents of this dissertation is provided.

1.1 FOUNDATIONAL KNOWLEDGE OF FERROELECTRICS

1.1.1 Basic definition of ferroelectric and polarization

Ferroelectrics are a kind of dielectric materials with a spontaneous electric polarization (P_s), and direction of this polarization can be reoriented between crystallographically defined states by an external electric field. Ferroelectricity was discovered by Valasek in Rochelle Salt ($NaKC_4H_4O_6$-$4H_2O$). Spontaneous polarization (P_s) is defined by the value of the dipole moment per unit volume, or by the value of the charge per unit area on the surface perpendicular to the axis of spontaneous polarization (P_s).

1.1.2 The perovskite structure

It was found that most of the ferroelectric materials can be described as the general formula ABX_3 which corresponds to perovskite type of structure. B^{x+} (Ti^{4+}, Zr^{4+}, Sn^{4+}, Nb^{5+}, Ta^{5+}, W^{6+}, etc.) is a cation of a small size, and it is surrounded by six anions (O^{2-} etc.) in an octahedral configuration, and A represents a cation with a large size. A cubic ABX_3 perovskite-type unit cell is shown in Fig. 1-1. The most useful perovskite-type ferroelectrics include barium titanate (BT), lead zirconate titanate (PZT), lead lanthanum zirconate titanate (PLZT), and potassium niobate ($KNbO_3$). Perovskite is the mineral name of calcium titanate ($CaTiO_3$).

The concept of tolerance factor for perovskite structure is useful to analyze the influence of the ionic radii on the crystal structure. The tolerance factor of ABX_3 is

defined by the formula as: [1]

$$t = \frac{R_A + R_X}{\sqrt{2}(R_B + R_X)} \tag{1-1}$$

Where R_A, R_B and R_X are the ionic radii of the A, B cation and the anoin (X), respectively. It is expected that when t=1.0, ideal cubic perovskite is obtained. In practice, those with t=0.95-1.0 exhibit cubic structure; those with lower t are slightly distorted but non-ferroelectric, and those with t slightly higher than 1.0 tend to be ferroelectric. [2]

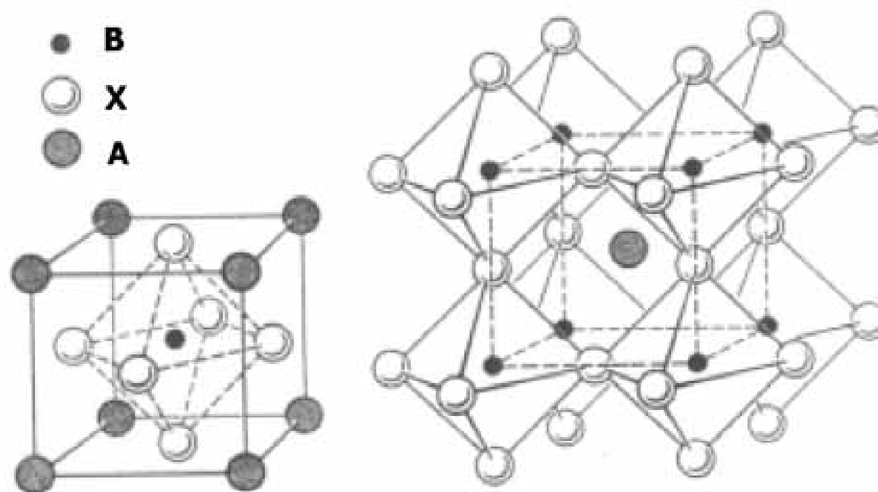

Fig. 1-1 Crystal structure of perovskite-type structure (a) unit cell (b) three-dimensional network of BO_6 octahedra [2].

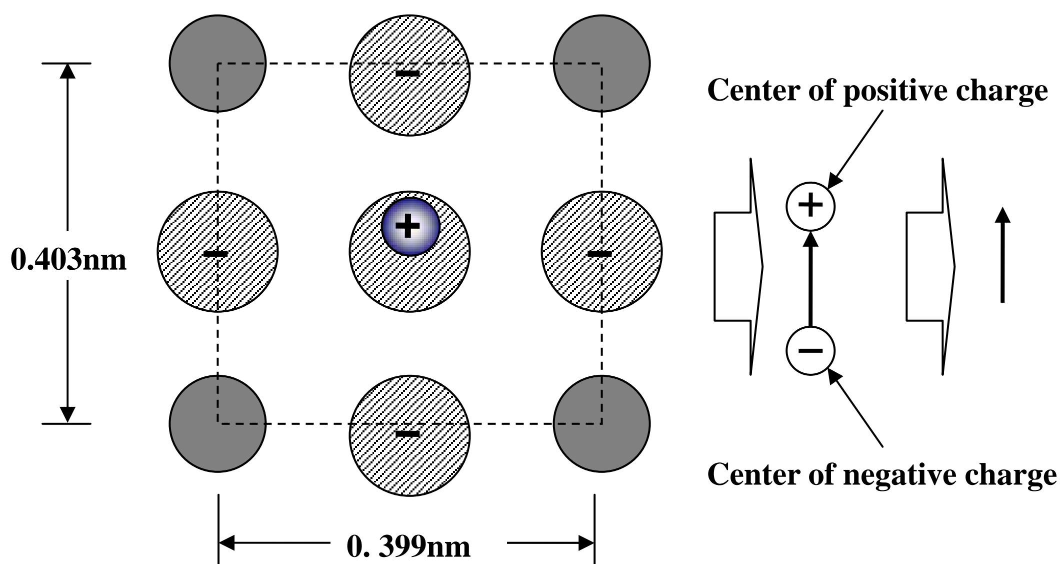

Fig. 1-2 Origin of dipole moment in ferroelectrics, B site off-centering model [3].

For most ferroelectrics, the origin of spontaneous polarization (P_s) comes from the ion off-centering. Figure 1-2 shows a B-site offset model that the B-site ion in an octahedron is off-centered, creating a nonzero dipole moment.

1.1.3 Domain, polarization and hysteresis loop

In a ferroelectric, the region with uniform polarization is called the domain. The interface between two domains is called the domain wall. [4,5] The domain structure of ferroelectrics depends on the structure of the ferroelectric crystal. Fig. 1-3 shows the two major types of ferroelectric domain wall.

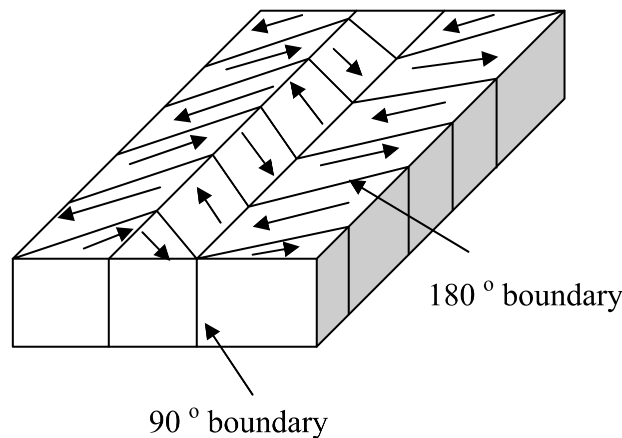

Fig. 1-3 Schematic illustration of 180 ° and 90 ° domain wall [6].

A strong field makes the reversal of the polarization in the domain, which is known as polarization switching or domain switching. Fig. 1-4 exhibits a typical P-E hysteresis loop in ferroelectrics. A small electric field results in a linear relationship between polarization (P) and electric filed (E) (segment OA). As the electric field strength increases, a number of the negative domains (which have a polarization opposite to the direction of the field) will be switched over in the positive direction (along the field direction) and the polarization will increase rapidly (segment AB). As the electric field strength decreases, the polarization will generally decrease but does not return to zero, and the ferroelectric exhibits a remnant polarization P_r. The strength of the field required to zero polarization is called 'coercive field', E_c (segment OF). Further increase of the negative field will cause a complete alignment of the domains, corresponding to G.

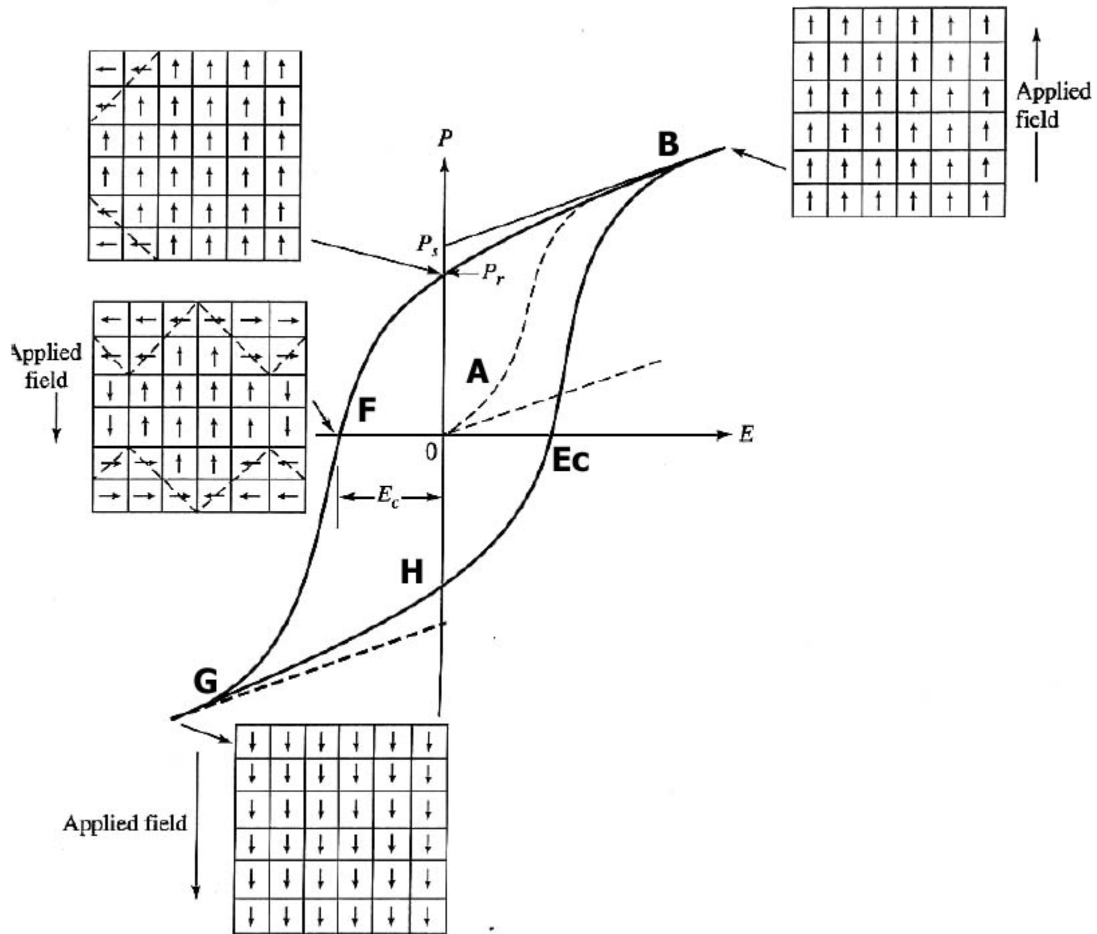

Fig. 1-4 Typical P-E hysteresis loop in ferroelectrics [3].

1.1.4 Curie point

Most ferroelectrics have a non-ferroelectric, and paraelectric form, which may or may not be polar. The temperature of phase transition between ferroelectric and paraelectric phase is called Curie point T_c. When the temperature decreases through the Curie point, a ferroelectric crystal undergoes a structural phase transition from a paraelectric phase to a ferroelectric phase. When the temperature is above T_c, the crystal does not exhibit ferroelectricity; on the other hand, when the temperature is below T_c, the crystal exhibits ferroelectricity. [7-9] If there are more than one ferroelectric phases, the temperature at which the crystal transforms from one ferroelectric phase to another is called the transition temperature. When the temperature is in the vicinity of the Curie point, thermodynamic properties (such as dielectric, elastic, optical, and thermal properties) of a ferroelectric crystal show anomalies. Taking the dielectric permittivity as an example, most ferroelectrics exhibit a very large value of

the dielectric permittivity when the temperature is close to Curie point. This phenomenon is usually called the 'dielectric anomaly', as shown in Fig. 1-5. Above T_c, the dielectric permittivity of most ferroelectrics follows the *Curie-Weiss* law:

$$\varepsilon = \varepsilon_0 + C/(T - T_0) \quad (T > T_0) \tag{1-2}$$

where C is the Curie-Weiss constant and T_0 the Curie-Weiss temperature. It should be noted that T_0 is different from the Curie point T_c. In the case of a first-order phase transition, $T_0 < T_c$, while for the second-order phase transition $T_0 = T_c$.

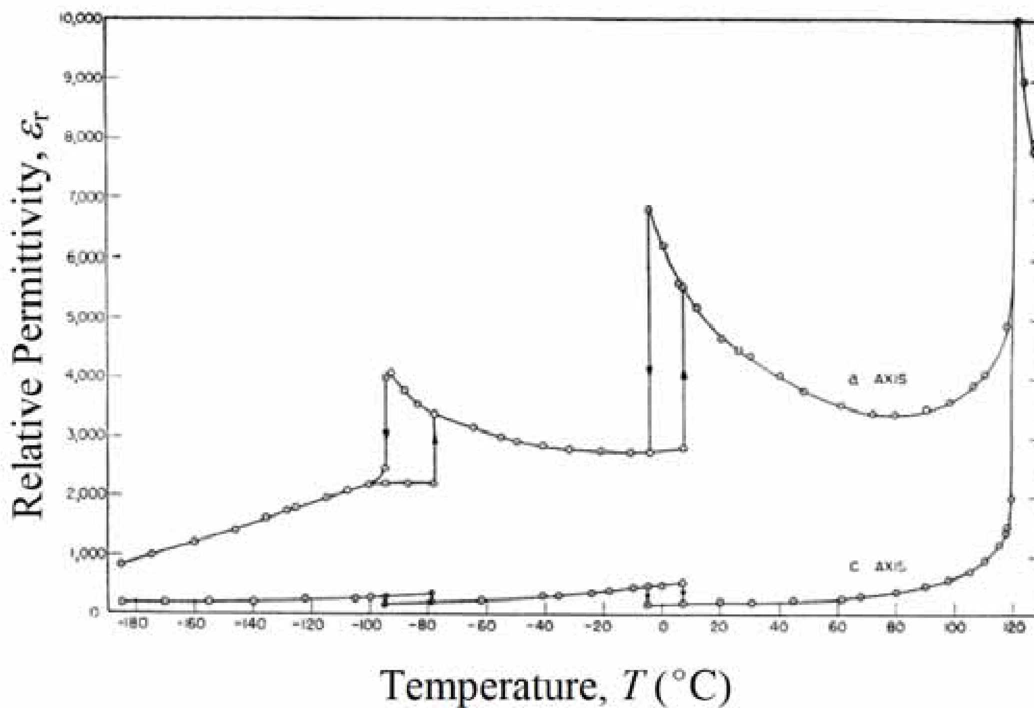

Fig. 1-5 Temperature dependence of the dielectric permittivity in $BaTiO_3$ [10].

The order of phase transition is defined by the discontinuity in the partial derivatives of the Gibbs free energy (G) of the ferroelectric at the phase transition temperature. Therefore, spontaneous polarization (P_s) changes continuously at the phase transition for a ferroelectric with the second order phase transition, and it is discontinuous for a first-order transition, as shown in Fig. 1-6.

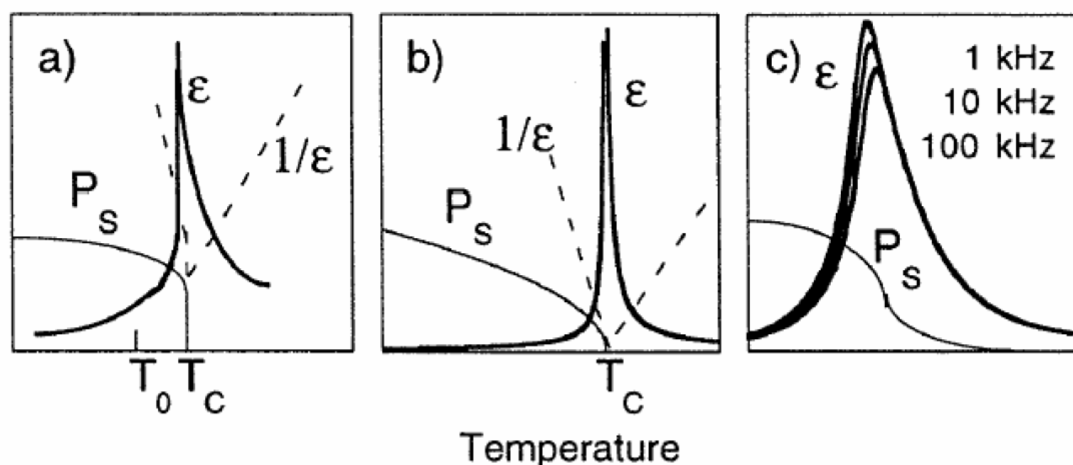

Fig. 1-6 Temperature dependence of the dielectric permittivity (ε) and spontaneous polarization (P_s) for a) a first- and b) a second-order ferroelectric and c) for a relaxor ferroelectric [11].

1.2 APPLICATION OF FERROELECTRIC FILMS (NON-VOLATILE FERROELECTRIC RANDOM ACCESS MEMORIES: NVFERAM)

Non-volatile memory is an essential part of all computer systems. It does not lose information when power is lost in a hostile environment. Tab. 1-1 shows the key characteristics of some current and future nonvolatile memory technology. (DRO: Destructive read out; NDRO: non-destructive read out). Considering all the selection requirements for a nonvolatile memory that fast read/write, radiation hardness, effective cost and compatibility with currently used integrated circuit (IC) processing technology, high endurance and retention, and nondestructive readout capability, the ferroelectric memory stands out as the logical choice for all the application where submicro-second programming is needed.[12] Fig. 1-7 shows two currently used types of NVFeRAM cells consisting a number of capacitor (C) and transistor (T) pair. The details of the nonvolatile ferroelectric memories can be found in several publications. [12-16]

Tab. 1-1. Key characteristics of candidate nonvolatile memory technologies [17].

	FLOATRIN GATE EEPROM	FLASH EEPROM	SNOS nvSRAM (Shadow)	SONOS nvSRAM (SNOS)	SONOS EEPROM	DRO FRAM	NDRO FRAM	MRAM	CORE
SPEED (ACCESS TIME)	150 nsec	120 nsec	35 nsec	150 nsec	150 nsec	100 nsec	200 nsec	Density Dependent 200 ns-2μs	150 nsec
WRITE TIME	10 msec Byte/Page	High	SRAM write 35 nsec; Download 11 msec	10 msec Byte	10 msec Byte	100-200 nsec	100-200 nsec	100-200 nsec	900 nsec
ENDURANCE	10^4-10^5 write cycles	10^4 write cycles	10^5 Power cycles	10^5 write cycles	10^6 write cycles	10^{10} Read/Write	10^{10} write cycles	No known limitation	No limits
RADIATION HARDNESS	Low-Moderate	Low-Moderate	Moderate	High	High	High	High	High	Moderate-High
LIMITATIONS	Write speed	Write speed Endurance	Density	Write speed	Write speed	Endurance DRO	None	Read speed Density	Speed Density Power
COST	Moderate	Low	Moderate-high	Low	Moderate	Potentially low	Potentially low to Moderate	Potentially Moderate	High

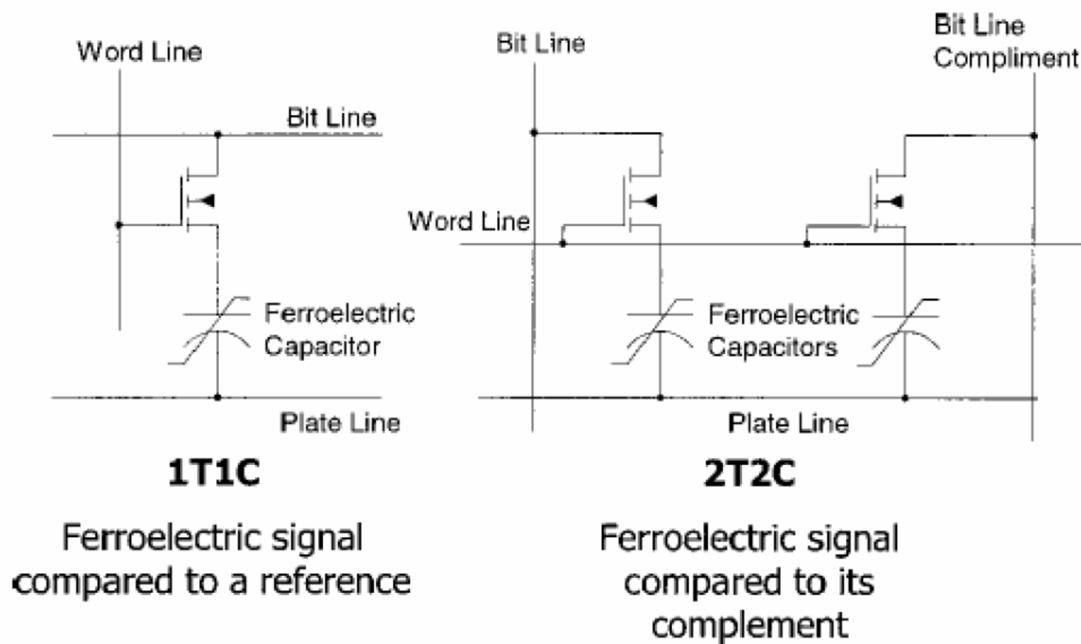

Fig. 1-7 Schematics of two types of NVFeRAM cells [15].

1.2.1 Basic operation of NVFeRAM

The memory application of ferroelectrics is based on the hysteretic behavior of polarization with electric field as shown in Fig. 1-8(a). At zero applied field, there are two polarization states, $\pm P_r$, and these two states could be encoded as “1” or “0”. Since no external field is required to maintain these states, the memory device is nonvolatile. To switch the state of the device, a threshold field greater than $\pm E_c$ is required. Therefore, ferroelectric film is suitable to reduce the required applied voltage (to within 5V) for a given E_c.

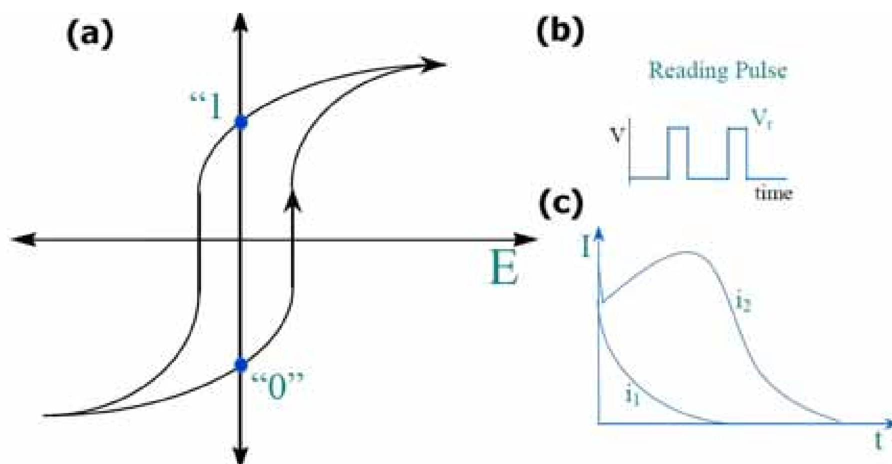

Fig. 1-8 Schematic of the read/write operation in a ferroelectric memory cell.

If a voltage is applied to a ferroelectric capacitor in a direction opposite to the previous voltage, as shown in Fig. 1-8(b), the remnant domains will switch, requiring compensating charge to flow onto the capacitor plates, responding to curve i_2 in Fig. 1-8(c). [18] If the field is applied in the direction of the previously applied field, no switching take place, no change occurs in the compensating charge, and a reduced amount of charge flows to the capacitor, responding to curve i_1 in Fig. 1-8(c).This property can be used to read the state or write a desired state into the capacitor.

1.2.2 Polarization fatigue

Polarization fatigue is a loss of polarization due to repeated switching, as shown in Fig. 1-9. It is a primary degradation effect in ferroelectrics, which is a major problem for the application of memory. Even though extensive works have been carried out to investigate mechanism of polarization fatigue, the main origin of polarization fatigue is still not well understood. Therefore, investigation on mechanism of fatigue still attracts extensive interesting.

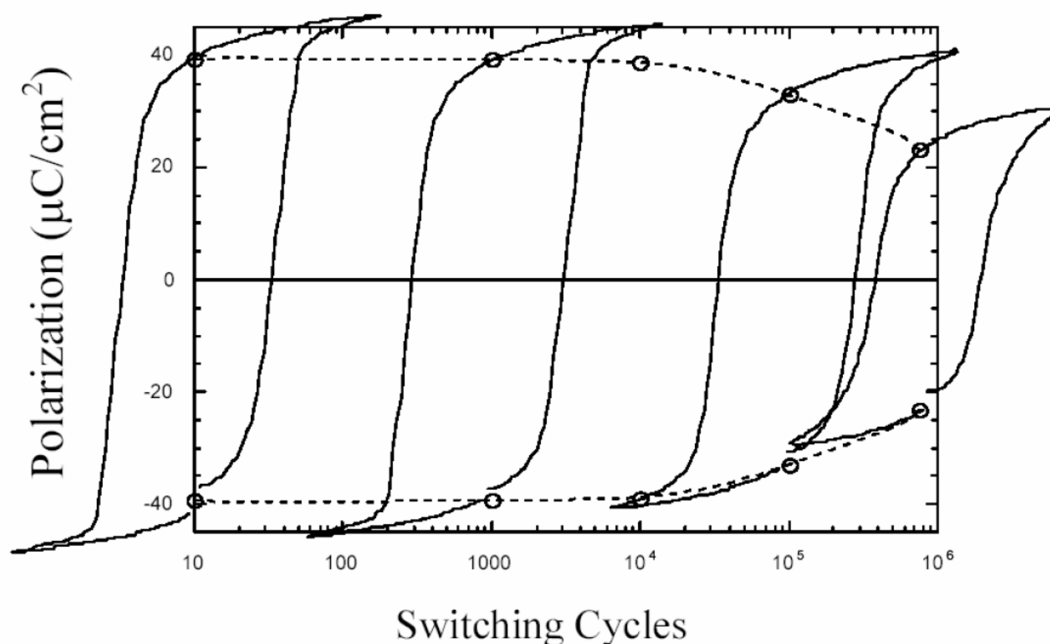

Fig. 1-9 Schematic illustration of polarization decay as a function of the number of the switching cycles.

1.2.3 Fatigue mechanisms

(1) Domain pinning-unpinning model

Dimos *et al.* investigated the fatigue behaviors of $SrBi_2Ta_2O_9$ (SBT) and $Pb(Zr_{1-x}Ti_x)O_3$ (PZT) ferroelectric filmss.[19-21] They found that a significant suppression of the switchable polarization could be induced in fatigue-free SBT by optical illumination combined with a bias voltage near the switching threshold. A similar effect was also found in PZT. Moreover, the optically fatigued SBT could be near-completely recovered by electric field cycling; however, fatigued PZT could not realize the recovery by the electric field cycling.

They proposed that the loss of switchable polarization in PZT due to light/bias combination results from trapping of photogenerated carriers (electrons or holes) at domain boundaries. Figure 1-10 shows the schematic illustration of domain wall pinning. Since the domain wall constitute strong electrostatic potential wells, charged defects are easy to be trapped at such domain wall, and trapped defects tend to pin the domains. It results in reducing the switchable polarization. However, for the fatigue-free ferroelectric such as SBT, the domain pinning is weak, and the cycling field can be expected to unpin the domain walls.

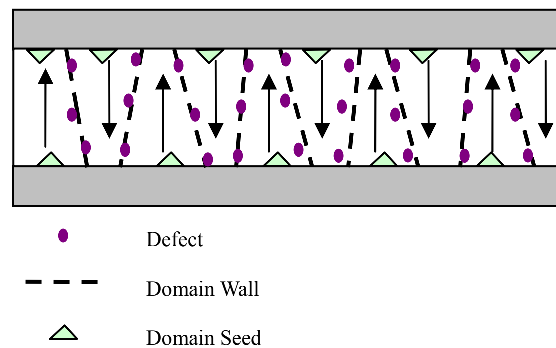

Fig. 1-10 Schematic illustration of domain wall pinning.

(2) $(Bi_2O_2)^{2+}$ layers

Park et al. [45] proposed that $(Bi_2O_2)^{2+}$ layers should make SBT and BiT fatigue-free because the layers have net electrical charges, and so their position in the lattice is self-regulated to compensate for space charges near the electrode (free energy during the growth process is minimized by compensating for space charge). Fig. 1-11 shows the crystal structure of bismuth-layer component.

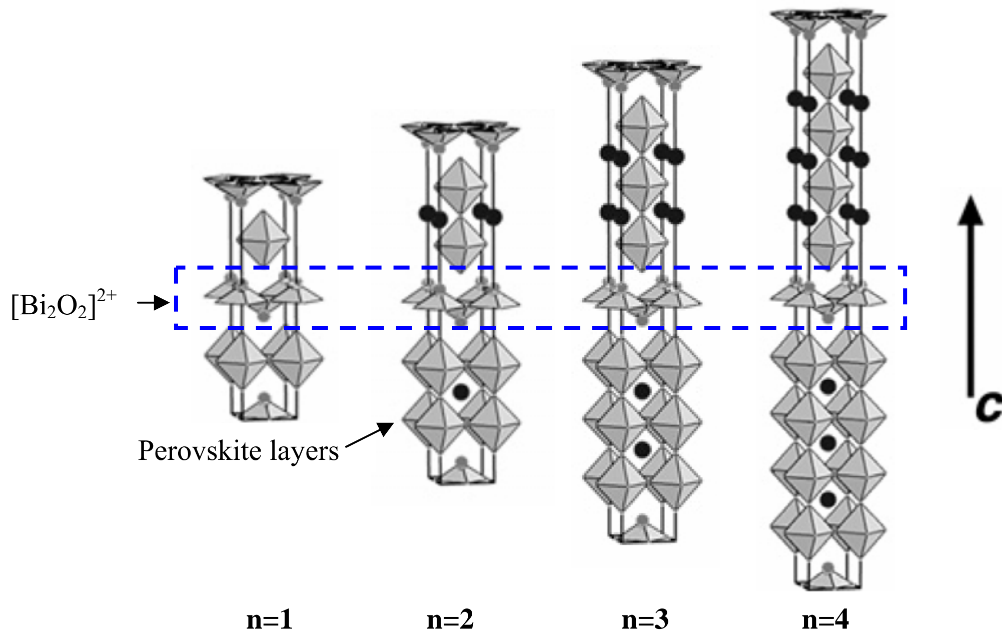

Fig. 1-11 Aurivillius phases, $(Bi_2O_2)(A_{n-1}B_nO_{3n+1})$, consist of interleaved Bi_2O_2 (or Pb_2O_2) and *n* number of ABO_3 perovskite crystallographic units.

(3) Low dielectric layer

It was found that dielectric permittivity exhibits a strong dependence of the thickness of films. [22] With decrease of the thickness, permittivity decreases, [22, 23] as shown in Fig. 1-12. Generally, this phenomenon is attributed to the existence of a low dielectric layer at the electrode/film interface, as shown in Fig. 1-13.

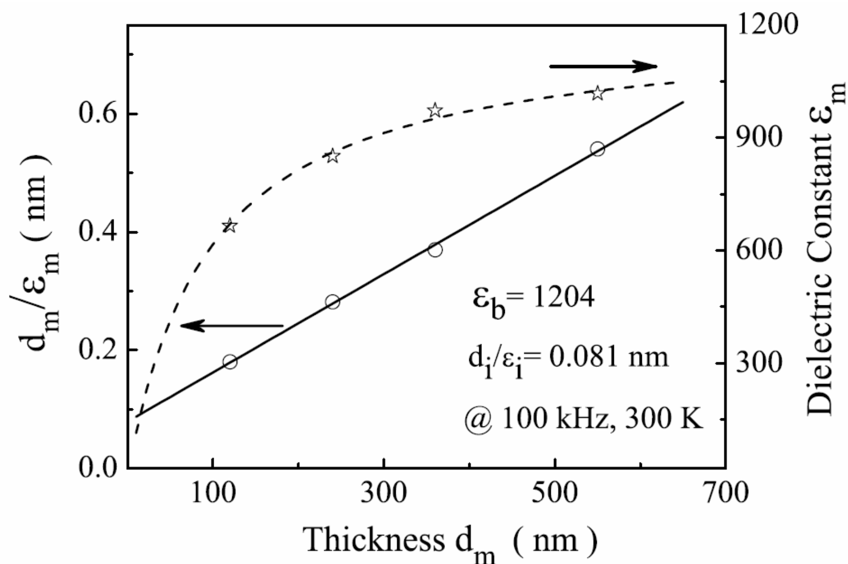

Fig. 1-12 Dependence of d_m/ε_m and ε_m on the thickness of films(d_m, d_i,: thickness of capacitance and interface; ε_m, ε_i and ε_b: dielectric permittivity of capacitance, interface, and bulk film)[24].

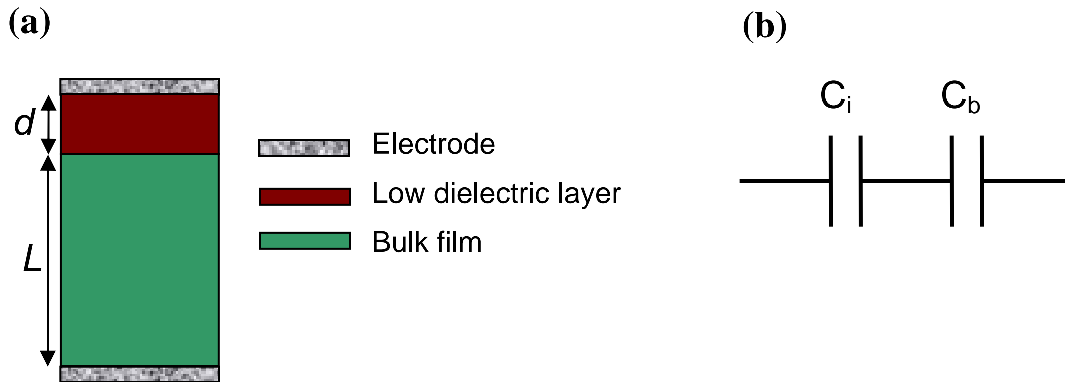

Fig. 1-13 Schematic illustration of the films with low dielectric layer. (a) structure of multilayer films, (b) equivalent circuit of multilayer films (C_i, C_b: Capacitance of interface and bulk film).

The existence of low dielectric layer is also understood to affect switching characteristics of ferroelectric films [25, 26]. The films with a low dielectric layer would be illustrated as an equivalent circuit, as shown in Fig. 1-13(b). Origin of the low dielectric layer was attributed to a thin layer with a gradient polarization or a second phase between the ideal bulk ferroelectric and the electrode.

Similar Point of the previously discussed mechanisms

As mentioned above that most proposed mechanisms for polarization fatigue involve a concept of defects. In the domain pinning-unpinning model, defects play an role on pinning domain wall; in $[Bi_2O_2]^{2+}$ layer model, fatigue-free behavior is attributed to the self-compensate for space charges (a kind of defect); in a low dielectric layer model, fatigue could result in an increase of the defect concentration near the interface between bulk ferroelectric and electrode. ***Therefore, the conception of defect is an important factor to investigate the mechanism of polarization fatigue.***

1.2.4 Potential materials for NVFeRAM application

Two ferroelectric families, perovskite (e.g. $PbZr_{1-x}Ti_xO_3$ (PZT); $BaTiO_3$ (BT)) and layered perovskite (e.g. $Bi_4Ti_3O_{12}$ (BiT) and $SrBi_2Ta_2O_9$ (SBT)) have been widely investigated for memory applications. The crystal structures of PZT and BiT are shown in Fig. 1-1. However, the realization of a commercially available NvFeRAM technology based on PZT has been hampered by the serious polarization fatigue when PZT films grows on metallic Pt electrode. One solution is to fabricate PZT thin film on the conducting oxide electrodes, involving $(La,Sr)CoO_3$ (LSCO),[27] $YBa_2Cu_3O_x$

(YBCO) and RuO_2.[28, 29] However, it results in high leakage current as well as being complex preparation process.[30, 31] Therefore, fatigue-free ferroelectric materials have an advantage over PZT-based ferroelectrics with metal electrodes such as Pt electrode. As a kind of primary fatigue-free ferroelectric materials, layered perovskite ferroelectric shows essentially no polarization fatigue with electric field cycling.[32] However, these fatigue-free ferroelectrics still show a slight decrease of polarization after extensive cycling. Therefore, it is important to find the origin of this polarization decrease to realize the high reliability of NVFeRAM application.

1.2.5 Bismuth titanate ($Bi_4Ti_3O_{12}$)

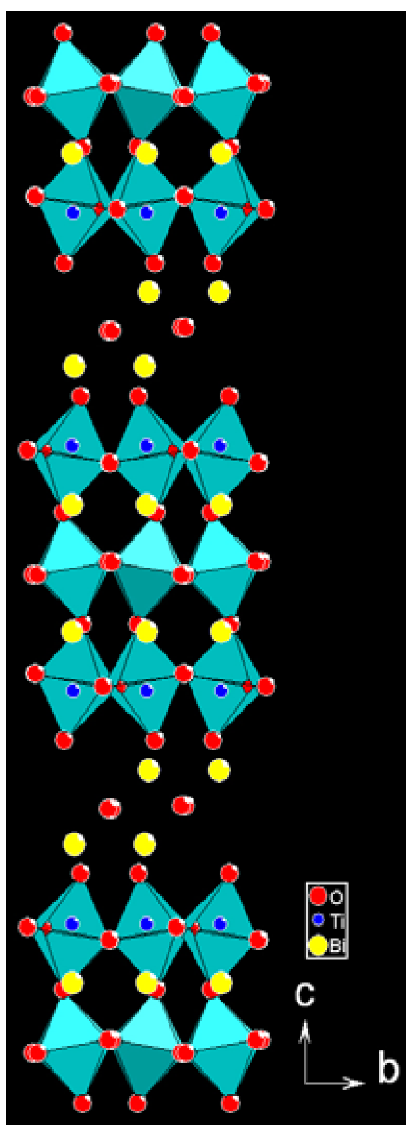

Fig. 1-14 Crystal structure of $Bi_4Ti_3O_{12}$.

$Bi_4Ti_3O_{12}$ (BiT) is one of the famous fatigue-free ferroelectrics. The crystal structure of BiT is shown in Fig. 1-14. The symmetry of BiT was reported to be monoclinic with β very close to 90°.[33] Recently, Hervoches *et al.* [34] used neutron diffraction to refine the structure, and they claimed that it is orthorhombic with the lattice parameter: a=5.4444 Å, b=5.4086 Å, and c=32.8425 Å. Investigation of BiT single crystal revealed that its Curie temperature is 676 °C and spontaneous polarizations along the a and c axis are 50±5 μC/cm^2 and 4±0.1μC/cm^2.[35-37]

Dielectric characteristics of BiT ceramics were investigated by Cross and Setter *et al.*.[38,39] Figure 1-15(a) shows the dependence of dielectric permittivity and loss tangent of BiT at 100 kHz and 1 MHz on temperature, which was reported by Kan *et al.* [39]. Figure 1-15(b) shows the dependence of dielectric permittivity of BiT at 20 Hz, 100 Hz, 1 kHz, 10 kHz, 100 kHz, and 1 MHz, reported by Shulman *et al.* [38]. It is found that the Curie temperature of BiT is about 675 °C, and dielectric permittivity and loss tangent exhibit abrupt increase above 200 °C, which was contributed to the relaxation of

oxygen vacancies ($V_O^{\bullet\bullet}$). Moreover, substitutes such as lanthanum (La) and niobium (Nb) exhibit effect on the dielectric relaxation behavior of BiT ferroelectrics, as shown in Fig. 1-16 which is believed to realize through the suppression of oxygen vacancies.

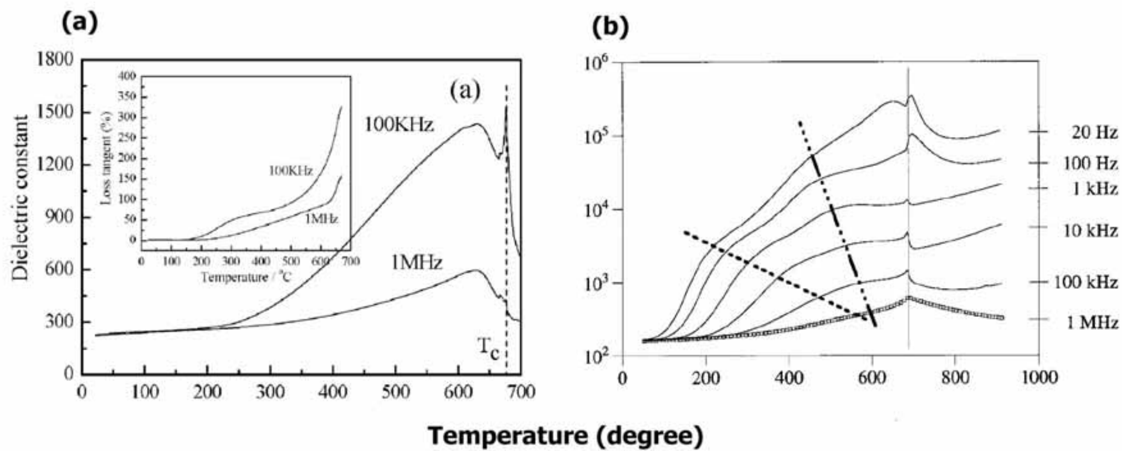

Fig. 1-15 Dielectric behavior of undoped BiT ceramics. (a) dielectric permittivity and loss tangent Vs. temperature [39], (b) dielectric permittivity vs. temperature [38].

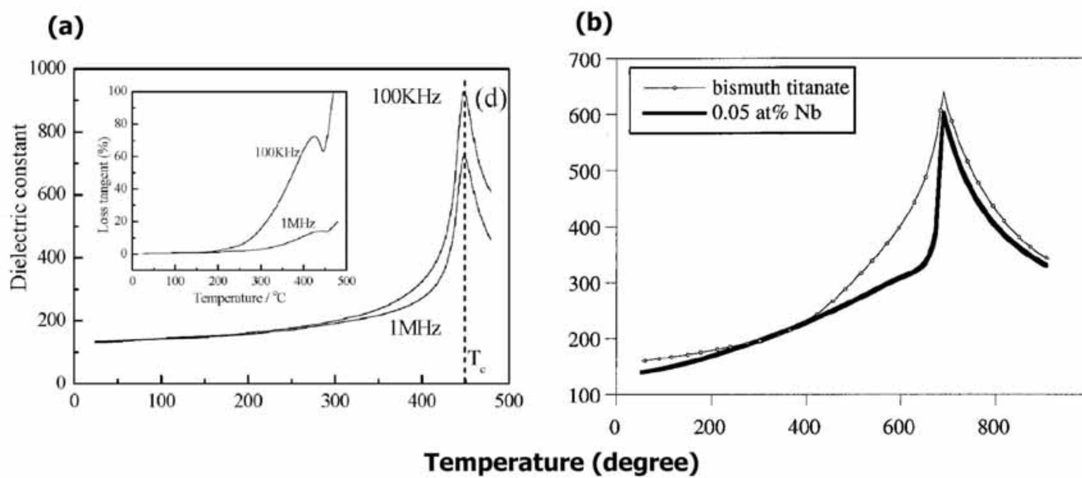

Fig. 1-16 Dielectric behavior of doped BiT ceramics (a) $Bi_{3.25}La_{0.75}Ti_3O_{12}$ [39] (b) BiT doped with 0.05% Nb [38].

1.3 DIELECTRIC RELAXATION [43]

1.3.1 Base knowledge

In ferroelectrics, a dielectric relaxation phenomenon reflects the delay (time dependence) in the frequency response of a group of dipoles submitted to an external applied field. As shown in Fig. 1-17, not all the polarization vector can always follow the variation of the alternating field. The frequency response is expressed in terms of the complex dielectric permittivity

$$\varepsilon^*(\omega) = \varepsilon'(\omega) - i\varepsilon''(\omega) \quad (1\text{-}3)$$

where $\omega = 2\pi f$ is the angular frequency; f is the circular frequency (in hertz) of the oscillating field and i a complex number ($i^2 = -1$). The real (ε': component in phase with the field) and imaginary (ε'': component in quadrature) parts of the permittivity are dependent on each other as shown by the Kramers-Kronig relations:

$$\varepsilon'(\omega) - \varepsilon_\infty = 2/\pi \int_0^\infty \varepsilon''(\omega') \frac{\omega'}{(\omega')^2 - \omega^2} d\omega' \quad (1\text{-}4)$$

$$\varepsilon''(\omega) = 2/\pi \int_0^\infty (\varepsilon'(\omega') - \varepsilon_\infty) \frac{\omega}{(\omega')^2 - \omega^2} d\omega' \quad (1\text{-}5)$$

where ω' is an integration variable and ε_∞ is the high frequency dielectric permittivity.

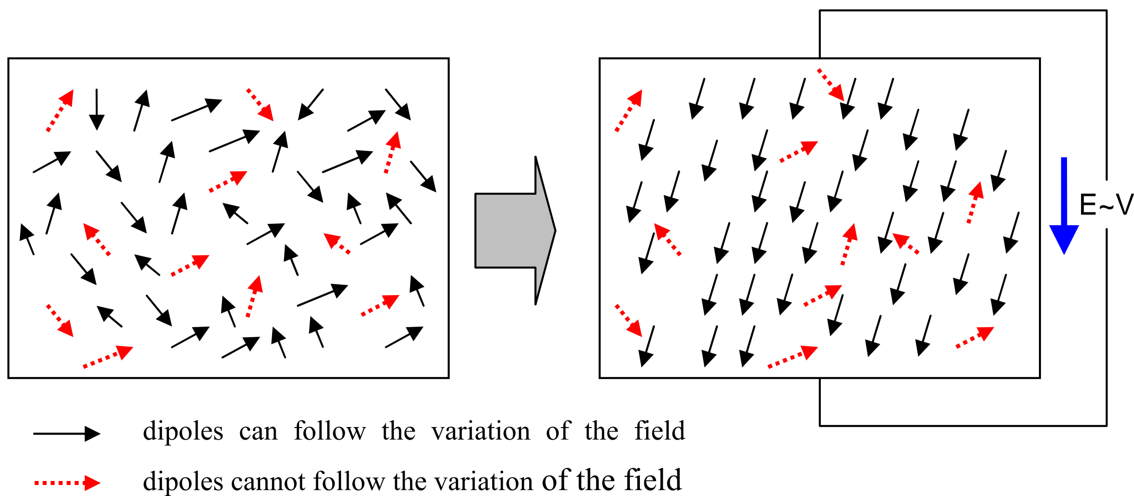

Fig. 1-17 Schematic illustration of dielectric relaxation.

Over a wide frequency range, different types of polarization cause several dispersion regions, as shown in Fig. 1-18. The critical frequency depends on the nature of the dipoles. When the frequency increases, the number of mechanisms involved in the dynamic polarization decreases. A decrease of ε' is observed with increasing frequency. Each polarization mechanism is characterized by a critical frequency f_r (relaxation frequency) corresponding to the maximal phase shift between the polarization (P) and the applied electric field (E); a maximum of dielectric losses ($\tan\delta = \varepsilon''/\varepsilon'$ is the loss factor) occurs. In Debye model, the reorientation of non-interacting dipoles in a purely viscous environment without an elastic restoring force is assumed. The expression for the complex permittivity is:

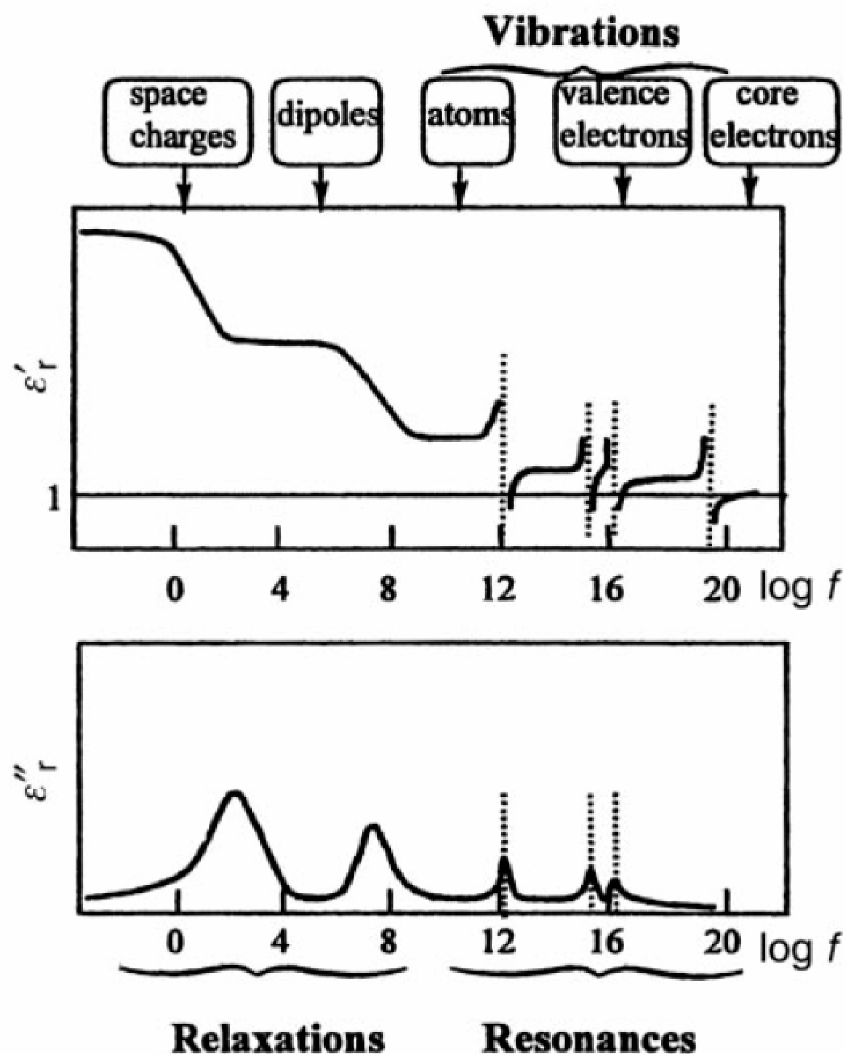

Fig. 1-18 Schematic representation of various relaxation and resonance types f/Hz.

$$\varepsilon^*(\omega) = \varepsilon_\infty + \frac{\varepsilon_s - \varepsilon_\infty}{1 + i\omega\tau} \qquad (1\text{-}6)$$

Separation of the real and imaginary parts of the permittivity gives:

$$\varepsilon' = \varepsilon_\infty + \frac{\varepsilon_s - \varepsilon_\infty}{1 + (\omega\tau)^2} \qquad (1\text{-}7)$$

$$\varepsilon'' = \frac{\varepsilon_s - \varepsilon_\infty}{1 + (\omega\tau)^2}\omega\tau \qquad (1\text{-}8)$$

Where τ is the relaxation time, ε_s is the permittivity at low frequency (f << relaxation frequency) and ε_∞ the one at high frequency (f >> relaxation frequency). ε' decreases to ε_∞ with increasing frequency and ε'' is maximal at the frequency $\omega = 1/\tau$, as shown in Fig. 1-19.

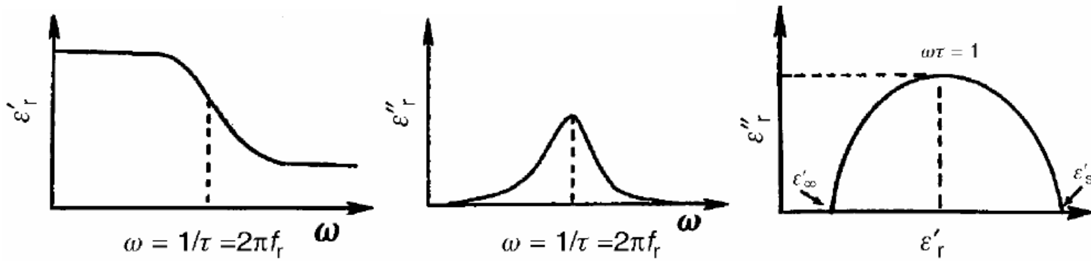

Fig. 1-19 Frequency dependence of $\varepsilon'_r, \varepsilon''_r$ and an Argand diagam: Debye model.

To describe the dielectric dispersion, the variation of ε'_r, ε''_r and $\tan\delta$ as a function of temperature and versus frequency are used. ε'_r is the relative real part of the permittivity $\varepsilon'_r = \varepsilon'/\varepsilon_0$ with the vacuum permittivity ε_0=8.84×10^{-12} C/(Vm).

1.3.2 Review of previous investigation using dielectric relaxation

A Debye-type dielectric relaxation is always reported at a temperature region of 400-700 ^{o}C for perovskite-type ferroelectric oxides such as $PbTiO_3$, $BaTiO_3$, $SrTiO_3$, $CaTiO_3$, and their solid solutions. This dielectric anomaly is a defect-related dielectric relaxation phenomenon.

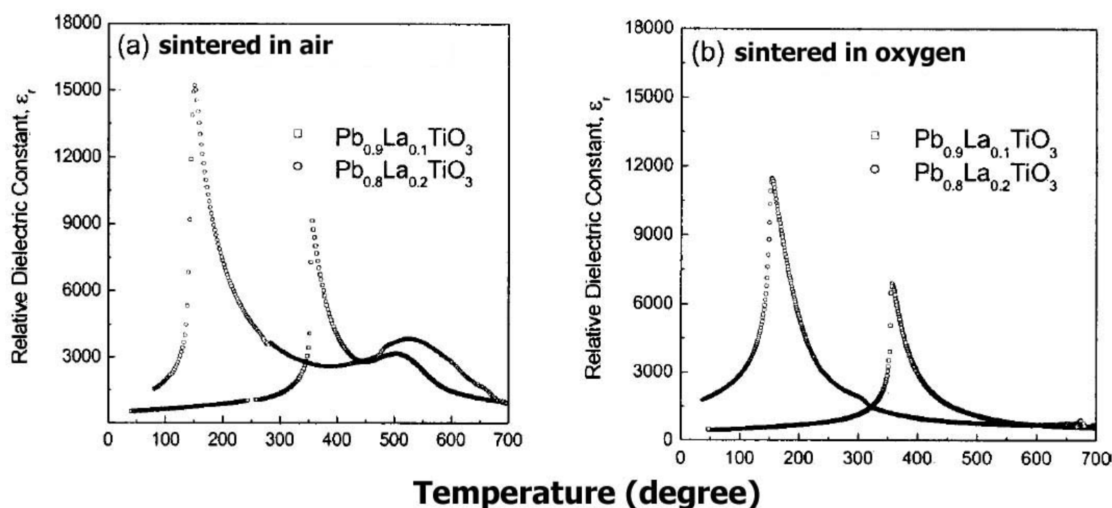

Fig. 1-20 Temperature dependence of the dielectric permittivity of $Pb_{0.9}La_{0.1}TiO_3$, and $Pb_{0.8}La_{0.2}TiO_3$ ceramics (@1kHz). (a) 1150 °C for 10 h, (b) 1100 °C for 10 h. [44]

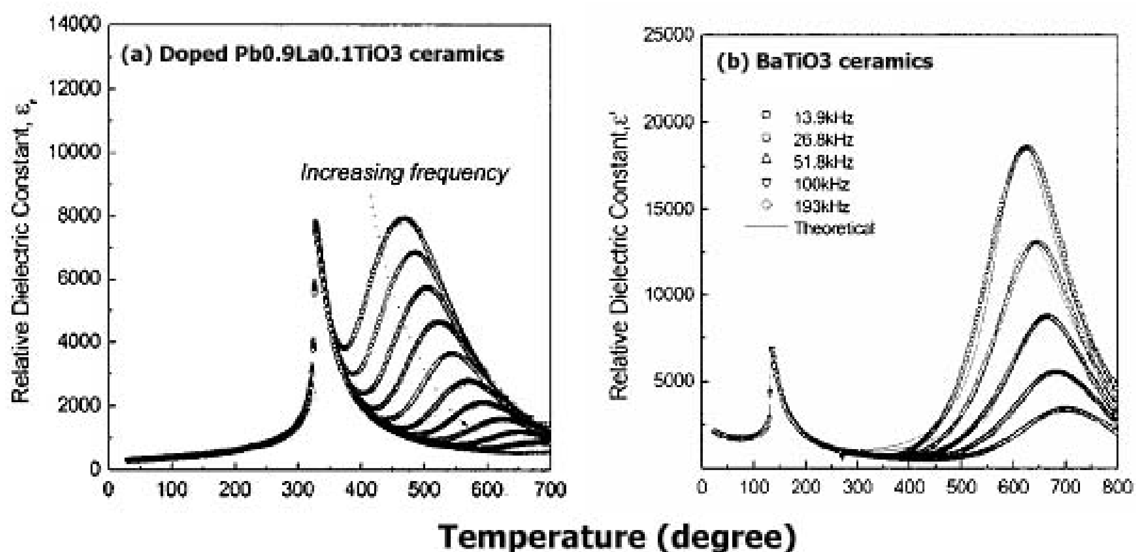

Fig. 1-21 Temperature dependence of dielectric permittivity of (a) MnO_2 doped $Pb_{0.9}La_{0.1}TiO_3$ ceramics annealed in O_2 at 1150 °C for 10h, (b) $BaTiO_3$ ceramics. [44]

As shown in Fig. 1-20, and Fig.1-21, at a temperature higher than Curie temperature (T_c), a diffuse dielectric anomaly occurs for $T>T_c$ at T ($\varepsilon'_{r\max}$). Moreover, the value of T ($\varepsilon'_{r\max}$) increases with frequency, and $\varepsilon'_{r\max}$ decreases, as shown in Fig. 1-21.

In the case of $Pb_{0.9}La_{0.1}TiO_3$ and $Pb_{0.8}La_{0.2}TiO_3$, the diffuse dielectric anomaly is strongly suppressed by annealing in O_2 atmosphere, as shown in Fig. 1-20, while the

sharp anomaly of the phase transition is not. It proves that the diffuse dielectric anomaly is very sensitive to the oxidative annealing atmosphere. It was proposed that the diffuse dielectric anomaly in perovskite-type oxides is an oxygen vacancy-related extrinsic phenomenon.

In case of MnO_2-doped $Pb_{0.9}La_{0.1}TiO_3$, it is believed that Mn^{2+} or Mn^{3+} ions are substituted for the Ti and act as acceptor ions, and they stabilize oxygen vacancies in the lattice to compensate the electric charge unbalance. Since the oxygen vacancies formed by the acceptor ions are expected to be hardly eliminated despite the O_2 atmosphere, therefore a diffuse dielectric anomaly is still found in MnO_2-doped $Pb_{0.9}La_{0.1}TiO_3$ ceramics annealed in O_2 atmosphere.

In conclusion, a diffuse dielectric anomaly in perovskite-type ferroelectric is always attributed to a space charge relaxation related to oxygen vacancies.

1.4 FABRICATION OF FERROELECTRIC FILMS

Recently, there is a rapid improvement in the thin film process. In the fabrication of ferroelectric thin film, most methods are classified into physical and chemical methods of film deposition.

Physical methods of film deposition consist of sputtering, electron beam deposition (EBD), pulsed laser deposition (PLD), and molecular beam epitaxy (MBE) *etc*. Chemical methods of film deposition consist of chemical vapor deposition (CVD) and chemical solution deposition (CSD).

In case of physical methods of film deposition, the deposition process should be carried out in the vacuum; therefore, the vacuum equipment is necessary. Even though, this method has the advantage of high clean degree, the deposition rate is low; the component control is difficult; and deposition area is limited. Thus, the shortcoming of physical methods of film deposition limits the industrial application of this method. Compared to the physical methods of film deposition, chemical methods show the high deposition rate, good component control, large deposition area, and high quality of films.

Due to the low cost, chemical solution deposition (CSD) has been applied in fabricating ferroelectric films, such as PZT, SBT, BiT, and $LiNbO_3$ etc.. However, it still has some shortcoming such as poison of precursor solution and low density of films. In this work, CSD has been selected as fabrication method to prepare $Bi_{4-x}R_xTi_3O_{12}$ (R=La and Nd) ferroelectric films.

1.5 OBJECTIVES

Bismuth titanate ($Bi_4Ti_3O_{12}$) ferroelectric materials are promising candidate for Non-volatile memory, due to its high spontaneous polarization, low processing temperature, and excellent fatigue characteristics. Recently, most works are carried out on doped BiT thin film, such as lanthanum (La^{3+}) substituted BiT,[45-48] neodymium (Nd^{3+}) doped BiT,[49-51] and vanadium (V^{5+}) ,tungsten or nitrogen (N^{3-}) etc. substituted BiT ferroelectric film.[40,52] However, most researches only paid attention on improving ferroelectric properties, including enhancing remnant polarizations (P_r)[49-51, 40] and decreasing coercive fields (E_c)[52], and effect of dopants on fatigue characteristic of BiT-based ferroelectric thin film has been rarely reported. So far, several models have been proposed to explain fatigue-free behavior of ferroelectrics belongs to bismuth layer compound family, such as $SrBi_2Ta_2O_9$ (SBT) and BiT-based ferroelectric films. Cycling field dependence of fatigue behavior, suggesting that fatigue-free behavior of BiT is attributed to field-assisted domain pinning, which is called domain pinning and unpinning model.[53, 54] Moreover, stability of oxygen perovskite layers and space charge compensation by self-regulating $[Bi_2O_2]^{2+}$ layers were also proposed as mechanisms of fatigue-free properties in bismuth layer compounds. It should be noted that all the proposed models involve a variation of concentration of defects. Therefore, it is expected that change of defect concentration may contribute to variation of fatigue behavior of BiT-based ferroelectrics.

As reported, substitution of rare-earth element such as lanthanum (La) and neodymium (Nd) improve the ferroelectric properties.[45-51] Compared to undoped BiT ferroelectric thin film, substituted BiT films exhibit higher fatigue resistance, it is proposed that rare-earth element substitution play a role on fatigue behavior of BiT films due to their suppression effect on defect formation in this ferroelectrics. Considering that La or Nd-substituted BiT films show good ferroelectric properties including high polarization and good fatigue behavior, they is considered as the most promising candidate materials for application of non-volatile ferroelectric random access memories. Moreover, even though extensive study on the influence of La or Nd on the polarization, coercive and orientation of BiT ferroelectric thin films have been reported,[45-51] the effect of La or Nd on the fatigue behavior has not been studied in detail, so far, which is necessary for their application of non-volatile ferroelectric random access memories. Therefore, La or Nd-substituted BiT films are selected to investigate, especially, the effect of substitution on fatigue behavior of BiT-based

ferroelectric thin film.

Moreover, it is found that dielectric relaxation is a useful measurement to detect possible defects in ferroelectric materials. Therefore, in this dissertation, we would like to propose the defect type in bismuth titanate ferroelectric films at first, and then fatigue behavior of the lanthanum (La) and neodymium (Nd)-substituted BiT ferroelectric thin films would be investigated. According to the dielectric relaxation properties and fatigue characteristics, the mechanism of fatigue behavior in bismuth titanate film would be proposed. On the basis of experimental results and proposed mechanisms of fatigue behavior of BiT-based ferroelectric thin films, the optimum condition such as concentration of substitute, annealing temperature, annealing atmosphere could be suggested.

REFERENCES

[1] F.S.Galasso, *Structure, Properties and Preparation of perovskite Type Compounds*, Pergamon Press, London, (1969).
[2] Yuhuan Xu, Ferroelectric *Materials and Their Application*, North-Holland, (1991).
[3] J. F. Shackelford, *Introduction to Materials Science for Engineers*, 2nd edition, Macmillan, (1988).
[4]H.Blattner, W. Kanzig, W. J. Merz and H. Sutter, Helv. *Phys. Acta*, **21**, 207 (1948).
[5] B. T. Batthias and A. von Hippel, *Phys. Rev.*, **73**, 1378 (1948).
[6] A. J. Moulson and J. M. Herbert, *Electroceramics,* Chapman and Hall Press, New York, (1996).
[7] M. E. Lines and A. M. Glass, *Principles and Applications of Ferroelectrics and Related Materials*, Clarendon Press, Oxford, (1977).
[8] H. D. Megaw, *Ferroelectricity in Crystals*, Methuen and Co., London, (1957).
[9] F. Jona and G. Shirane, *Ferroelectric Crystals*, Pergamon Press, Oxford, (1962).
[10] W. J. Merz. *Phys. Rev*., **76**, 1221 (1949).
[11] D. Damjanovic, *Rep. Prog. Phys*., **61**, 1267 (1998).
[12] S. Sinharoy, H. Buhay, D.R. Lampe, and M.H. Francombe, *J. Vac. Sci. Technol.* A, **10**, 1554 (1992).
[13] F. Scott, and C. A. Paz De Araujo, *Science*, **246,** 1400 (1989).
[14] A. I. Kingon and S. K. Streiffer, *Curr. Opin. Sol. St*. M., **4**, 39 (1999).
[15] G. R. Fox, F. Chu, and T. Davenport, *J. Vac. Sci. Technol. B*, **19**, 1967 (2001).
[16] R. Ramesh, *Thin film ferroelectric materials and devices*, Kluwer Press, Massachusetts, (1997).
[17] 1. Bob Peters, *Defense Electronics.*,82 (1991).
[18] J. T. Evans and R. Womack, *IEEE J. Solid State. Circuits.*, **23**, 1171 (1988).
[19] W. L. Warren, D. Dimos, B. A. Tutttle, G. E. Pike, R. W. Schwartz, P. L. Clews, and D. C. Mclntyre, *J. Appl. Phys.*, **77**, 6695 (1995).
[20] D. Dimos, W. L. Warren, M. B. Sinclair, B. A. Tuttle, and R. W. Schwartz, *J. Appl. Phys.*, **76**, 4305 (1994).
[21] H. N. Al-Shareef, D. Dimos, T. J. Boyle, W. L. Warren, and B. A. Tuttle, *Appl. Phys. Lett.*, **68**, 690 (1996).
[22] P. K. Larsen, J. M. Dormans, D. J. Taylor, and P. J. van Veldhoven, *J. Appl. Phys.* **76**, 2405 (1994).
[23] D. Wu, A. D. Li, H. Q. Ling, T. Yu, Z. G. Liu, and N. B. Ming, *J. Appl. Phys.*, **87**, 1795 (2000).

[24] J. Miao, Y. Wang, H. Y. Tian, X. Y. Zhou, H. L. W. Chan, C. L. Choy, L. X. Cao, and B. R. Zhao, *J. Phys. D. Appl. Phys.,* **39**, 2565(2006).
[25] A. K. Tagantsev, M. Landivar, E. Colla, and N. Setter, *J. Appl. Phys.*, **78**, 2623 (1995).
[26] H. Z. Jin, and Jing Zhu, *J. Appl. Phys.*, **92**, 4594 (2002).
[27] J. Lee and R. Ramesh, *J. Appl. Phys.* **68**, 484 (1996).
[28] V. G. Keramidas, D. K. Fork, J. Lee, and A. Safari, *Appl. Phys. Lett.*, **61**, 1537 (1992).
[29] S. D. Bernstein, T. Y. Wong, Y. Kisler, and R. W. Tustison, *J. Mater. Res.*, **8**, 12 (1993).
[30] P. C. Fazan, *Integ. Ferroelect.*, **4**, 247 (1994).
[31] W. Kinney, *Integ. Ferroelect.*, **4**, 131 (1994).
[32] C. A. Paz de Araujo, J. D. Cuchiaro, L. D. Mcmillan, M, C, Scott, and J. F. Scott, *Nature*, **374**, 627 (1995).
[33] S. E. Cummins and L. E. Cross, *Appl. Phys. Lett.*, **10**, 14 (1967).
[34] C. H. Hervoches and P. Lightfood, *Chem. Mater.*, **11**, 3359 (1999).
[35] B. Frit, J. P. Mercurio, *J. Alloys Compds.*, **188**, 27 (1992).
[36] A. Fouscova and L. E. Cross, *J. Appl. Phys.*, **41**, 2834 (1970).
[37] S. E. Cummins and L. E. Cross, *J. Appl. Phys.*, 3**9**, 2268 (1968).
[38] H.S. Shulman, D. Damjanovic, and N. Setter, *J. Am. Ceram. Soc.*, **83**, 528 (2000).
[39] Y. Kan. X. Jin, G. Zhang, P. Wang, Y. Cheng, and D. Yan, *J. Mater. Chem.*, **14**, 3566 (2004).
[40] Y. Noguchi and M. Miyayama, *Appl. Phys. Lett.*, **26**, 1903 (2001).
[41] A. Q. Jiang, Z. X. Hu and L. D. Zhang, *Appl. Phys. Lett.*, **74**, 114 (1999).
[42] C. Jovalekic, M. Pavlovic, P. Osmokrovic and L. Atanasoska, *Appl. Phy. Lett.*, **72**, 1051 (1998).
[43] C. Elissalde and J. Ravez, *J. Mater. Chem.*, **11**, 1957 (2001).
[44] B. S. Kang, S. K. Choi, and C. H. Park, *J. Appl. Phys.*, **94**, 1904 (2001).
[45] B. H. Park, B. S. Kang, S. D. Bu, T. W. Noh, J. Lee and W. Jo, *Nature* (London) **401**, 682 (1999).
[46] D. Wu, A. Li, T. Zhu, Z. Li, Z. Liu, and N. Ming, *J. Mater. Res.*, **16**, 1325 (2001).
[47] H. N. Lee, D. Hesse, N. Zakharow, and U. Gösele, *Science*, **296**, 2006 (2002).
[48] T. Kojima, T. Sakai, T. Watanabe, H. Funakubo, K. Saito, and M. Osada, *Appl. Phys. Lett.*, **80**, 2746 (2002).
[49] D. Wu, A. Li, and N. Ming, *J.Appl. Phys.*, 95, 4275 (2004).

[50] T. Watanabe, H. Funakubo, M. Osada, H. Uchida and I. Okada, *J. Appl. Phys.*, **98**, 024110 (2005).
[51] C. J. Lu, Y. Qiao, Y. J. Qi, X. Q. Chen, and J. S. Zhu, *Appl. Phys. Lett.*, **87**, 222901 (2005).
[52] H. Irie, H. Saito, S. Ohkoshi, and K. Hashimoto, *Adv. Mater.*, **17**, 491 (2005).
[53] H. N. Al-shaareef, B. A. Tuttle, W. L. Warren, T. J. Headley, D. Dimos, J. A. Voige, and R. D. Nasby, *J. Appl. Phys.*, **79**, 1013 (1996).
[54] D. Dimos, H. N. Al-Shareef, W. L. Warren, and B. A. Tuttle, *J. Appl. Phys.*, **80**, 1682 (1994).

Chapter 2

Experiment

This chapter provides the preparation process of the films investigated in this thesis. Two kinds of precursor solutions were used. One is a purchased solution from Toshima Co., Japan, and the other is prepared in our laboratory. The detailed fabrication procedure will be presented in following sections. This processing exhibits low cost, easy control of stoichiometry, simplicity, and potential commercial application to deposit uniform films over large areas. The fabrication processing of $Bi_4Ti_3O_{12}$-based ferroelectric films using the two different precursor solutions is introduced. Moreover, a brief introduction of the characteristics of structure and the electrical measurement methods are also given in this chapter. Specially, due to the importance of the ferroelectric properties such as hysteresis loop measurement and fatigue measurement, the working principle of the two measurements is also introduced.

2.1 PRECURSOR SOLUTION

2.1.1 Precursor solution 1# (Toshima Co., Japan)

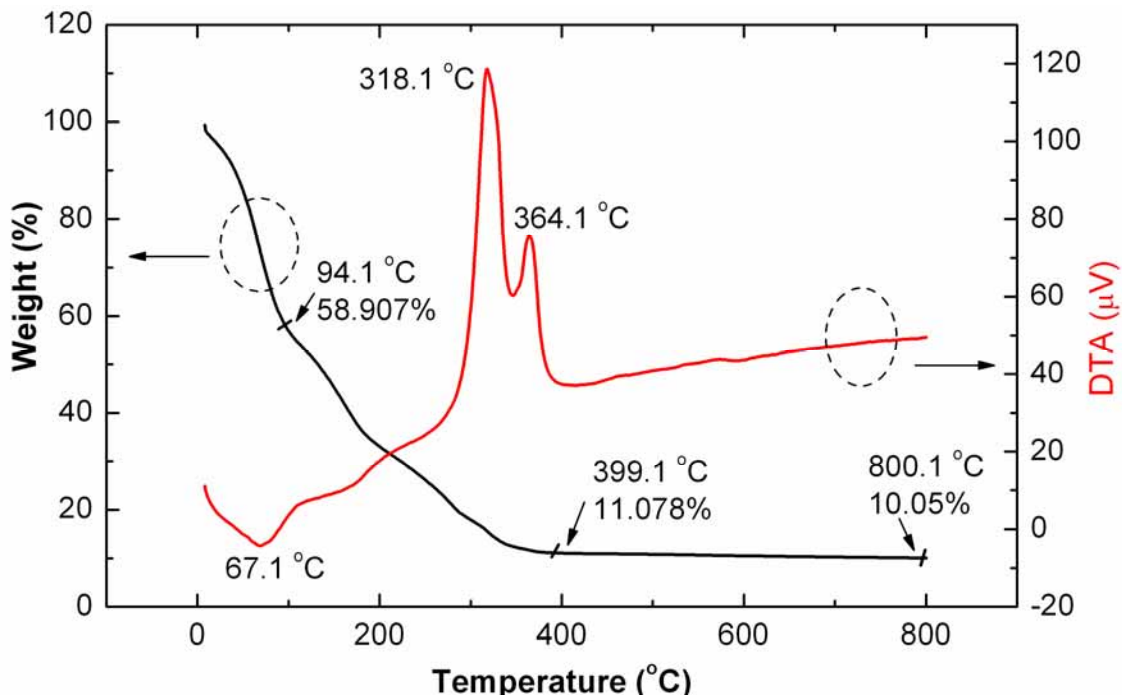

Fig. 2-1 Thermal analyses on precursor solution 1# $Bi_{3.25}La_{0.75}Ti_3O_{12}$.

The component of precursor solution 1# is $Bi_{3.25}La_{0.75}Ti_3O_{12}$ (BLT0.75). To identify the heat treatment processing, Thermal analysis thermo gravimetric analysis (TGA)-differential thermal analysis (DTA) measurement was conducted in air from room temperature to 800 ^{o}C with a temperature ramp rate of 10 ^{o}C/min, as shown in Fig. 2-1.

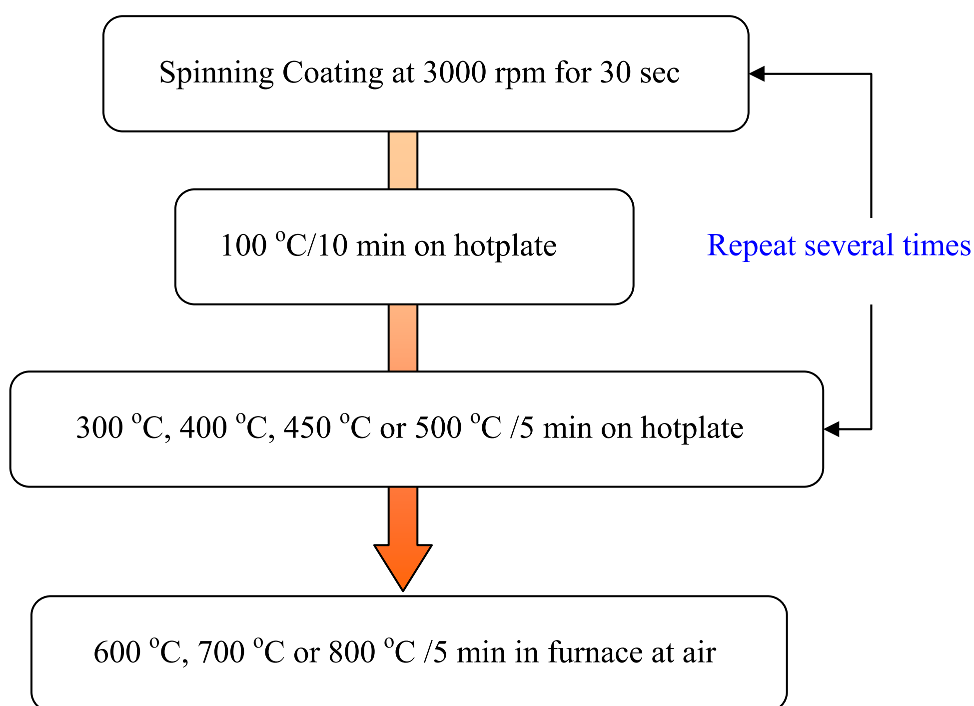

Fig. 2-2 Heat treatment process for precursor solution 1#.

It is found that a rapid decrease of weight between room temperature to 94.1 ^{o}C, because of the evaporation of solvents. The weight shows almost unchanged above 399.1 ^{o}C. Two exothermal peaks are found at 318 ^{o}C and 364 ^{o}C, which may consistent with the decomposition of precursor. According to the thermal analysis results, the heat treatment for the films fabricated from precursor solution 1# was decided, as shown in Fig. 2-2.

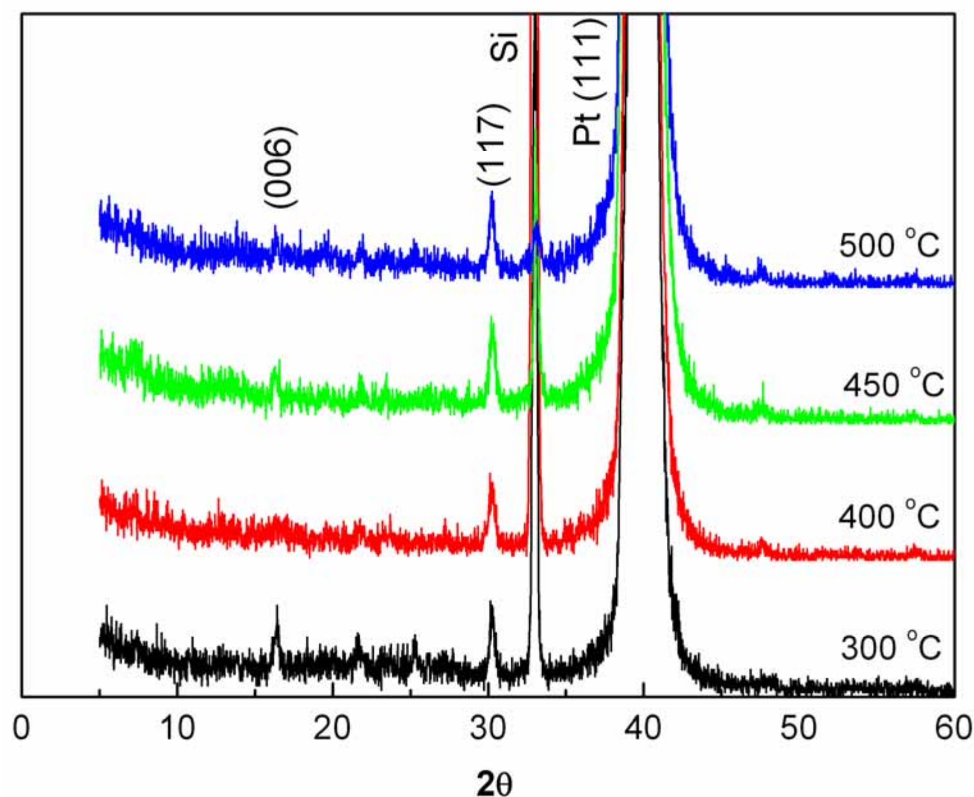

Fig. 2-3 X-ray diffraction of BLT0.75 at different intermediate annealing temperature.

As shown in Fig.2-2, the heat treatment is divided into three steps. Recently, it was reported that intermediate annealing plays an important role on the orientation and crystallization of films.[1-3] According to the thermal analysis results, four intermediate annealing temperatures (300 °C, 400 °C, 450 °C, and 500 °C) were selected. To compare the effect of intermediate annealing temperature on orientation and crystallization, the annealing temperature is fixed as 700 °C.

The XRD patterns of BLT0.75 films prepared at 300 °C, 400 °C, 450 °C and 500 °C intermediate annealing temperature are shown in Fig. 2-3. All the XRD peaks of the samples agreed well with the XRD data of crystalline $Bi_4Ti_3O_{12}$, no other phase were detected, suggesting that La^{3+} ions were incorporated into the $Bi_4Ti_3O_{12}$ lattice. The effect of intermediate annealing temperature on orientation of BLT0.75 was not found in present work.

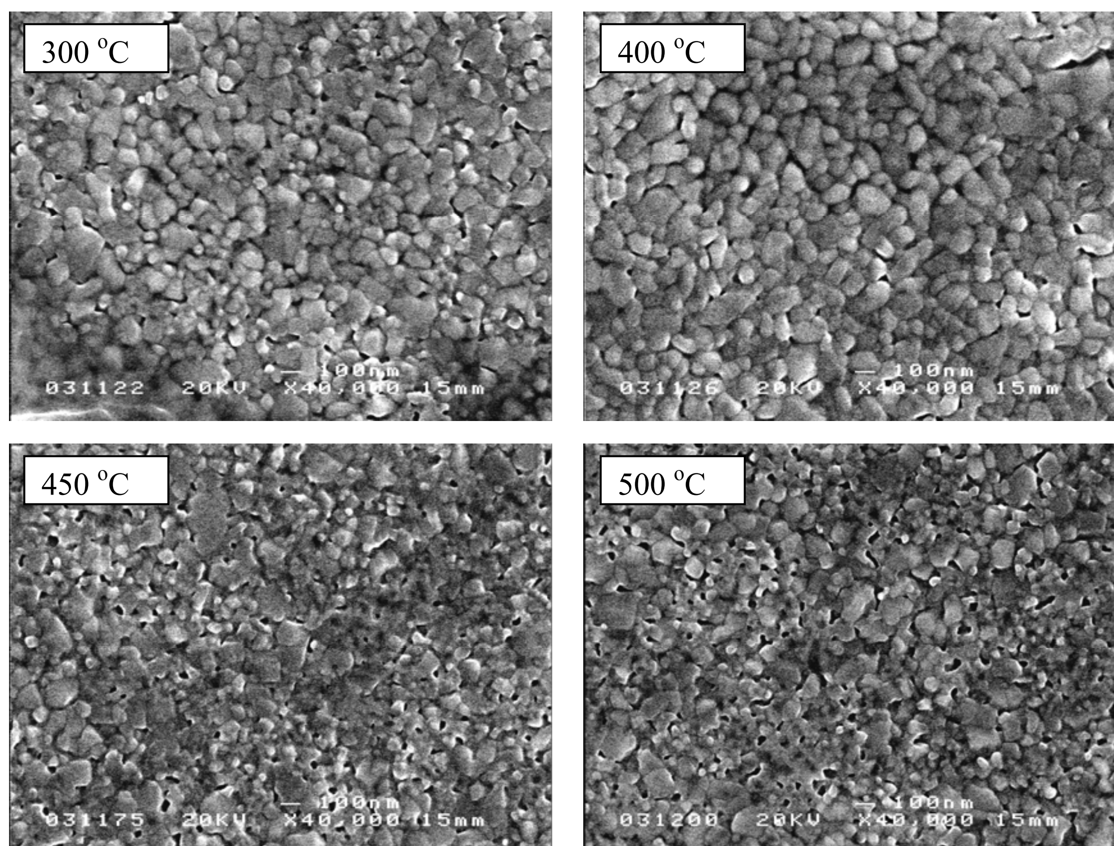

Fig. 2-4 SEM images of the films annealed at 700 °C at different intermediate annealing temperature.

Figure 2-4 shows the typical morphology of the BLT0.75 films fabricated at intermediate annealing temperature 300 °C, 400 °C, 450 °C, and 500 °C, respectively. It is observed that BLT0.75 prepared at the intermediate temperature of 400 °C exhibits the dense morphology and homogenous grain size, while the other films show poor morphology. It suggests that an intermediate annealing temperature of 400 °C is favorable condition for growth of dense BLT films. Therefore, an intermediate annealing temperature of 400 °C was selected in the following experiments.

2.1.2 Precursor solution 2# (Prepared in Laboratory)

Bismuth nitrate ($Bi(NO_3)_3 \cdot 5H_2O$), n-tetrabutyl titanate ($(C_4H_9O)_4Ti$) and lanthanum nitrate ($La(NO_3)_3 \cdot 5H_2O$) or neodymium nitrate ($Nd(NO_3)_3 \cdot 6H_2O$) were selected as starting materials. Acetic acid (CH_3COOH) and 2-methoxyethanol were solvents. Firstly, bismuth nitrate ($Bi(NO_3)_3 \cdot 5H_2O$) was dissolved in acetic acid (CH_3COOH), and tetrabutyl titanate $(C_4H_9O)_4Ti$ was added to the solution slowly with constant stirring. 10 mol% excess of bismuth nitrate was added to compensate the Bi

loss during annealing process. Finally, 2-methoxy ethanol was added to adjust solution concentration to 0.05mol/l. This solution was transparent without any participation. The general steps of this processing are shown in Fig. 2-5.

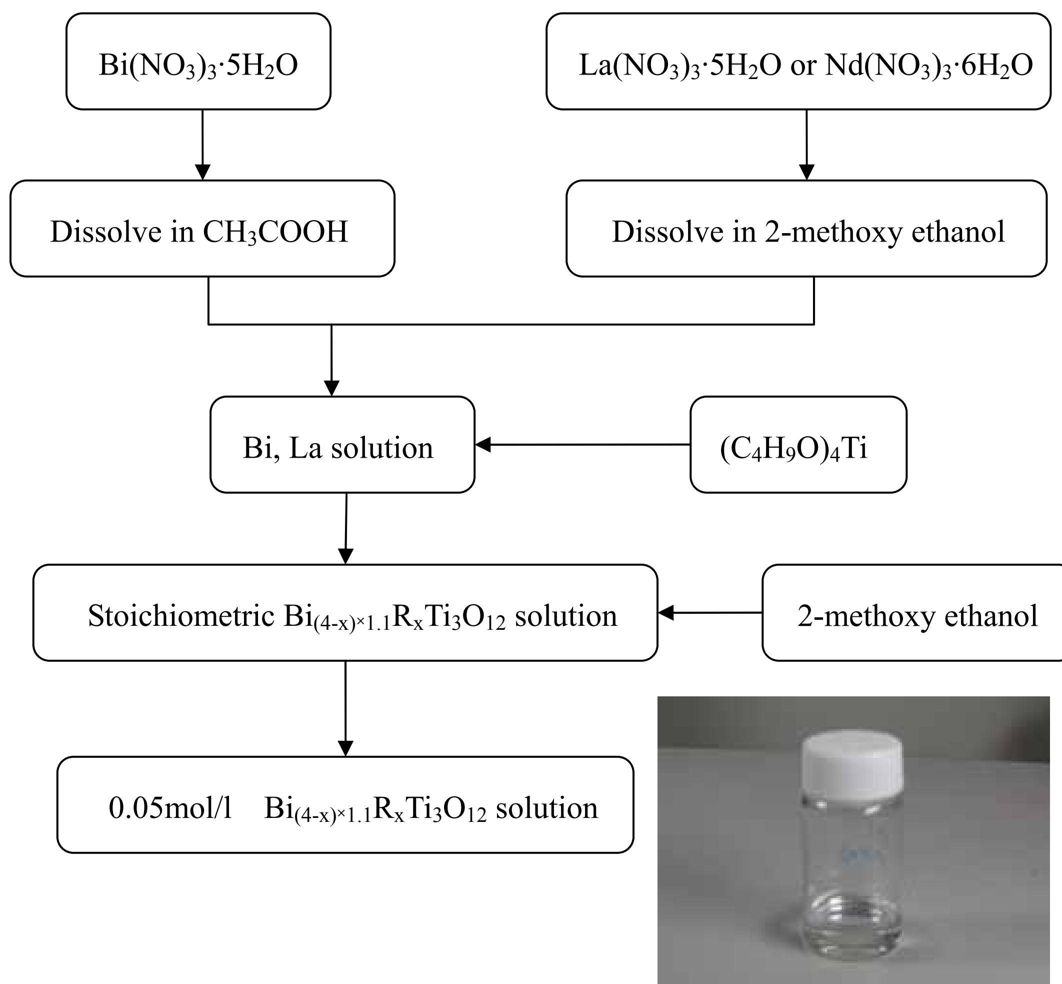

Fig. 2-5 Preparation processing of $Bi_{4-x}R_xTi_3O_{12}$ precursor solution.

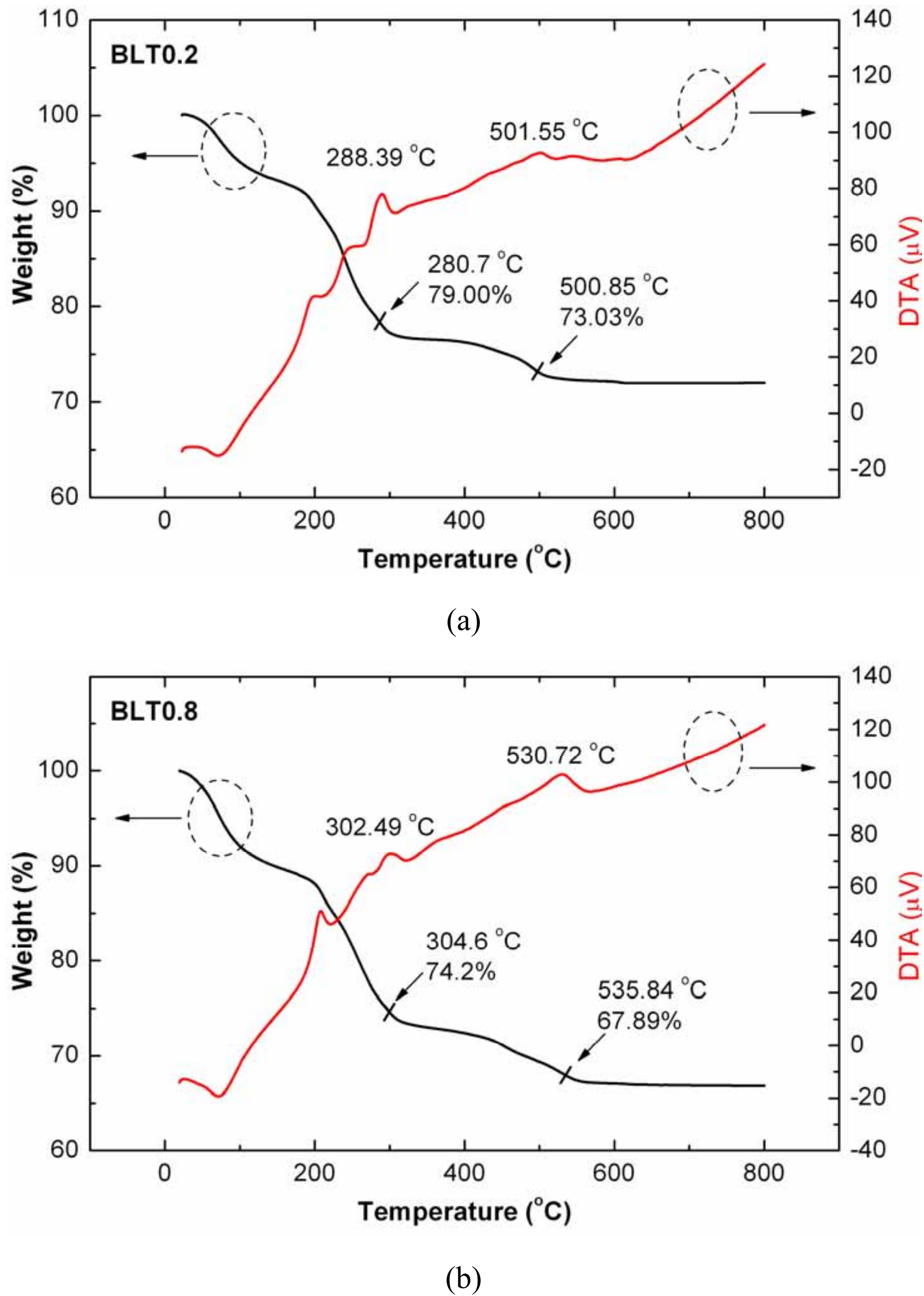

Fig. 2-6 Thermal analyses of precursor solution 2# (a) $Bi_{3.8}La_{0.2}Ti_3O_{12}$ and (b) $Bi_{3.2}La_{0.8}Ti_3O_{12}$.

Thermal analysis was also performed at the powder after heating precursor solution 2# at 120 ^oC for 2 hours, as shown in Fig. 2-6. The results of two components $Bi_{3.8}La_{0.2}Ti_3O_{12}$ (BLT0.2) and $Bi_{3.2}La_{0.8}Ti_3O_{12}$ (BLT0.8) are similar, therefore the heat treatment process are selected as same for all the compositions. All the weight loss is found below 300 ^oC, which is responding to the decomposition of precursor solution. The broad peaks at about 500 ^oC may be related to crystallization of BLT films.[4]

Nanosized powders were prepared after heating precursor solution 2# after 600 °C for 1 hour. Typical morphology of the powders is shown in Fig. 2-7. It is observed that all compositions exhibit spherical grain with similar size. With the increase of substitute of La, grain size decreases. It agrees with previous reports that with increase of substitutes, such as La and Nd etc., the grain size of BiT-based ferroelectric decrease due to the suppression effect of the substitute on growth of BiT-based grains.[5, 6]

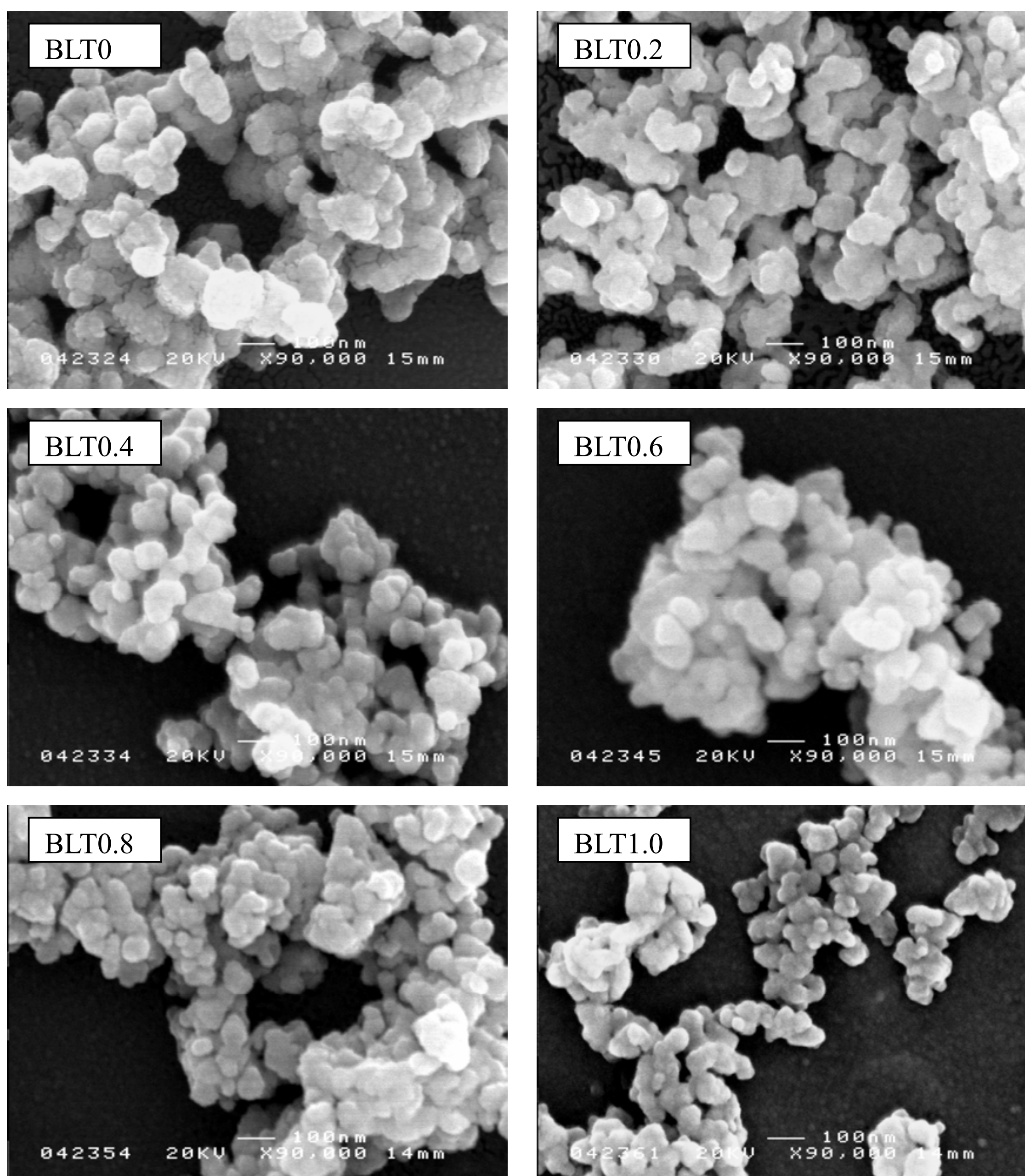

Fig. 2-7 SEM images of BLT powders (2# solution) after heated at 600 °C for 1 hour.

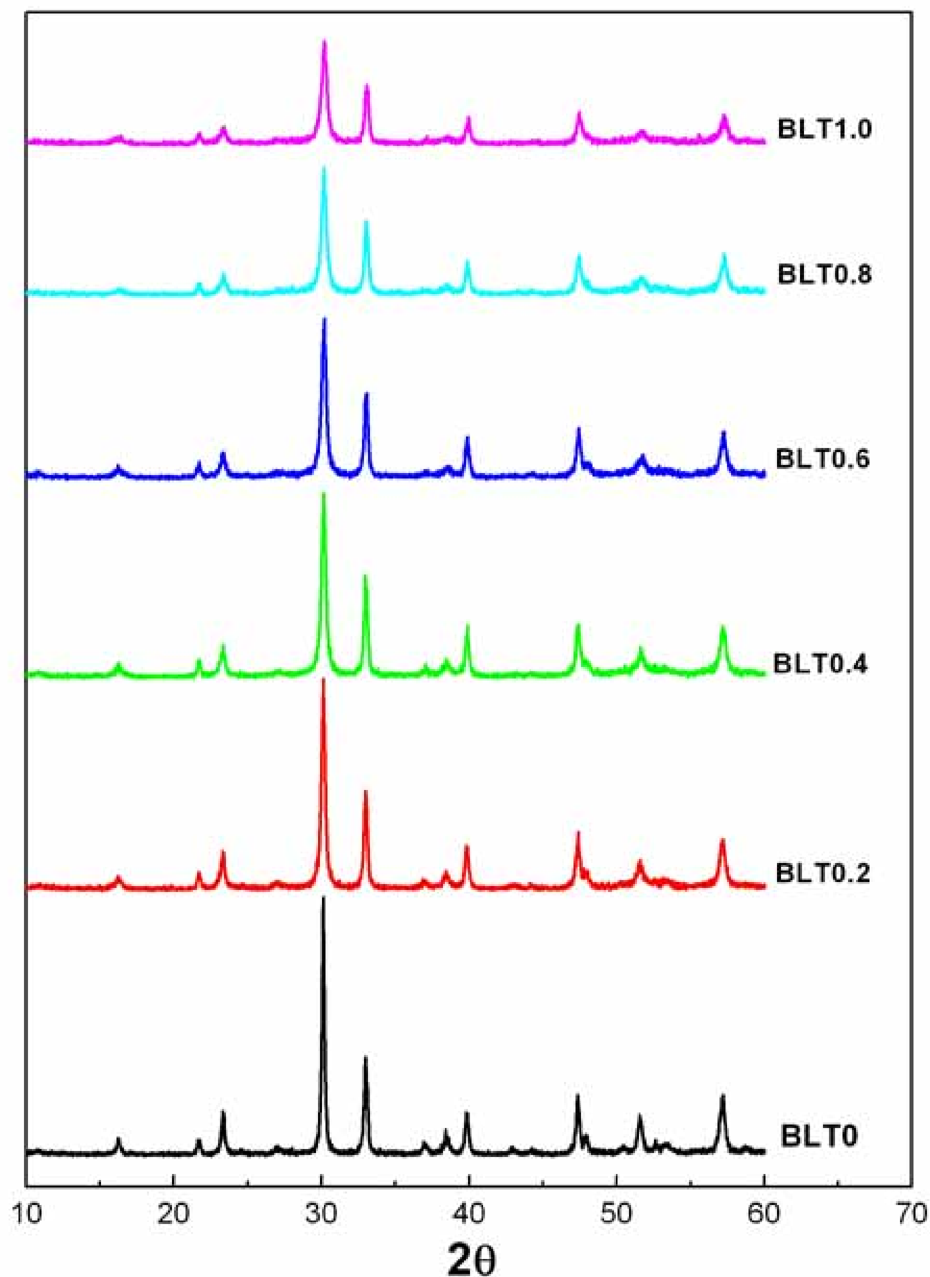

Fig. 2-8 XRD patterns of BLT powders (2# solution) after heated at 600 ^{o}C for 1 hour.

Figure 2-8 shows the XRD patterns of powders obtained from 2# solution after heated at 600 ^{o}C for 1 hour. It is clear that all samples exhibit a single BiT phase, and no second phase was observed. Moreover, with increase of substitute La, the intensity of peaks decreases. This result agrees with the above SEM results that doping of La suppresses the growth of BiT grain. It should be noted that all substituted La would incorporate into the lattice of BiT due to the absence of second phase in XRD patterns.

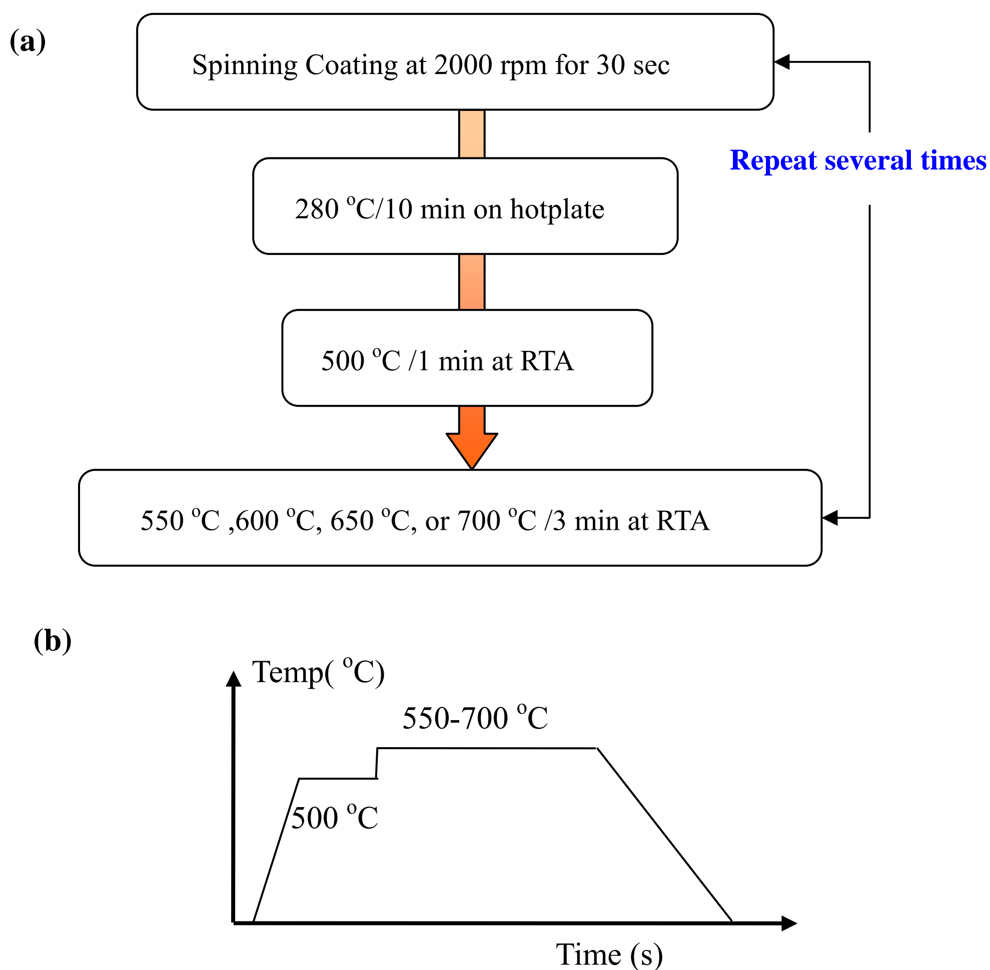

Fig. 2-9 Heat treatment process for precursor solution 2#. (a) whole process, (b) RTA process.

According to the thermal analysis, SEM and XRD results, the heat treatment of films fabricated from precursor solution 2# is decided as shown in Fig. 2-9.

2.2 FABRICATION OF TOP ELECTRODE

For the electrical measurement, the capacitor structure of electrode/film/electrode is needed. The structure of substrate is Pt/TiO_2/SiO/Si, and the top electrode is fabricated in laboratory. First, a Pt top electrode with a thickness of 200nm was deposited using a shadow mask at room temperature, and then one corner of the film was etched by a mix solution of HCl and HF to make the bottom electrode of Pt visible. The schematic illustration of top and cross section of Pt/BiT/Pt capacitor is shown in Fig. 2-10.

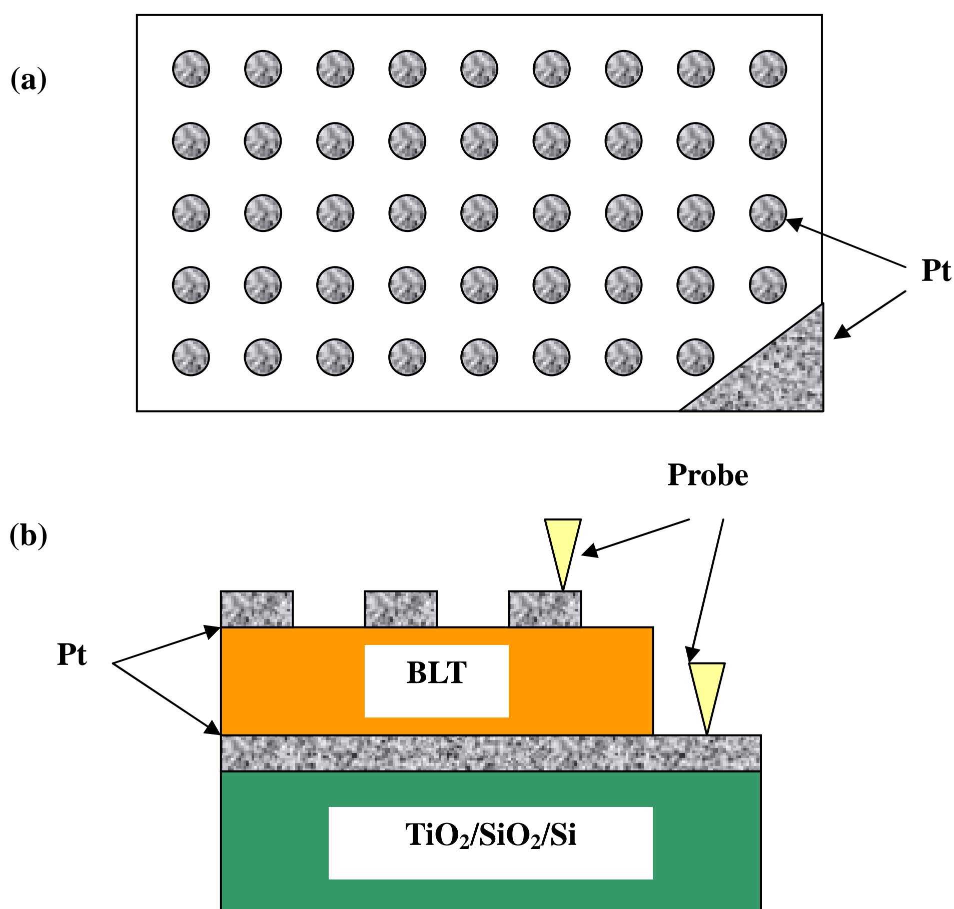

Fig. 2-10 Schematic illustration of ferroelectric capacitor. (a) surface, (b) cross section.

2.3 PHASE AND STRUCTURE CHARACTERISTICS

The crystal structure of BiT-based films are determined by X-ray diffraction (XRD) using a Philips XPert with Cu-K_α as the radiation source. The film morphology was observed using a Jeol JSM-6301F field emission scanning electron microscope (FESEM).

2.4 CHARACTERIZATION OF ELECTRICAL PROPERTIES

2.4.1 Dielectric properties

The dielectric behavior of BiT-based films has been measured by an impedance analyzer (HP4194A). Dielectric permittivity is calculated by the capacity, according to the Eq. 2-1:

$$\varepsilon_r = \frac{Cd}{\varepsilon_0 s} \tag{2-1}$$

where ε_r is dielectric permittivity; C capacity of BiT-based capacitor, s the area of top electrode, ε_0 permittivity of free space (8.85419×10^{-12} F/m), d the thickness of BiT bulk film.

Temperature dependence of dielectric permittivity and loss tangent is also measured using a temperature controller and HP4194A at a rate of 3°C/min from room temperature to 600 °C. To set the connection between the BiT-based films and the impedance analyzer (HP4194A), thin gold wire was used, and the schematic illustration of the connection is shown in Fig. 2-11.

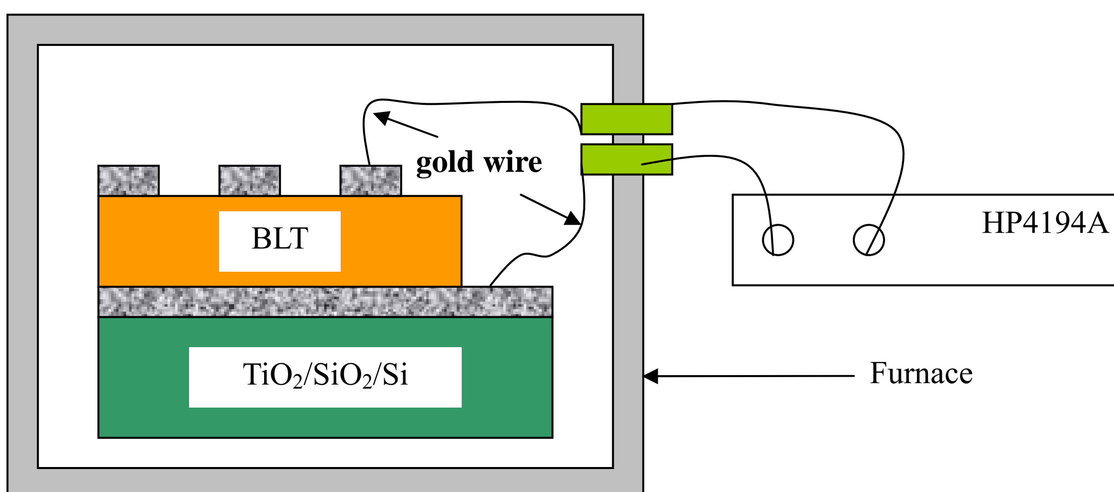

Fig. 2-11 Schematic illustration of the connection between films and HP4194A.

2.4.2 Ferroelectric measurement

The ferroelectric measurements including hysteresis loop and fatigue are carried out using TF analyzer 2000 (aixACCT). The measurement principle of TF analyzer 2000 would be introduced briefly.[7] In TF analyzer 2000 system, feedback method is used to correct data. Fig. 2-12 shows the circuit design in principle.

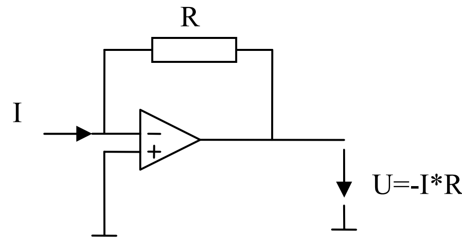

Fig. 2-12 Principle of the feedback method.

2.4.2.1 Dynamic hysteresis measurement (DHM)

In case of triangular voltage excitation, the voltage excitation signal is shown in Fig. 2-13. The prepolarization pulse establishes a defined polarization state, a negative state of relaxed remnant polarization. The prepolarization pulse is followed by three consecutive bipolar excitation signals, each signal is separated by 1 second relaxation time. The corresponding hysteresis loops to the bipolar excitation signal are shown in Fig. 2-14. The hysteresis loop corresponding to pulse no. 1 starts in the negative relaxed remnant polarization state (P_{rrel-}) and turns into the positive saturation ($P_{\max+}$). When the voltage is equal to zero, the polarization reaches to the positive remnant polarization state (P_{r+}), afterwards it turns into the negative saturation ($P_{\max-}$) and back to the remnant polarization state (P_{r-}). This point is normally not equal to the start point (P_{rrel-}), because of the polarization loss over time.

The second loop establishes the sample into the positive remnant polarization state without sampling data. The third loop starts in the positive relaxed remnant polarization state (P_{rrel+}), turns into the negative saturation ($P_{\max-}$), and crosses the polarization axis at zero volts excitation signal in the negative remnant polarization state (P_{r-}). Afterwards the samples is driven into the positive saturation ($P_{\max+}$) and ends in the positive remnant polarization state (P_{r+}) when the voltage is zero. Afterwards the hysteresis loop is balanced respectively to the values P $(+V_{\max})$ and P $(-V_{\max})$. From the data of the parameters V_{c-}, P_{r-} and P_{rrel-} are determined and from the data of the third loop the parameters V_{c+}, P_{r+}, and P_{rrel+} are determined. The closed hysteresis loop is calculated from the second half of the first and the second half of the third loop.

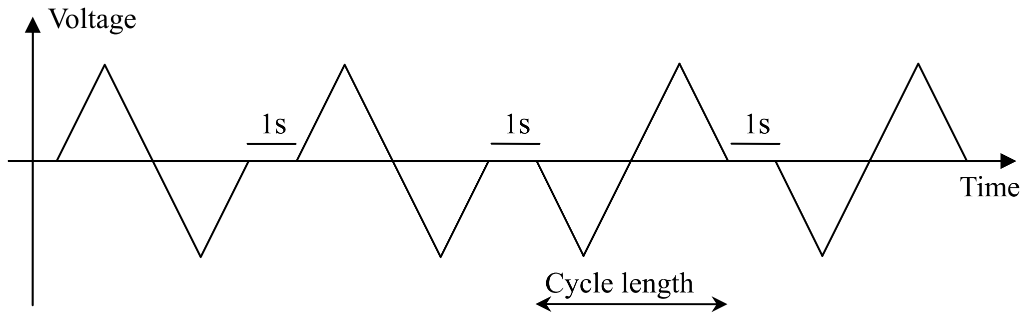

Fig. 2-13 Excitation signal for hysteresis measurement.

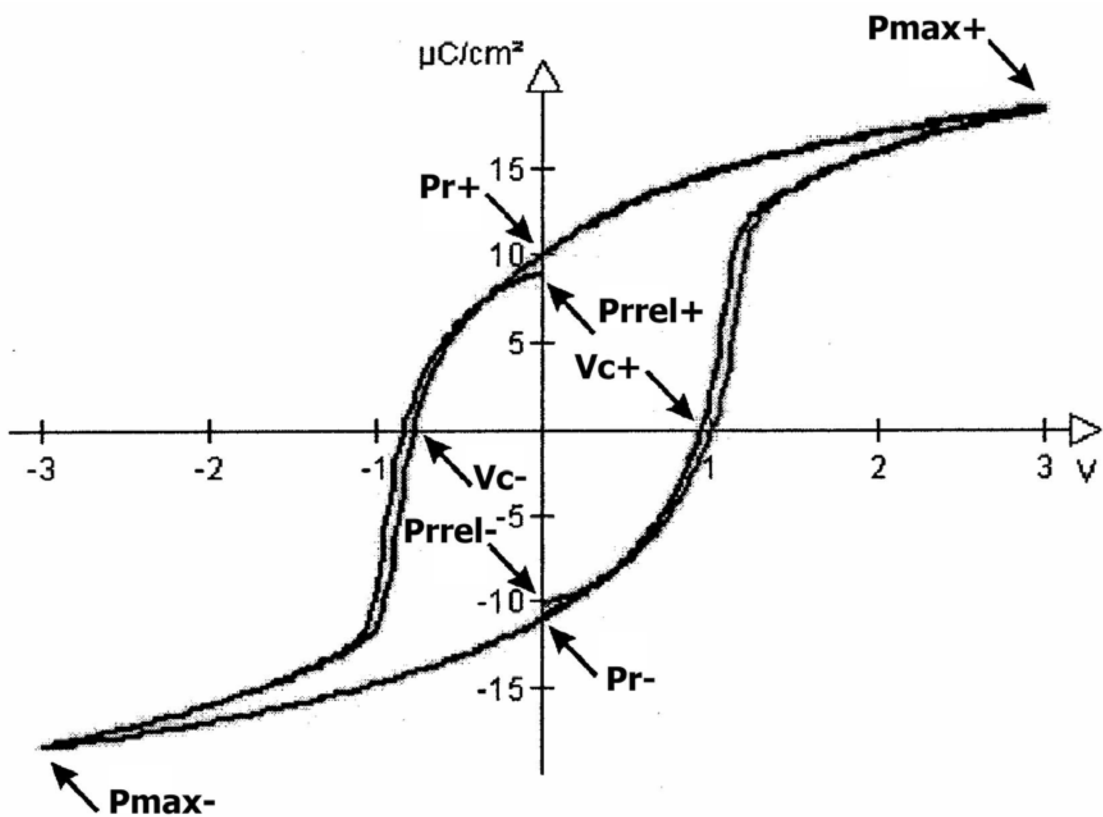

Fig. 2-14 Typical hysteresis measurement graph.

2.4.2.2 Fatigue measurements

A typical result of a fatigue measurement is shown in Fig. 2-15. It displays remnant polarizations of recorded hysteresis loops versus the logarithm of the total number of applied cycles. After measuring an initial hysteresis, the fatigue signal sequence, as shown in Fig. 2-16, is applied to the sample. The fatigue treatment is interrupted regularly for hysteresis measurements. These intermediate hysteresis measurements are performed with time intervals in such way that in a logarithmic plot data points are depicted with an equal spacing.

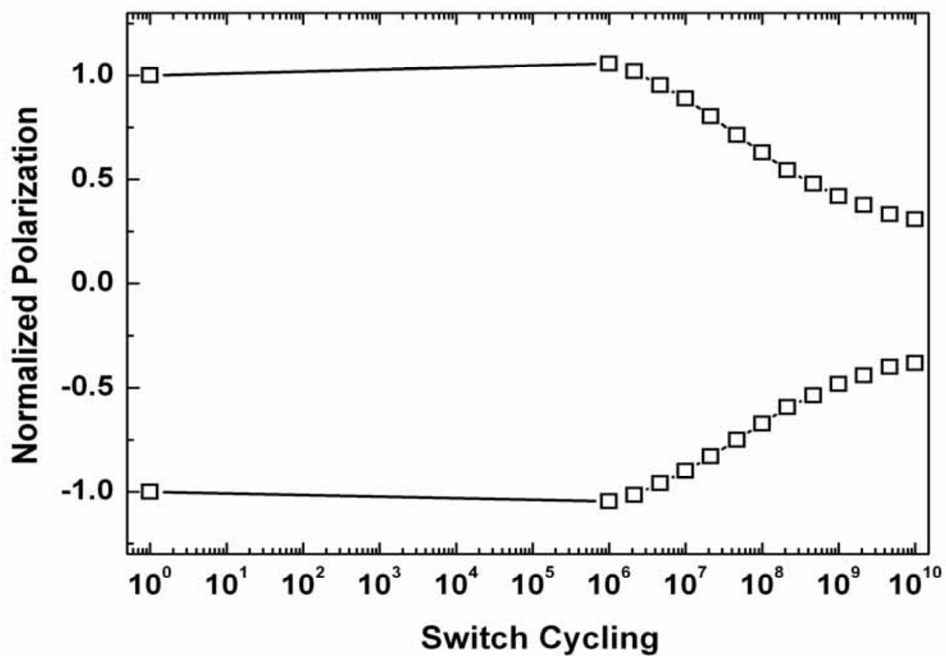

Fig. 2-15 Typical results of a fatigue measurement (remnant polarization vs. log cycles of the excitation signal.

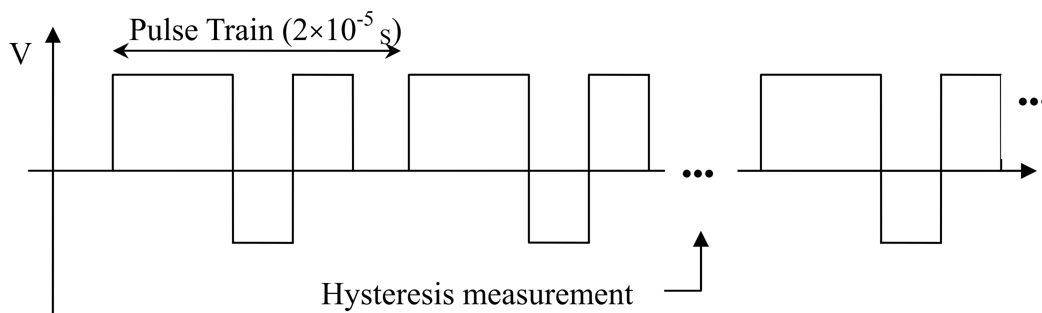

Fig. 2-16 Typical excitation signal for Fatigue measurement.

REFERENCES

[1] S. O. Ryu, W. J. Lee, N. Y. Lee, W. C. Shin, I. K. You, S. M. Cho, S. M. Yoon, B. G. Yu, J. K. Koo, and J. D. Kim, *Jpn. J. Appl. Phys.*, **42**, 1665 (2003).
[2] T. Kijima, Y. Fujisaki, and H. Ishiwara, *Jpn. J. Appl. Phys.*, **40**, 2977 (2001).
[3] W. S. Yang, N. K. Kim, S. J. Yeom, S. Y. Kweon, E. S. Choi and J. S. Roh, Jpn. *J. Appl. Phys.*, **40**, 5569 (2001).
[4] D. Wu, A. Li, T. Zhu, Z. Li, Z. Liu, and N. Ming, *J. Mater. Res.*, **16**, 1325 (2001).
[5] Y. Kan, X. Jin, G. Zhang, P. Wang, Y. Cheng, and D. Yan, *J. Mater. Chem.*, **14**, 3566 (2004).
[6] P. H. Xiang, Y. Kinemuchi, K. Watari, *Mater. Lett.*, **60**, 2837 (2006).
[7] TF analyzer 2000 measurement system, operating manual, aixACCT.

Chapter 3

Fabrication and Characterization of $Bi_{3.25}La_{0.75}Ti_3O_{12}$ Films

In this chapter, $Bi_{3.25}La_{0.75}Ti_3O_{12}$ (BLT) thin films were prepared using a chemical solution deposition technique. Commercially available BLT precursor solutions purchased from Toshima Co., Japan, were used for experiment in this chapter. The films were fabricated at 600 °C, 700 °C and 800 °C, respectively. The effect of annealing temperature on the ferroelectric and dielectric properties was studied. Several dielectric relaxations were found in $Bi_{3.25}La_{0.75}Ti_3O_{12}$ thin films, which may be attributed to the defect-related dielectric relaxation. The mechanism of the observed dielectric relaxation is proposed.

3.1 INTRODUCTION

As a well known bismuth-layered ferroelectrics for non-volatile ferroelectric random access memory (NVFeRAM) applications, $Bi_4Ti_3O_{12}$ (BiT)-based ferroelectric films, especially La doped BiT-based films attract extensive interests, since their high remnant polarization, excellent fatigue characteristics, and relatively low processing temperature.[1-5] However, thin films and ceramics of BLT often suffer from large leakage current and imprint properties which have been reported to be closely related to point defects.[6] Meanwhile, point defects often act as pinning sites of domain motion, resulting in low values of remnant polarization (P_r) of BLT film, as low as 7.5 μC/cm^2, which extensively limit the practical application of these ferroelectric materials.[7,8] Therefore, many researchers are focusing on improving the properties of these kinds of ferroelectric materials by methods such as incorporating excess bismuth; doping nitrogen, vanadium, or tungsten into titanium site, to obtain large P_r, low coercive field(E_c) or good fatigue properties for application of NVFeRAM.[9,10] Irie *et al.*[13] reported that nitrogen substitute enhances P_r, and at the same time reduces the coercive field (E_c). However, it brought large leakage current and worse fatigue properties.[11,12] It is believed that the incorporation of substitutes could control these defects in these ferroelectric materials.[14] Due to the strong relationship between defect and ferroelectric properties, such as P_r, leakage current, E_c and fatigue properties, extensive studies on defects in BLT-related ferroelectric film using in NVFeRAM application is desirable. Recently, several works examined by dielectric relaxation

phenomena to investigate defects, such as space charge of electrons and oxygen vacancies.[13,14] However, the investigation on defects, which has been reported to relate with the fatigue behavior, is still few.[15] In this chapter, $Bi_{3.25}La_{0.75}Ti_3O_{12}$ fabricated by solution 1# was investigated. To identify the potential defects in this ferroelectric films, temperature dependence of dielectric permittivity and loss tangent was studied.

3.2 FABRICATION AND MEASUREMENT OF $Bi_{3.25}La_{0.75}Ti_3O_{12}$ (BLT) FILMS

The films investigated in this chapter were fabricated by the precursor solution purchased from Toshima Co., Japan. As mentioned in chapter 2, $Bi_{3.25}La_{0.75}Ti_3O_{12}$ thin films were deposited on the substrate with a structure of Pt(111)(200 nm)/Ti(5nm)SiO_2(600nm)/Si by spin coating at a speed of 3000 rpm for 30 s. After depositing, the films were first dried at 100 ^oC for 10 min and then heated at 400 ^oC for 5 min. These two steps are all carried out on a hotplate. The above processing was repeated several times to obtain a desired thickness. Finally, the films were annealed for 30 min at 600, 700, 800 ^oC (hereafter abbreviated as BLT600, BLT700, and BLT800, respectively,). The annealed films were about 800 nm in thickness. For dielectric measurement, a Pt top electrode with a diameter of 0.64 mm was deposited at room temperature using a shadow mask. Dielectric measurements were carried out at the temperatures from room temperature to 600 ^oC at a rate of 3 ^oC/min using a temperature controller and LCR meter (HP 4194A) with an applied voltage of 0.05 V. For ferroelectric measurement, a Pt top electrode with a diameter of 0.1 mm was deposited at room temperature. The measurement was carried out using TF analyzer 2000 (aixACCT).

3.3 PHASE CHARACTERISTICS AND MORPHOLOGY OF BLT FILMS

3.3.1 X-ray diffraction (XRD) results

As shown in Fig. 3-1, all samples exhibit a well-crystallized phase, and no secondary phase was observed. It should be noted that all prepared films showed the same random orientation within experimental error.

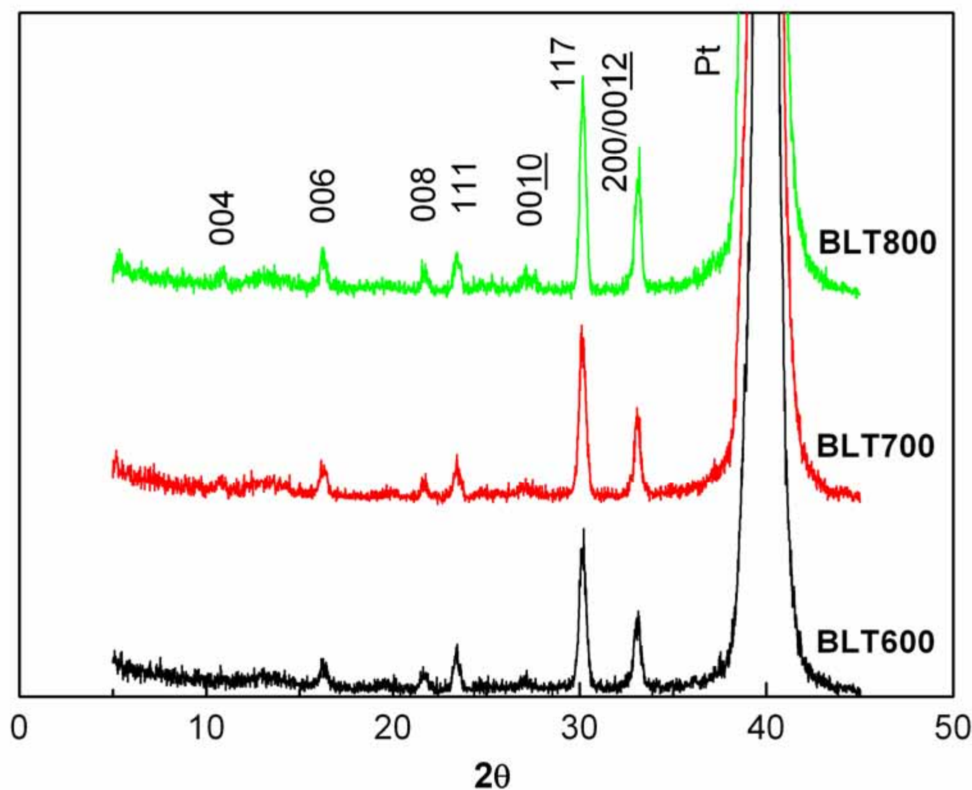

Fig. 3-1 XRD patterns of BLT600, BLT700 and BLT800.

3.3.2 Surface morphology

Surface morphologies of BLT films annealed at various temperatures were observeded by scanning electron microscopy (SEM). Figure 3-2 shows SEM micrographs of BLT600, BLT700 and BLT800 films, respectively. It can be seen that all films consist of rodlike grains. BLT600 exhibits the grains with 30-40 nm, and BLT700 and BLT800 exhibit the grains with 100-130 nm. With the increase of annealing temperature, the grain size of BLT increases.

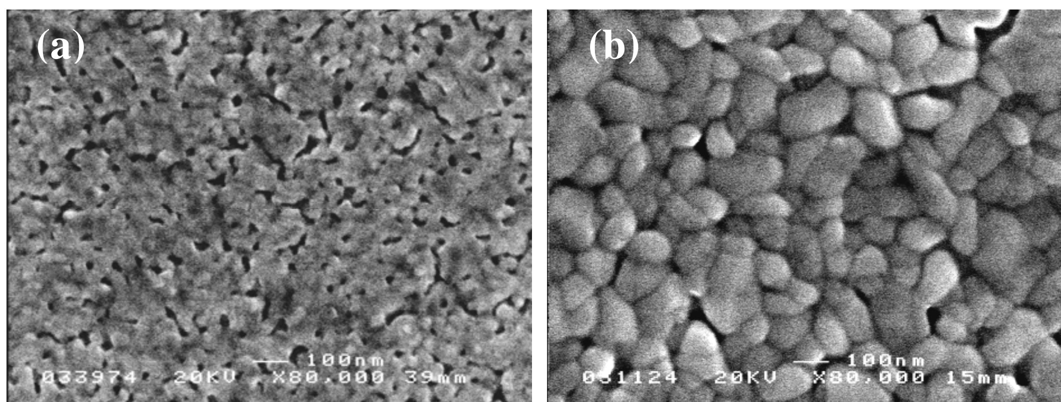

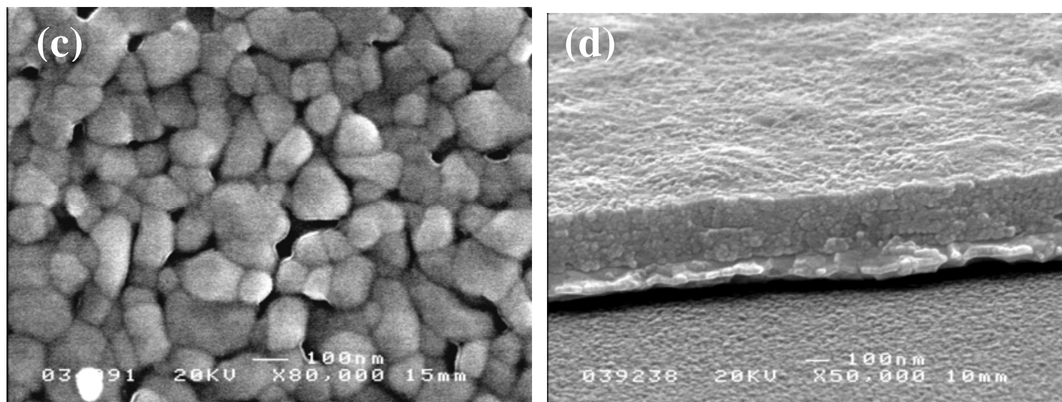

Fig. 3-2 SEM micrographs of (a)BLT600, (b)BLT700, (c) BLT800 and (d) cross section.

It is well known in ferroelectric thin films that larger grains lead to large remnant polarization, which is favorable to NVFeRAM application.

3.4 ELECTRIC PROPERTIES

3.4.1 Hysteresis loop

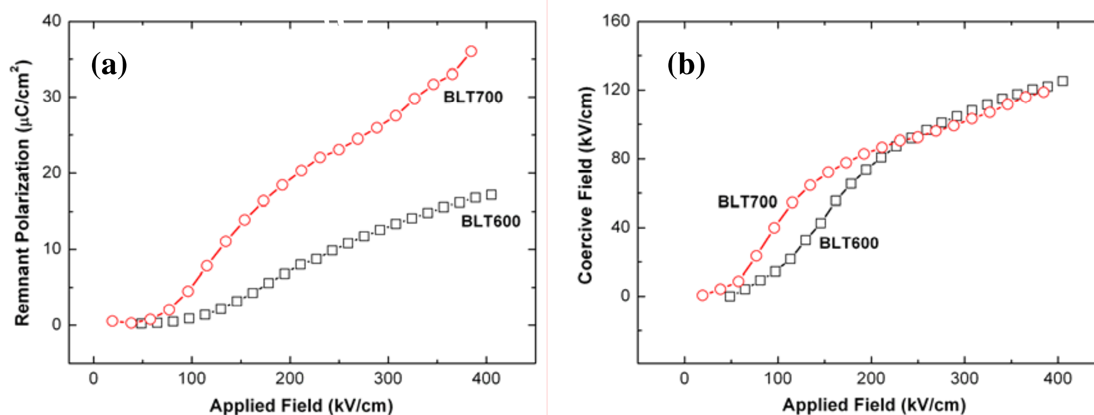

Fig. 3-3 Remnant polarization (P_r) (a) and coercive field (E_c) (b) as function of applied field for BLT600 and BLT700 thin films.

Figure 3-3 displays the field dependence of remnant polarization (P_r) and coercive field (E_c). It is clear that BLT700 exhibits higher Pr than that of BLT600, which agrees with the SEM results that BLT700 shows larger grain size than BLT600. However, the coercive fields of BLT600 and BLT700 are similar.

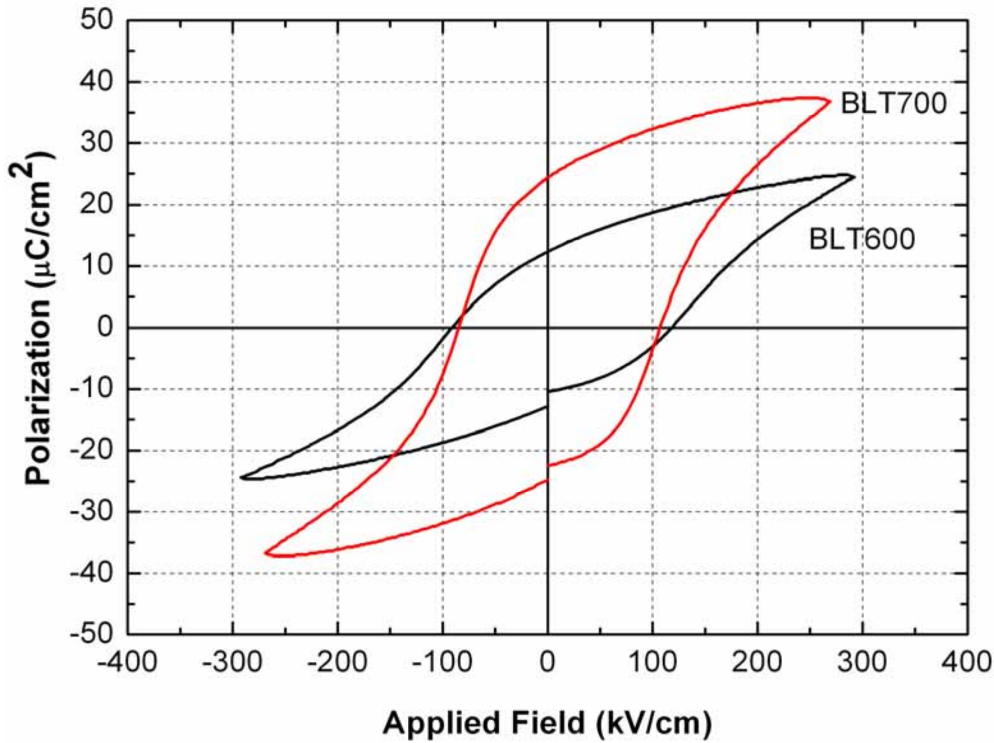

Fig. 3-4 P-E hysteresis loops of BLT600 and BLT700 thin films.

P-E hysteresis loops of BLT600 and BLT700 at applied field 300 kV/cm are shown in Fig.3-4. The P_r and E_c value of BLT600 and BLT700 are 12.6 μC/cm^2, 104.7 kV/cm; 24.5 μC/cm^2, 96.0 kV/cm, respectively. Since the large leakage current of BLT800, ferroelectric property was failed to be measured.

3.4.2 Dielectric relaxation

3.4.2.1 Dielectric behavior in temperature range of 25 ^{o}C–600 ^{o}C

Figure 3-5 shows the temperature (*T*) dependence of the dielectric permittivity (ε') for BLT600. Two peaks are observed at around 400 ^{o}C and 500 ^{o}C, which we designate as Mode 1 and Mode 2, respectively. Moreover, a slight peak appears in the low-temperature side of Mode 2 at high frequencies which is signified in Fig. 3-5(a) with "?", however, due to the large amount of noise in this temperature range, we could not confirm its existence.

There has been only one report on the observation of Mode 1 in $Bi_4Ti_3O_{12}$ ceramics. [16] The appearance temperature range in Ref.16 is a little higher than that of mode 1 in Fig.3-5, which may be attributed to the difference in composition between their ceramics ($Bi_4Ti_3O_{12}$) and our thin film ($Bi_{3.25}La_{0.75}Ti_3O_{12}$). Mode 1 in $Bi_4Ti_3O_{12}$ ceramics exhibit strong diffusion, and it is difficult to distinguish it from other peaks. In

BLT films, Mode 1 is well separated, and it also shows strong frequency dependency. Additionally, it was found that Mode 1 almost disappears at frequencies higher than 10^5 Hz. This result demonstrates that it is related to a low frequency relaxation process.

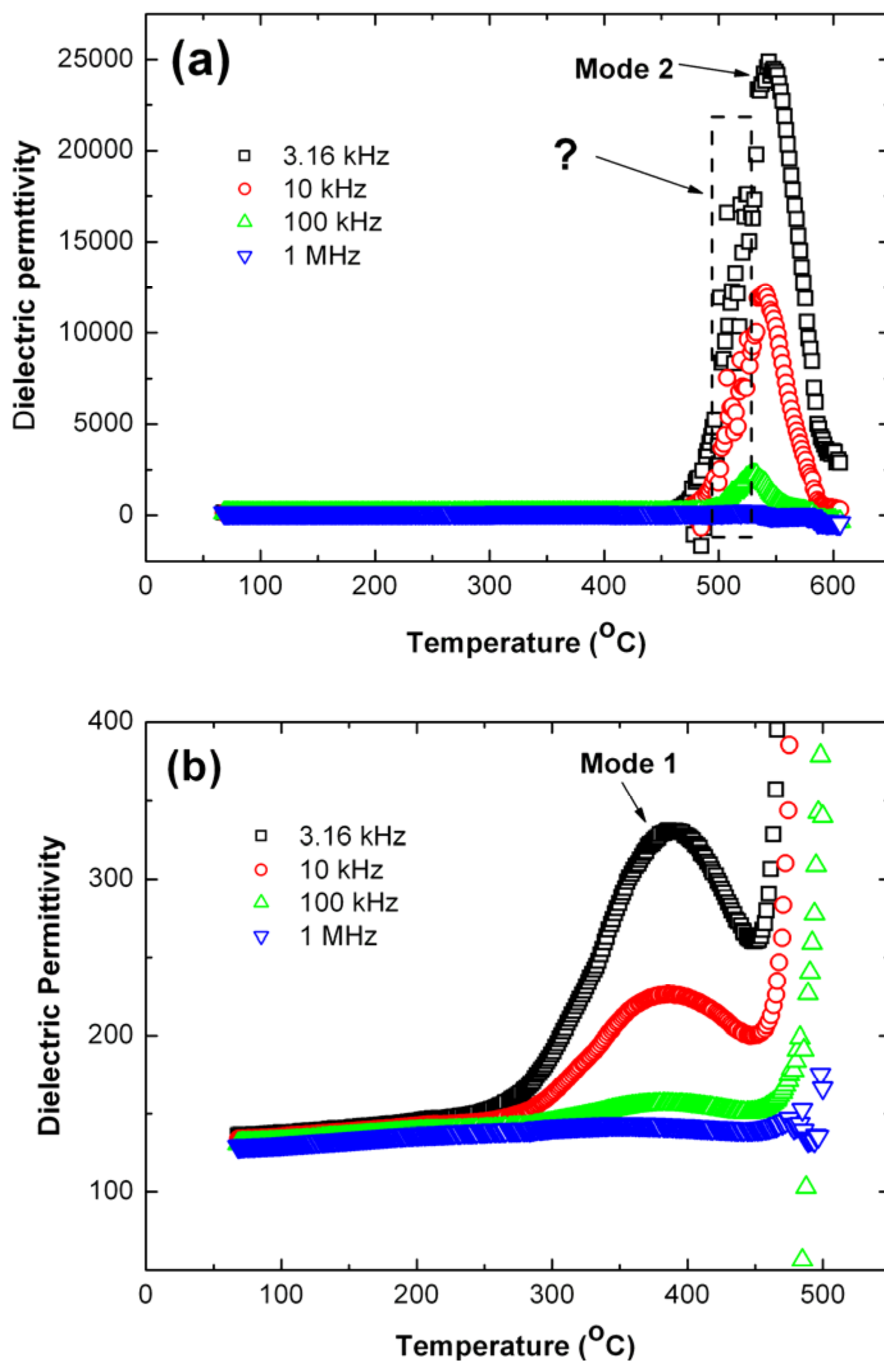

Fig. 3-5 Temperature dependence (T) of ε' for BLT600 (a) and enlarged figure (b).

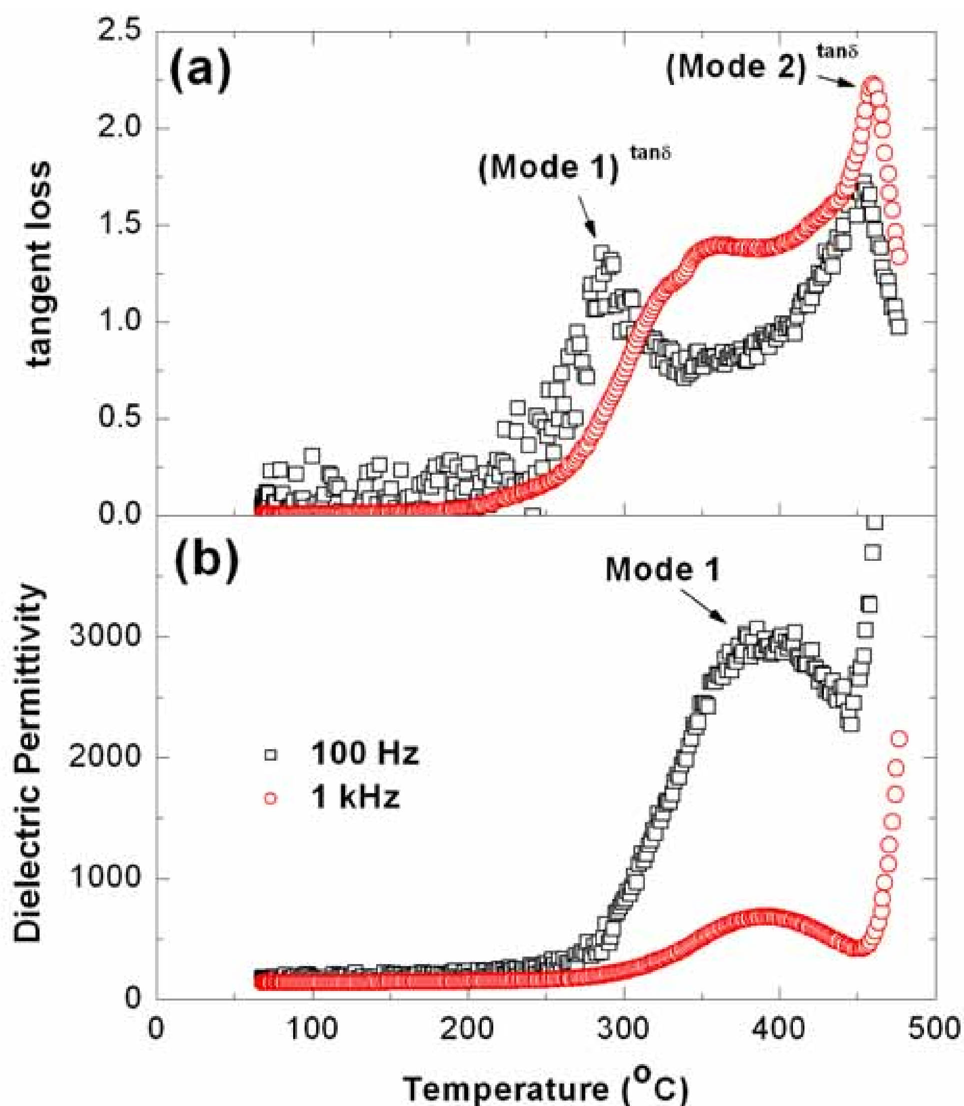

Fig. 3-6 Temperature dependence (T) of tanδ (a) and ε' (b) for BLT600.

There have been several reports on the observation of Mode 2 both in single crystals and in ceramics.[16,17] However, this is the first time to find it in ferroelectric film. The two characteristics of this mode are: (1) Strongly frequency dependence in dielectric permittivity (as shown in Fig. 3-5(a), magnitudes of Mode 2 decrease markedly when frequency increases); (2) Appears around 500 ^{o}C. It should be noted that the peak temperature of Mode 2 exhibits slight dependency on the composition of BiT-based materials. All the reported temperatures of Mode 2 were around 500 ^{o}C, including for pure BiT single crystal,[17] and for Nd-doped BiT ceramics.[16] However, Mode 2 found in BLT600 thin film exhibits negative frequency dispersion, which means that the temperatures where Mode 2 decreases with increasing frequency. This is in

contrast to previously reported results in a single crystal that Mode 2 showed positive frequency dispersion characteristics.[17]

Temperature dependence (*T*) of the dissipation factor (tan δ) for BLT600 is shown in Fig. 3-6(a). Due to the high conductivity at temperatures higher than 500 °C, the value of tan δ is extensively high, so we only show the results in the temperature range from 25 °C to 500 °C. Two tan δ peaks are also found, which are called as $(\text{Mode 1})^{\tan\delta}$ and $(\text{Mode 2})^{\tan\delta}$ hereafter.

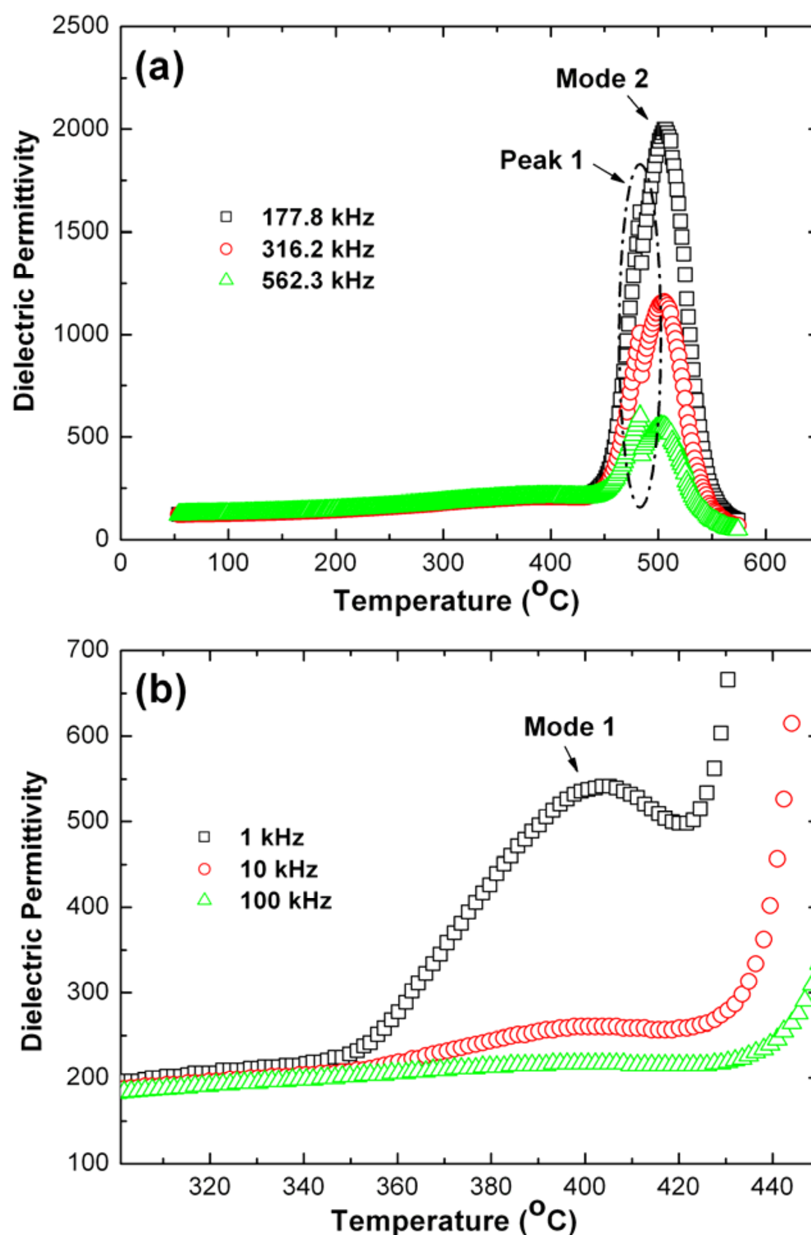

Fig. 3-7 Temperature dependence (*T*) of ε' for BLT700 (a) and enlarged figure (b).

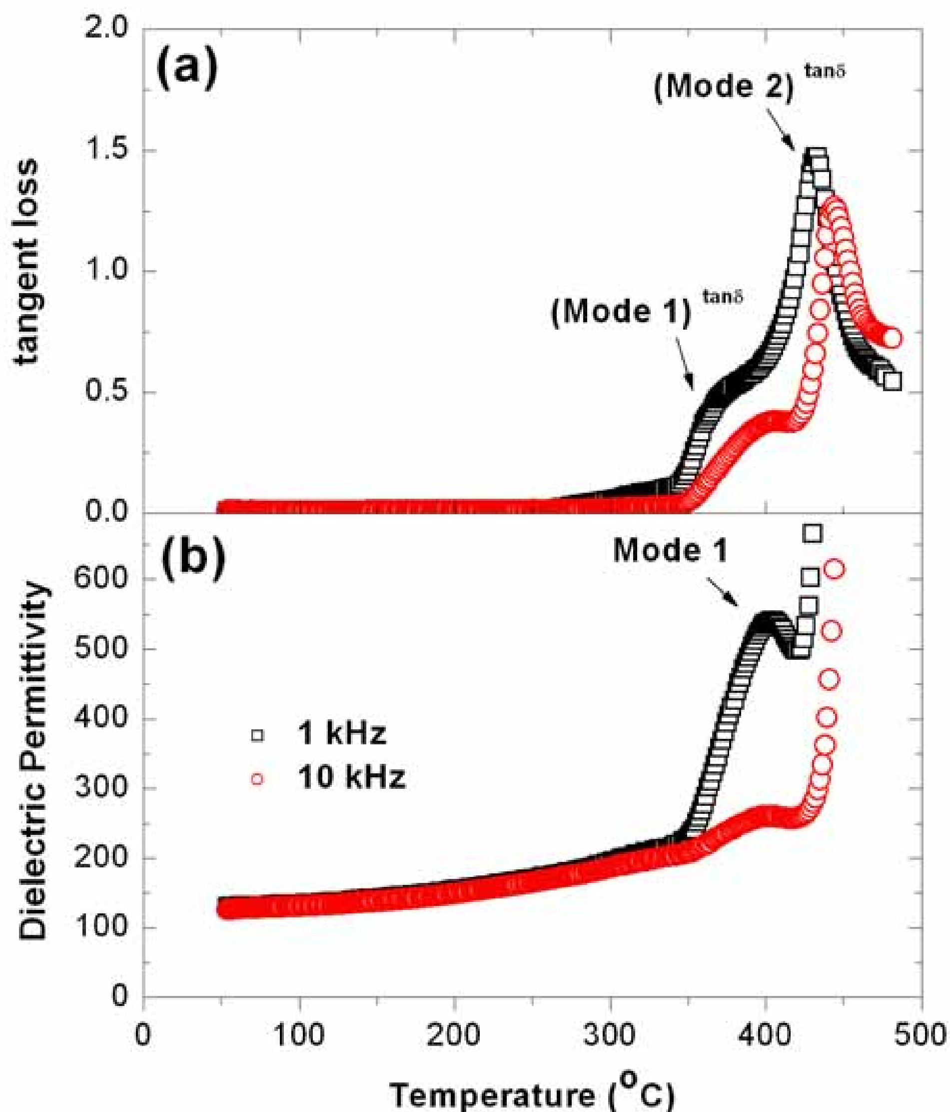

Fig. 3-8 Temperature dependence (*T*) of tanδ (a) and ε' (b) for BLT700.

Dielectric measurements were also carried out on BLT700 and BLT800. As shown in Fig. 3-7,8, BLT700 exhibits similar characteristics to BLT600, on the permittivity curve: (1) An extensive high peak around 500 °C (Mode 2); (2) A broad peak around 400 °C (Mode 1), on the tanδ curve (two anomalies ((Mode 1)$^{\tan\delta}$ and (Mode 2)$^{\tan\delta}$) appear in the temperature range of 25 °C–500 °C); (3) On the low temperature side of Mode 2, a sharp peak (@483 °C) is found at high frequencies, which does not exhibit any frequency dispersion (abbreviated as Peak 1, hereafter), and agrees with the one found in a BLT600 film.

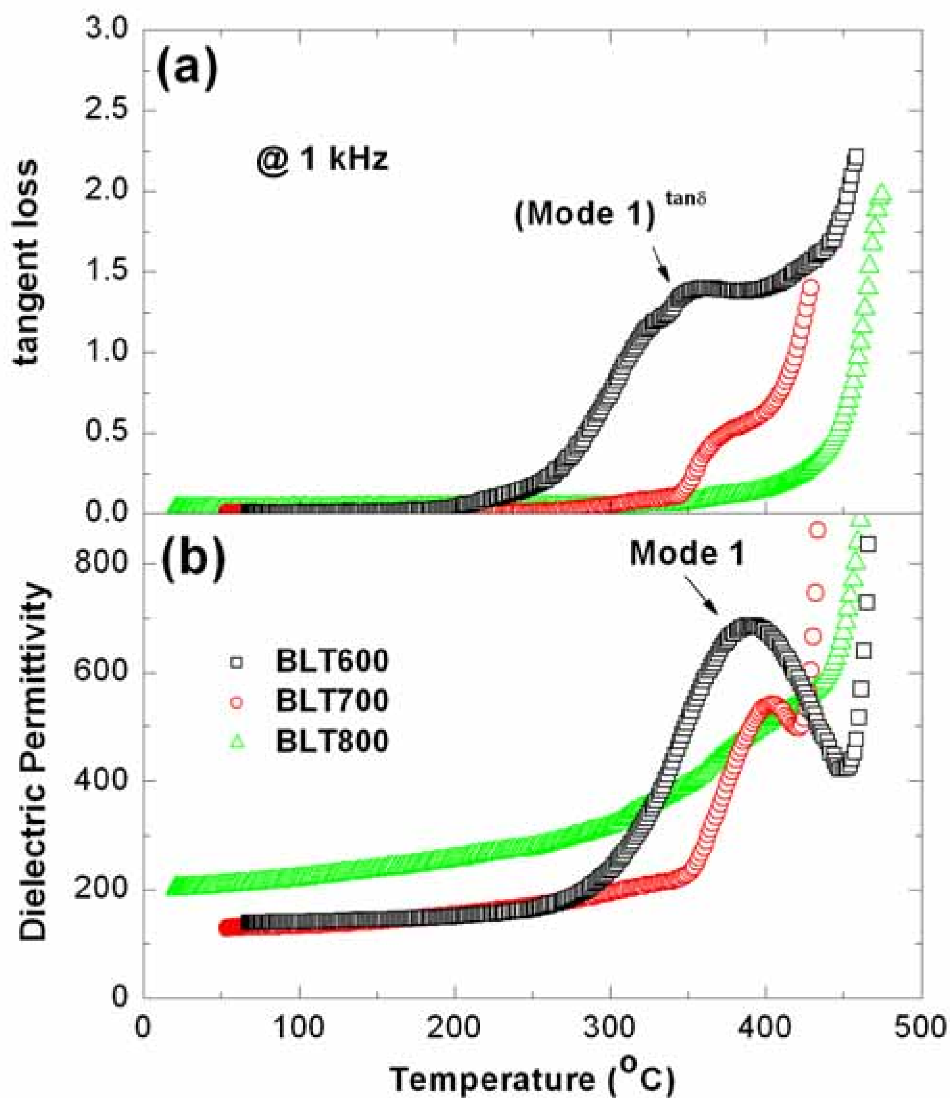

Fig. 3-9 Temperature dependence (*T*) of tanδ (a) and ε' (a) for BLT600, BLT700 and BLT800 at 1 kHz.

After comparing the results of BLT600, BLT700, and BLT800, it was found that annealing temperature plays an important role in Mode 1 and (Mode 1)$^{\tan\delta}$. Figure 3-9 shows the results of BLT600, BLT700, and BLT 800 at 1 kHz. It indicates that both Mode 1 and (Mode 1)$^{\tan\delta}$ decrease with increasing annealing temperature, and finally they disappear in BLT800. On the other hand, Mode 2, (Mode 2)$^{\tan\delta}$, and Peak 1 show a slight dependence on annealing temperature.

3.4.2.2 Influence of annealing on dielectric behavior

Further annealing treatment was carried out on BLT600. BLT600 was first annealed in oxygen (O_2) atmosphere at 600 °C for 24 hours (abbreviated as BLT600-O_2), and then annealed in nitrogen (N_2) atmosphere at 600 °C for another 24 hours (abbreviated as BLT600-O_2-N_2). After each annealing, dielectric measurement was conducted. It was found that annealing in oxygen atmosphere decreases the value of tanδ markedly, and an expected result was obtained in the whole measurement temperature range of 25 °C–600 °C. Interestingly, Peak 1 remains unchanged under all annealing treatments, while Mode 1, $(\text{Mode 1})^{\tan\delta}$ and Mode 2 show several changes after post-annealing treatment. Another new mode (Mode 3) at low temperature (250 °C) was appeared after post-annealing treatment.

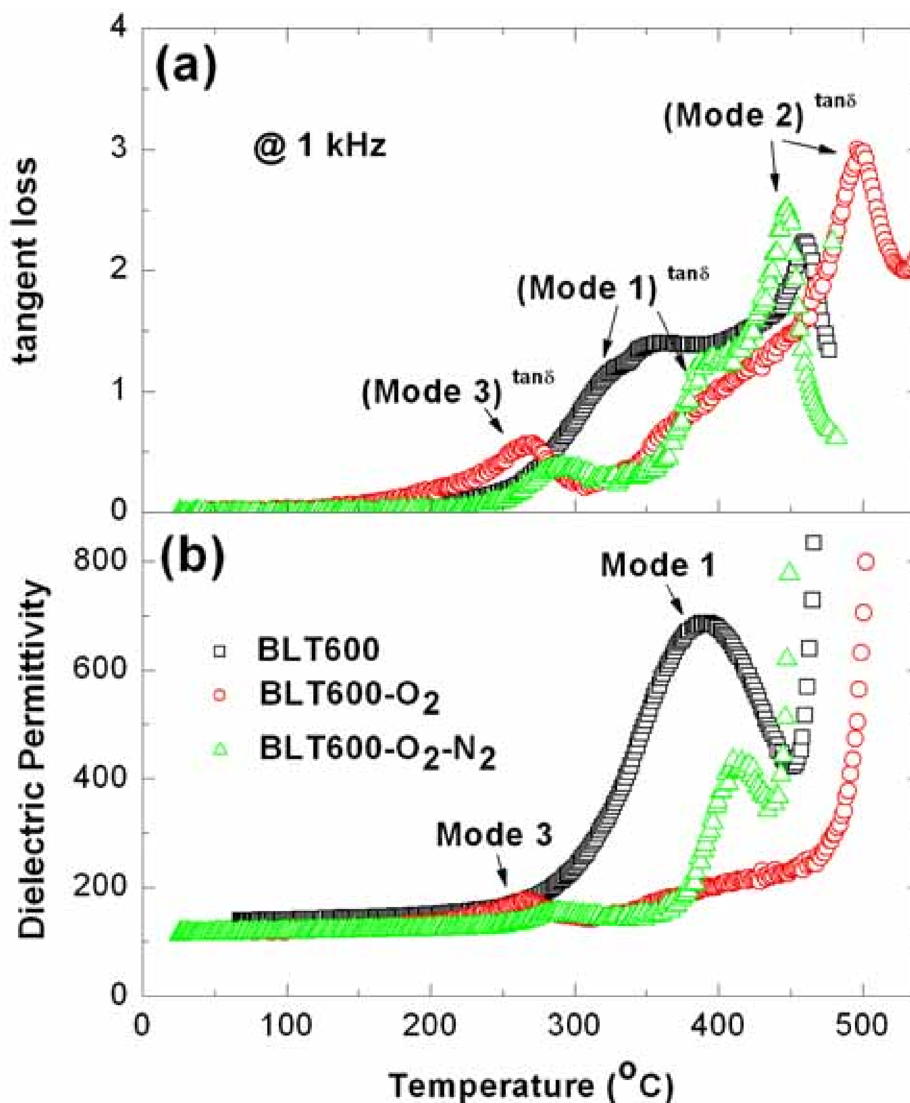

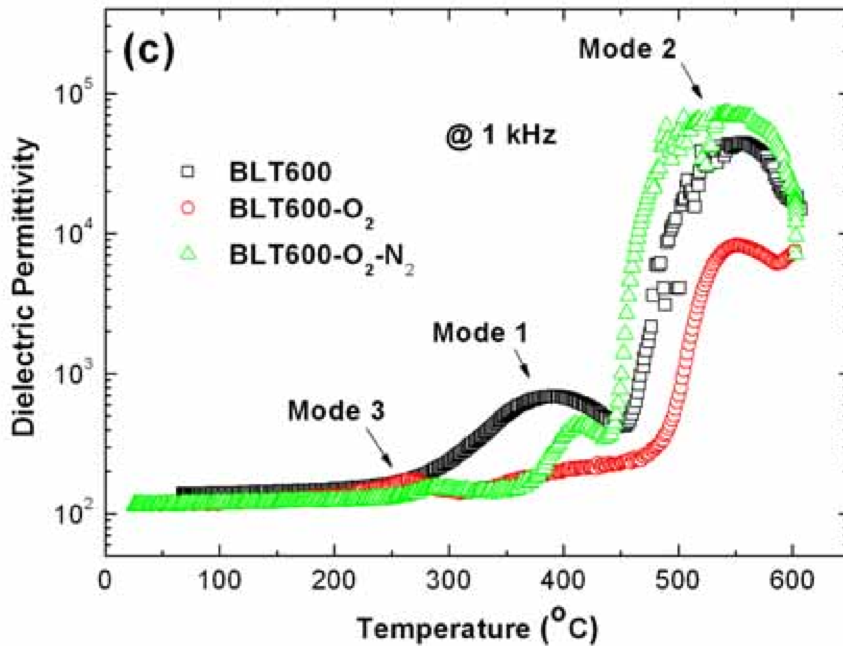

Fig.3-10 Temperature dependence of dielectric properties under different annealing conditions at 1kHz. tan δ Vs T (a), ε' Vs T (b), and log ε' Vs T (c).

(1) Mode 1 and (Mode 1)$^{\tan\delta}$

As shown in Fig. 3-10(b), annealing in oxygen atmosphere made Mode 1 and (Mode 1)$^{\tan\delta}$ disappear, and subsequent annealing in nitrogen atmosphere induced them again, suggesting that the Mode 1 and (Mode 1)$^{\tan\delta}$ are closely related to the oxygen vacancies.

(2) Mode 2

Figure 3-10(c) shows the dielectric permittivity at 1 kHz of BLT600, BLT600-O_2 and BLT600-O_2-N_2 at various temperatures in a semilogarithmic scale. After annealing in oxygen atmosphere, the intensity of Mode 2 decreases, and after annealing in nitrogen atmosphere, it increases again. Taking the maximum permittivity ($\varepsilon'_{\max}$) of Mode 2 (@ 1kHz) as an example, $\varepsilon'_{\max}$ of BLT600 was about 4.4×10^5, and it decreased to 8.2×10^3 after oxygen annealing, and in the end it increased up to 7.0×10^5 after nitrogen annealing.

(3) Mode 3

At around 250 °C, a new dielectric peak (Mode 3) was appeared both after the first annealing (in oxygen atmosphere) and after the second annealing (in nitrogen

atmosphere). The induced Mode was weak, and the peak was somewhat broad.

3.4.2.3 Ac electric conductivity propertiesΩ

Figure 3-11 shows the temperature dependence (*T*) of ac conductivity of BLT600. It was found that conductivity increases markedly, at temperatures higher than 450 °C, and two slopes were found at (300–450 °C) and (450–600 °C), respectively.

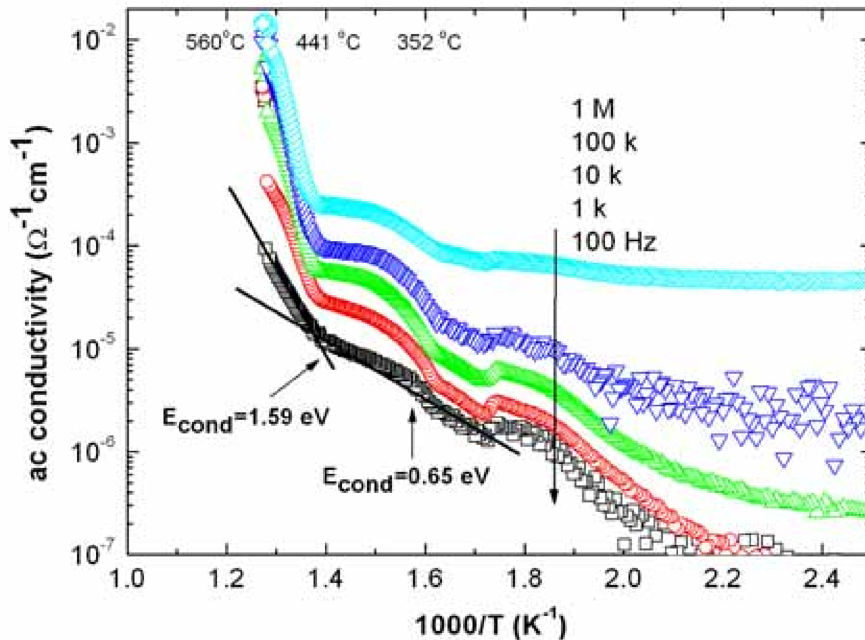

Fig. 3-11 Temperature dependence of ac conductivity of BLT600.

3.4.2.4 Discussion of the mechanisms

Review of reported dielectric anomaly in $Bi_4Ti_3O_{12}$ ferroelectric system

(1) Mode around 250 °C

Shulman et.al observed this mode in $Bi_4Ti_3O_{12}$ and $Bi_{3.26}Nd_{0.74}Ti_3O_{12}$ ceramics,[16] and they attributed it to an oxygen-ion-jump mechanism. Most recently, Li *et al.*[9] investigated this mode in pure $Bi_4Ti_3O_{12}$ ceramics, and they attributed it to short-range diffusion of oxygen ions via vacancies.

(2) Mode around 350 °C

In pure $Bi_4Ti_3O_{12}$ and $Bi_{3.26}Nd_{0.74}Ti_3O_{12}$ ceramics, a broad slope was first found (Fig. 3–5,9 in reference 16). To our knowledge, no detailed investigation on this mode has been reported.

(3) Curie temperature at 449 °C

Recently, Kan *et al.* [18] has reported that the Curie temperature of $Bi_{3.25}La_{0.75}Ti_3O_{12}$ ceramics is 449 °C. The corresponding peak was sharp, and the

permittivity was about 700–900 at frequencies from 100 kHz to 1MHz (see Fig. 6 in Ref. 18).

(4) Mode around 500 ^oC

There have been several reports on this mode, and Fouskova and Cross found this anomaly in a pure $Bi_4Ti_3O_{12}$ single crystal, and they attributed it to a space charge.[16]

Dielectric anomalies in this work

As can be seen in the above review of dielectric anomalies in this material, $Bi_4Ti_3O_{12}$-based ferroelectrics exhibit complex dielectric behavior. However, due to the different measurement temperatures and different compositions of investigated $Bi_4Ti_3O_{12}$-based ferroelectrics, the dielectric behavior of $Bi_4Ti_3O_{12}$-related ferroelectric is still ambiguous. In current study, all the reported dielectric anomalies were observed, which gives a chance to distinguish and clarify these relaxation anomalies.

To find out the mechanism of each mode, it is necessary to find the corresponding modes in the permittivity and dissipation factor curves at first. Four sets of anomalies are clarified in this experiment, and the mechanisms are also shown in Tab. 3-1. The details of analysis are presented in following sections.

Tab. 3-1. Dielectric anomalies observed in this work.

Temperature range	*～250 ^oC*	*～400 ^oC*	*483 ^oC*	*～500 ^oC*
Anomaly	Mode 3	Mode 1 and $(\text{Mode1})^{\tan\delta}$	Peak 1	Mode 2 and $(\text{Mode2})^{\tan\delta}$
Mechanism	V_O and V_{Bi}	$V_O^{\bullet}$	Ferroelectric-paraelectric phase transition	Space charge related to $V_O^{\bullet\bullet}$

(1) ～250 ^oC: Mode 3

Mode 3 is an induced dielectric anomaly in this study. Similar to Mode 1 and Mode 2, it also exhibits strong frequency dependence. Additionally, it is unobserved at frequencies higher than 10^5 Hz. It has been proposed that this is related to oxygen vacancies, due to the change of intensity of this mode after oxygen or reduced annealing (see Fig. 3 in Li's work [19]). However, it does not account for our result here that it appears after oxygen or reduced annealing. Therefore, I proposed that bismuth vacancies as well as oxygen vacancies contribute to this mode. It is expected that a large amount of bismuth vacancies are formed regardless of oxygen or reduced annealing, and this has been confirmed by degradation of ferroelectric properties after annealing.

(2) ~400 °C: Mode 1

Figure 3-8(a), 3-9(a), and 3-10(a) show that the $(\text{Mode1})^{\tan\delta}$ peak occurs at the temperature where ε' exhibits the highest increase speed in Mode 1, which is a well-known characteristics of corresponding ε' and tanδ mode. Additionally, Mode1 and $(\text{Mode1})^{\tan\delta}$ show the same change when annealing temperature increases or post annealing is conducted in oxygen or nitrogen atmosphere, as shown in Fig. 3-9 and 3-10. Therefore, we considered that Mode1 and $(\text{Mode1})^{\tan\delta}$ are corresponding and they are attributed to the same mechanism.

Since Mode 1 could be eliminated by oxygen annealing and be induced again by nitrogen annealing, it is reasonable to believe that this mode is closely related to oxygen vacancy. Moreover, this mode can be greatly suppressed and finally eliminated by high annealing temperature, as shown in Fig. 3-9. This result indicates that Mode 1 is related to oxygen vacancies.

It is well known that oxygen vacancies can be formed annealing process due to the escape of oxygen from the lattice at low oxygen partial pressure, and it is expected that the higher the annealing temperature, the larger amount of $V_O^{\bullet\bullet}$. Therefore, the dielectric anomaly related to $V_O^{\bullet\bullet}$ should be enhanced by higher annealing temperature, which is contrary to our findings that Mode 1 is suppressed by higher annealing temperature (700 °C) and finally eliminated by highest annealing temperature (800 °C), shown in Fig. 3-9. Therefore, the possibility that Mode 1 only relates to double-ionized oxygen vacancy ($V_O^{\bullet\bullet}$) can be excluded.

We considered two possible mechanisms of Mode 1:

(1) Dipole formed by $V_O^{\bullet\bullet}$ and a defect that could be suppressed by high annealing temperature.

Another potential defect in BiT is bismuth vacancy V_{Bi}''', however, it is expected that the amount of bismuth vacancy V_{Bi}''' would increase with annealing temperature. So far, this defect has not been identified.

(2) Single-ionized oxygen vacancy $V_O^{\bullet}$.

Here, we found that the mechanism of Mode 1 could be explained by $V_O^{\bullet}$. After oxygen escapes from the lattice, ionization of oxygen vacancy is shown as following:[20]

$$V_O \Leftrightarrow V_O^{\bullet} + e' \quad (3\text{-}1)$$

$$V_O^{\bullet} \Leftrightarrow V_O^{\bullet\bullet} + e' \quad (3\text{-}2)$$

According to Eq. 3-1, high temperature will enhance the formation of $V_O^{\bullet}$.

Meanwhile, according to Eq. 3-2, transformation of $V_O^{\bullet}$ to $V_O^{\bullet\bullet}$ would be enhanced by evaluating temperature. Therefore, it is expected that Eq. 3-1 in which the amount of $V_O^{\bullet}$ increases, and Eq. 3-2 in which the amount of $V_O^{\bullet}$ decreases are in competition. And we believe that at high annealing temperature, Eq. 3-2 plays a dominant role, thus the amount of $V_O^{\bullet}$ decreases. This assumption agrees with the present results where Mode 1 is suppressed by high annealing temperature and finally eliminated. As a kind of oxygen vacancy, $V_O^{\bullet}$ would be eliminated by oxygen annealing, which is the reason that Mode 1 disappears after anneal BLT600 in oxygen atmosphere.

Relaxation behavior of Mode 1 is fitted according to Arrhenius law:

$$\tau = \tau_0 \exp\frac{-E_{relax}}{k_B T} \qquad (3\text{-}3)$$

where τ is the relaxation time, τ_o the relaxation time at infinite temperature (characteristic relaxation time), k_B Boltzmann's constant, and T temperature.

Since, $(\text{Mode1})^{\tan\delta}$ is relatively sharp at low frequency, BLT600 dielectric measurements were carried out from 100–500Hz. Figure 3-12 shows the ln(2πf) plotted against the inverse of k_BT for various frequencies. It is clearly seen that there is an excellent linear relationship between ln(2πf) and $1/(k_BT)$, demonstrating that relaxation of Mode 1 is in accordance with Arrhenius law. Moreover, the activation energy for this dielectric relaxation ($E_{relax\text{-}Mode1}$) is 1.89 eV and the characteristic relaxation time $\tau_{o\text{-}Mode1}=1.08\times10^{-14}$ s (a frequency of 9.29×10^{13} Hz). Activation energy related to oxygen vacancy has been reported as 1.9 eV in $(Pb,La)TiO_3$,[21] 0.97 eV in $SrBi_2Ta_2O_9$,[22] 0.98–1.13 eV in $SrTiO_3$.[23] Compared to these results, the calculated value $E_{relax\text{-}Mode1}$= 1.89 eV is quite reasonable. Therefore, we concluded that Mode 1 is related to $V_O^{\bullet}$, and the activation energy of this dielectric relaxation is 1.89 eV.

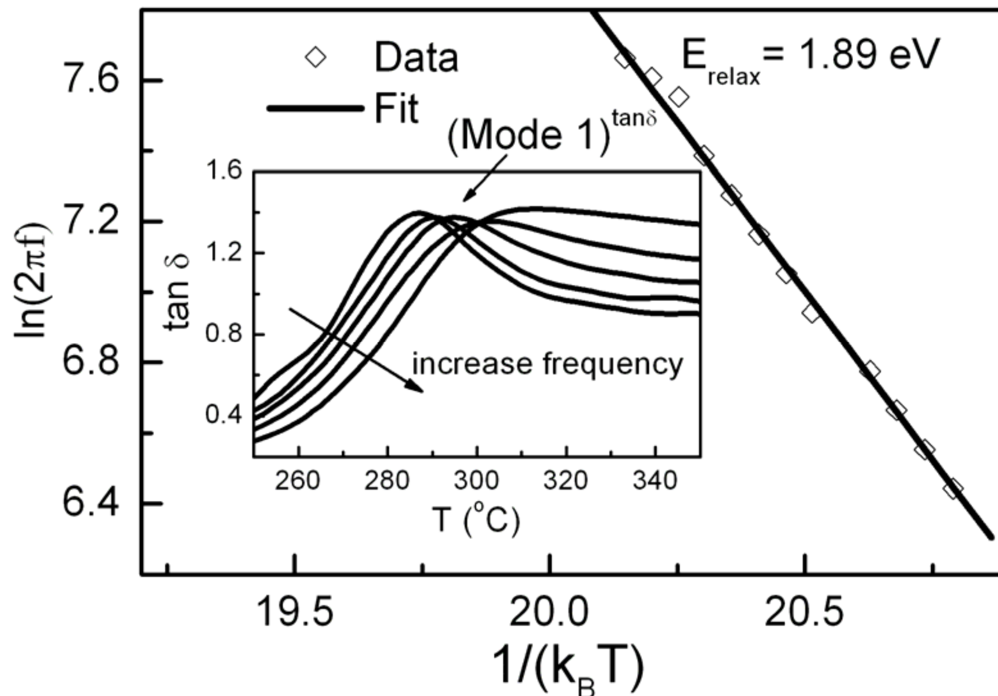

Fig. 3-12 ln(2πf) as a function of $1/(k_BT)$ (the insert: the plot of tanδ Vs. temperature) of BLT600.

(3) ～483 °C: Peak 1

Similar to Kan et al.'s report [18], Peak 1 (shown in the insert of Fig. 3-6(a)) is sharp and exhibits permittivity of about 600–1600 at frequencies from $10^{5.25}$–$10^{5.75}$Hz. Moreover, Peak 1 does not show any frequency dispersion, and it did not changed after oxygen annealing or after reduced annealing. Therefore, Peak 1 is attributed to the para-ferrelectric phase transition. The difference between the Curie temperature reported by Kan *et al.* and temperature of Peak 1 in the present work may be attributed to the difference of composition (evaporation of bismuth in the process of annealing), and different form of investigated materials (ceramics and film).

(4) Mode 2

Bidault *et al.* [13] have reported that a dielectric anomaly in the vicinity of 500–600 °C was found in a number of pervoskite-based ferroelectrics containing titanium,[24] and they attributed it to space charge, which is related to the density of oxygen vacancies. We designated this anomaly as Space Charge Mode (SC Mode, hereafter). Fouskova and Cross [17] have reported Mode 2 in BiT single crystal, and they proposed that it arises from a space charge developed through the high conduction current at elevated temperatures. However, no evidence for this is shown in their report.

To confirm Fouskova and Cross's assumption, we compared the characteristics between Mode 2 and SC Mode: (1) Both modes exhibit strong frequency dependence behavior; (2) As shown in Fig. 3-8(b), it is found that the intensity of Mode 2 decreases after annealing in oxygen atmosphere, and increases again after annealing in reduced atmosphere, suggesting that Mode 2 is related to density of oxygen vacancy. It should be noted that ε' after reduced annealing is higher than the initial value. For example, permittivity of BLT600 (@ 1kHz) after reduced annealing is 7×10^5, which is larger than that of BLT600 (@ 1kHz: 4.4×10^5). And this result is very similar with SC Mode characteristics (seen Fig. 2 in Ref. 13 It means that oxygen vacancies related to Mode 2 are continuously formed easily after reduced annealing. It is somewhat different with Mode 1, since the intensity of Mode 1 after reduced annealing is smaller than the initial one, shown in Fig. 3-8 (a). The best explaination is that Mode 1 is related to $V_O^{\bullet}$ and Mode 2 is related to $V_O^{\bullet\bullet}$. As shown in Eq. 3-1 and Eq. 3-2, $V_O^{\bullet}$ is a byproduct in the process of $V_O^{\bullet\bullet}$ formation, therefore, the increase of $V_O^{\bullet\bullet}$ amounts can be created by long-time reduced annealing. On the other hand, the increase of $V_O^{\bullet}$ amounts is difficult because that $V_O^{\bullet}$ will be further ionized to form $V_O^{\bullet\bullet}$. In short, $V_O^{\bullet}$ is more easily eliminated than produced, which in accordance with our results. In conclusion, Mode 2 is attributed to space charge which is related to the density of $V_O^{\bullet\bullet}$.

Due to the strong frequency dispersion characteristics of $(\text{Mode 2})^{\tan\delta}$, the possibility that $(\text{Mode 2})^{\tan\delta}$ corresponds to Peak 1 (para-ferroelectric phase transition) is excluded. Therefore, $(\text{Mode 2})^{\tan\delta}$ is the corresponding loss anomaly of Mode 2. Experimental results are shown in Tab.2, and the activation energy of dielectric relaxation of Mode 2 has been calculated by $(\text{Mode 2})^{\tan\delta}$. First, we tried to fit the results using Arrhenius law Eq.3-3, however, poor fitting result and unreasonable activation energy $E_{relax\text{-}Mode2}$=8.8 eV were obtained. Therefore, Vögel-Fulcher law was used:[24,25]

$$\tau = \tau_0 \exp\frac{-E_{relax}}{k_B(T-T_f)} \tag{3-4}$$

where τ is relaxation time, τ_o the relaxation time at infinite temperature (characteristic relaxation time), k_B Boltzmann's constant, T temperature, and T_f static freezing temperature. As shown in Fig. 3-13, dielectric relaxation of $(\text{Mode 2})^{\tan\delta}$ can be fitted with Vögel-Fulcher relation. The solid line is the fitting curve that gives $\gamma_0=2.54\times10^{-14}$ s, T_f=578.26K, and E_{relax}=0.31eV.

In conclusion, Mode 2 is attributed to the space charge related with density of $V_O^{\bullet\bullet}$, and the activation energy of this mode is $E_{relax\text{-}Mode2}$=0.31eV.

Tab. 3-2 Experimental results of T_m and ε_{max} for Mode 2 (BLT700).

ω (Hz)	T_m (^oC) @(Mode 2)$^{tan\delta}$	ε_{max}@ (Mod 2)
10^2	423.1	-
$10^{2.25}$	426	-
$10^{2.5}$	427.6	40743
$10^{2.75}$	430.5	34896
10^3	433.5	29048
$10^{3.25}$	434.9	23201
$10^{3.5}$	438.1	18070
$10^{3.75}$	441	13618
10^4	441.1	9959
$10^{4.25}$	446.9	7375
$10^{4.5}$	450	7299
$10^{4.75}$	454.5	5583
10^5	459	
$10^{5.25}$	463.5	

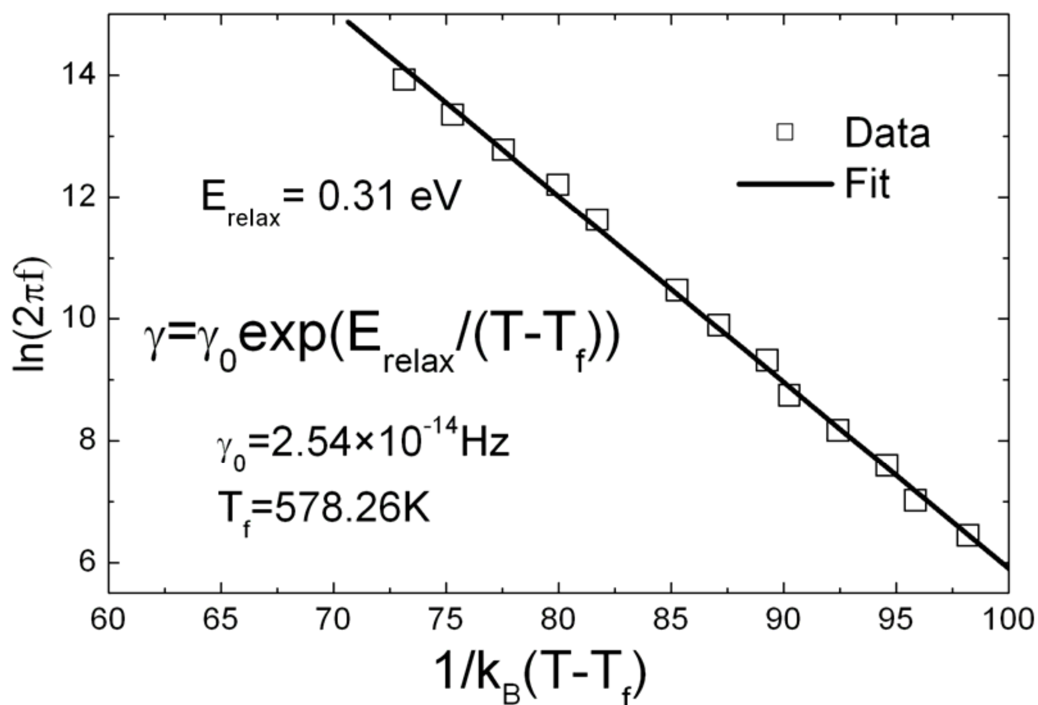

Fig. 3-13 Vögel-Fulcher behavior of BLT700.

Ac conductivity and its activation energy

Activation energy of conductivity has been calculated by:

$$\sigma = \sigma_0 \exp(-E_{cond} / k_B T) \quad (3\text{-}5)$$

where σ_0 is a constant and E_{cond} is the activation energy for conduction. It was found that E_{cond}(@450～600 °C)=1.59 eV, and E_{cond}(@300～450 °C)=0.65 eV. Different slopes appear in different regions of temperature, indicating multiple activation processes with different energies. We propose that different mechanisms dominate in these two temperature ranges of 300–450 °C and >450 °C.

If the relaxation mechanism is governed by trap-controlled ac conduction, the value of E_{relax} should be close to or less than that of E_{cond}. Therefore, the larger E_{relax} (1.89 eV) in the present work may suggest that the relaxation process in the temperature range (300-450 °C) does not govern the electrical conduction, which is similar to the research conducted on $La_{0.8}Sr_{0.2}GaO_{3-\delta}$.[26] The larger value of E_{relax} may suggest that the relaxation is a dipolar type, which is similar to amorphous $SrTiO_3$.[20] Moreover, Long *et al.* [27] have reported that the activation energy of the reaction of Eq.3-2 to be 1.4-1.6 eV. Therefore, if it is assumed that the electrical conduction in the temperature range (300-450 °C) is governed by the thermal excitation of carrier from $V_O^{\bullet}$. The activation energy should be 0.7-0.8 eV (E_D/2), which is very close to the fitted result E_{cond}=0.65 eV in the temperature range of 300-450 °C. The larger value of $E_{relax\text{-}Mode1}$ than E_{cond}(@300～450) suggests that the relaxation process in the temperature range 300–450 °C does not govern the electrical conduction and indicates that the relaxation is a dipolar type. Moreover, it is proposed that the electrical conduction in the temperature range of 300–450 °C is governed by the thermal excitation of the carrier from $V_O^{\bullet}$.

3.4.2.5 Summary

Dielectric properties at the temperature range of 25–600 °C were investigated in $Bi_{3.25}La_{0.75}Ti_3O_{12}$ ferroelectric films. Four dielectric anomalies were found at ～250 °C, ～400 °C, 483 °C, and ～500 °C. Long-time post-annealing processes were carried out in either oxygen or nitrogen atmospheres. It was found that subsequent heating treatments critically influenced the anomalies at ～250 °C, ～400 °C, and ～500 °C but not ～483 °C . Moreover, annealing temperature plays an important role on anomaly at ～400 °C, while heat treatment and annealing temperature show little influence on the anomaly at483 °C. It is proposed that the anomaly at～ 483 °C exhibits phase transition between para-ferroelectric. The other anomalies at ～250 °C, ～400 °C, and ～500 °C are related to oxygen vacancies. Detailed analysis demonstrates that the anomaly at ～250 °C is related to oxygen vacancies and bismuth vacancies; the

anomaly at ～400 ^{o}C is attributed to single-ionized oxygen vacancies $V_O^{\bullet}$; and the anomaly at ～500 ^{o}C is attributed to space charge which is came from double-ionized oxygen vacancies $V_O^{\bullet\bullet}$.

3.5 CONCLUSION AND SUMMARY

In this chapter, $Bi_{3.25}La_{0.75}Ti_3O_{12}$ ferroelectric thin films were fabricated from a precursor solution purchased from Toshima Co., Japan. Ferroelectric and dielectric properties of the $Bi_{3.25}La_{0.75}Ti_3O_{12}$ films were studied.

Three annealing temperatures: 600 ^{o}C, 700 ^{o}C and 800 ^{o}C were selected to prepare BLT600, BLT700 and BLT800. Phase characteristics were investigated by X-ray diffraction (XRD), suggesting that all samples exhibit a well-crystallized phase, and no secondary phase was observed. Moreover, all prepared films showed the same orientation within experimental error. Surface morphology of the films was observed by SEM, and it was found that all samples exhibit rodlike grains. As expected, with the increase of annealing temperature, grain size increases. Hysteresis loop measurement was also carried out on BLT600 and BLT700. It exhibits that higher remnant polarization was found in BLT700, which is attributed to the larger grain size in BLT700.

Dielectric and ac conductivity measurements at frequencies from 10^2 Hz to 10^6 Hz, were carried out on the fabricated $Bi_{3.25}La_{0.75}Ti_3O_{12}$ ferroelectric films, in the temperature range of 25–600 ^{o}C. In addition to a dielectric peak at 483 ^{o}C attributed to the para-ferroelectric phase transition, three dielectric relaxations were found at ～250 ^{o}C,～400 ^{o}C, and ～500 ^{o}C, respectively. The dielectric relaxation (～400 ^{o}C) can be eliminated by a higher annealing temperature and oxygen post-annealing, and it can be induced again by a subsequent nitrogen post-annealing process. The activation energy of dielectric relaxation of this mode is estimated to be 1.89 eV. The dielectric relaxation (～500 ^{o}C) is not influenced by annealing temperature but is by the post-annealing process. The intensity of this anomaly decreases after oxygen annealing and then increases after nitrogen annealing. The relaxation behavior of this dielectric relaxation is not in accordance with Arrhenius law but is in accordance with Vögel-Fulcher law, and the activation energy is calculated as 0.31eV. Mechanisms for the observed dielectric relaxations at ～250 ^{o}C,～400 ^{o}C, and ～500 ^{o}C are proposed.

REFERENCES

[1] D. Wu, A. Li, T. Zhu, Z. Li, Z. Liu and N. Ming, *J. Mater. Res.*, **16**, 1325 (2001).
[2] U. Chon, H. M. Jang, S. H. Lee, and G. Yi, *J. Mater. Res.*, **16**, 3124 (2001).
[3] H. N. Lee and D. Hesse, *Appl. Phys. Lett.*, **80**, 1040 (2002).
[4] D. Bao, X. Zhu, M. Alexe and D. Hesse, *J. Appl. Phys.*, **98**, 014101 (2005).
[5] B. H. Park, B. S. Kang, S. D. Bu, T. W. Noh, J. Lee, and W. Jo, *Nature* (London) **401**, 682 (1999).
[6] J. Lee and R. Ramesh, *Appl. Phys. Lett.*, **68**, 484 (1996).
[7] P. C. Joshi, S. B. Krupanidhi, A. Mansingh, *J. Appl. Phys.*, **72**, 5517 (1992).
[8] X. Du, I. W. Chen, *J. Am. Ceram. Soc.*, **81**, 3253 (1998).
[9] Y. Noguchi and M. Miyayama, *Appl. Phys. Lett.*, **78**, 1903 (2001).
[10]D. H. Bao, T. W. Chiu, N. Wakiya, K. Shinozaki, and N. Mizutani, *J. Appl. Phys.*, **93**, 497 (2003).
[11] H. Irie, H. Saito, S. Ohkoshii, and K. Hashimoto, *Adv. Mater.*, **17**, 491 (2003).
[12] Y. Noguchi, M. Miayama, *Appl. Phys. Lett.*, **78**, 1903 (2001).
[13] O. Bidault, P. Goux, M. Kchikech, M. Belkaoumi, and M. Maglione, *Phys. Rev. B*, **49**, 7868 (1994).
[14] B. S. Kang, S. K. Choi, and C. H. Park, *J. Appl. Phys.*, **94**, 1904 (2003).
[15] C. Jovalekic and M. Pavlovic, P. Osmokrovic, and Lj. Atanasoka, *Appl. Phys. Lett.*, **72**, 1051 (1998).
[16] H.S. Shulman, D. Damjanovic, and N. Setter, *J. Am. Ceram.Soc.*, **83**, 528(2000).
[17] A. Fouscova and L. E. Cross, *J. Appl. Phys*., **41**, 2834 (1970).
[18] Y. Kan, X. Jin, G. Zhang, P. Wang, Y. Cheng and D. Yan, *J. Mater. Chem.*, **14**, 3566 (2004).
[19] W. Li, A. Chen, X. Lu, and J. Zhu, *J. Appl. Phys.*, **98**, 024109 (2005).
[20] K. Morii, H. Kawano, I. Fujii, T. Matsui, and Y. Nakayama, *J. Appl. Phys.*, **78**, 1914 (1995).
[21] M. Kuwabara, K. Goda, and K. Oshima. *Phys. Rev. B*, **42**, 10012 (1990).
[22] Z. Y. Wang and T. G. Chen, *Phys. Status Solidi A*, **167**, R3(1998).
[23] A. E. Paladino, *J. Am. Ceram. Soc.*, **48**, 476 (1965).
[24] D. Viehland, S.J. Jang and L.E. Cross, *J. Appl. Phys.*, **68,** 2916 (1990).
[25] F. Chu and N. Setter, *J. Appl. Phys.*, **74,** 5129 (1993).
[26] E. Iguchi, S. Nakamura, F. Munakata, M. Kurumad, and Y. Fujie, *J. Appl. Phys.*, **93**, 3662 (2003).
[27] S. A. Long and R. N. Blumenthal, *J. Am. Ceram, Soc.*, **54**, 577 (1971).

Chapter 4

Ferroelectric Behavior of $Bi_{4-x}Nd_xTi_3O_{12}$ Thin Films

In this chapter, $Bi_{4-x}Nd_xTi_3O_{12}$ (BNT) ferroelectric films were fabricated by the precursor solution prepared in laboratory. The influence of annealing temperature and concentration of Nd on the ferroelectric properties of the BNT films was investigated. The influence of annealing temperature and composition on fatigue properties of the films were also studied.

4.1 INTRODUCTION

Ferroelectrics are materials that possess spontaneous polarization, whose direction could be reversed by applied external electric fields. Recently, ferroelectric thin films are considered as a promising candidate for nonvolatile ferroelectric random access memories (NvFeRAM).[1] Due to the good ferroelectric properties and low annealing temperature, $Pb(Zr_xTi_{1-x})O_3$ (PZT) thin film was initially studied for NvFeRAM application, however it exhibits severe polarization fatigue during electric field cycling, when configured with metal electrodes such as platinum (Pt). Polarization fatigue is a decrease in switchable polarization with electric field cycling, which is an important factor when consider the long-term reliability of devices. To avoid fatigue phenomenon, there has been interest in preparing fatigue-free ferroelectric, when configured with metal electrode. It was discovered that many ferroelectric materials belonging to layered bismuth ferroelectric family show excellent fatigue properties with electric field cycling. As a member of layered bismuth ferroelectric family, $Bi_4Ti_3O_{12}$ (BiT) based ferroelectric films have attracted extensive interest due to its superior fatigue resistance, giant spontaneous polarizations (P_s), and relatively low processing temperature.[2] Due to the low fatigue resistance and low polarization of pure BiT ferroelectric film, most works are carried out on doped BiT thin film; such as lanthanum (La^{3+}) substituted BiT,[2-5] neodymium (Nd^{3+}) doped BiT,[6-8] and vanadium (V^{5+}) ,tungsten or nitrogen (N^{3-}) etc. substituted BiT ferroelectric films.[9,10] Neodymium (Nd^{3+}) and Lanthanum (La^{3+}) substituted BiT have been extensively studied due to the high polarization and easy controlling. In the reported works on doped BiT ferroelectric thin films, investigation on the mechanism of the fatigue-free

behavior of ferroelectric thin films have attracted extensive interesting; however, the major origin is still ambiguous. The reported works on cycling field dependence of fatigue behavior, suggesting that fatigue-free behavior of BiT is attributed to field-assisted domain pinning, which is called domain pinning and unpinning mode.[11,12] Moreover, stability of oxygen perovskite layers and space charge compensated by self-regulating $[Bi_2O_2]^{2+}$ layers were also proposed as mechanisms of fatigue-free properties in bismuth layer compounds. It should be noted that all the proposed models involve a variation of concentration of defects. Therefore, it is expected that change of defect concentration may contribute to variation of fatigue behavior of BiT-based ferroelectrics. Because of the influence of substitution concentration on defect concentration in BiT-based ferroelectrics, $Bi_{4-x}Nd_xTi_3O_{12}$ (BNT) is selected to investigate in this chapter. $Bi_{4-x}La_xTi_3O_{12}$ (BLT) will be studied in the following chapter, due the extensive study in these two ferroelectric thin films.

4.2 EXPERIMENT

The whole process of fabricating BNT films is shown in Fig. 4-1. The process consists of two parts: preparation process of precursor solution and heat treatment process for BNT thin films.

4.2.1 Preparation of precursor solution

Thin films were fabricated by the metal organic solution deposition (MOSD) technique. Bismuth nitrate ($Bi(NO_3)_3 \cdot 5H_2O$), n-tetrabutyl titanate ($(C_4H_9O)_4Ti$) and lanthanum nitrate ($Nd(NO_3)_3 \cdot 5H_2O$) were selected as starting materials. Acetic acid and 2-methoxyethanol were solvents. Firstly, bismuth nitrate ($Bi(NO_3)_3 \cdot 5H_2O$) was dissolved in acetic acid (CH_3COOH), and then tetrabutyl titanate ($(C_4H_9O)_4Ti$) was added to this solution slowly with constant stirring. 10 mol.% excess amount of bismuth nitrate ($Bi(NO_3)_3 \cdot 5H_2O$) was added to compensate the Bi loss during annealing process. Finally, 2-methoxy ethanol was added to adjust the last concentration of solution to 0.05 mol/l, and the formed solution was transparent.

4.2.2 Fabrication of $Bi_{4-x}Nd_xTi_3O_{12}$ films

After filtered, precursor solution was spinning coated at substrate with a structure of Pt(200nm)/TiO_2(50nm)/SiO_2(500nm)/Si from Panasonic company. Spinning was carried out on at a speed of 3000rpm for 30 seconds. The deposited film was dried on a hot plate at 260 ^oC for 10 min. To crystallize films, a 2-step Rapid Thermal

Annealing (RTA) was employed. The dried films were heated at temperature of 500 °C for 60 s, and then were heated at 550 °C, 600 °C, 650 °C, or 700 °C for 60 s. This process was repeated several times to get the final thickness to about 120 nm.

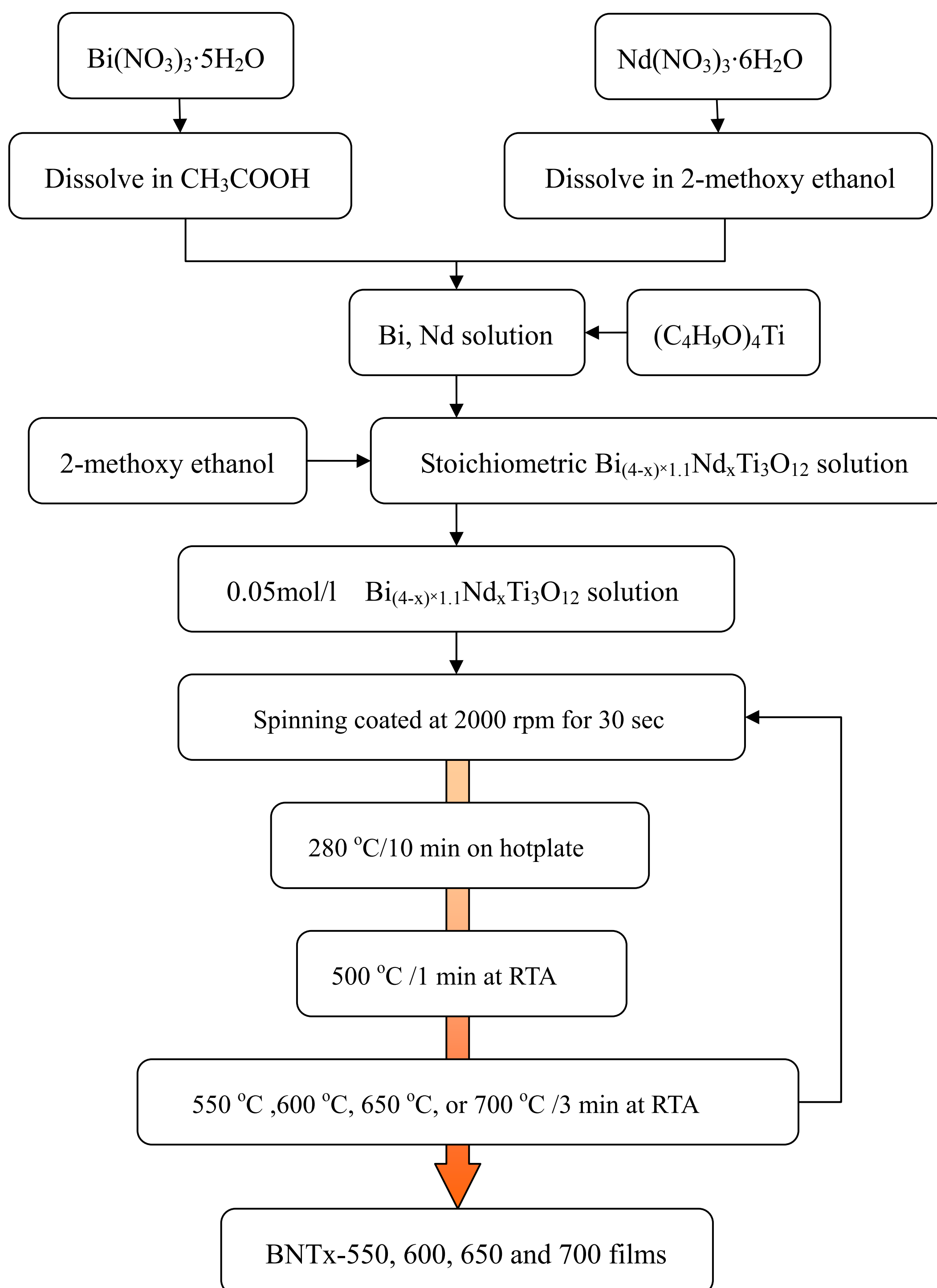

Fig. 4-1 Fabrication flow chart for BNTx ferroelectric films.

Five compositions, $Bi_{3.8}Nd_{0.2}Ti_3O_{12}$, $Bi_{3.6}Nd_{0.4}Ti_3O_{12}$, $Bi_{3.4}La_{0.6}Ti_3O_{12}$, $Bi_{3.2}Nd_{0.8}Ti_3O_{12}$, and $Bi_{3.0}Nd_{1.0}Ti_3O_{12}$, were prepared, which are abbreviated as BNT0.2, BNT0.4, BNT0.6 BNT0.8 and BNT1.0, respectively. Moreover, BNTx annealed at 550 ^oC, 600 ^oC, 650 ^oC and 700 ^oC is abbreviated as BNTx-550, BNTx-600, BNTx-650, and BNTx-700, hereafter.

4.2.3 Characterization

The crystallinity of BNT film was analyzed by X-ray diffraction (XRD). Scanning electron microscopy (SEM) was used to observe cross section and define the thickness of BNT films. For ferroelectric measurement, a Pt top electrode in the form of 100 μm dots and 200 Å thickness was deposited using a shadow mask at room temperature. Fatigue measurements were carried out at room temperature using TF analyzer 2000 (aixACCT) at 50 kHz up to 10^9 cycles. Capacitance measurements were carried out at room temperature using *LCR* meter (HP 4194A)

4.3 RESULTS AND DISCUSSION

4.3.1 Crystalline phase and morphology

Crystalline structure of BNT ferroelectric films was examined using X-ray diffraction (XRD) with Cu K_α radiation. Figure 4-2 shows XRD patterns of BNT films, which were indexed according to the standard powder diffraction data of $Bi_4Ti_3O_{12}$ (PDF#73-2181). In current work, all prepared films were single phase without second phase. As shown in Fig. 4-2, BNT films could be crystallized at as low as 550 ^oC. Compared with the annealing temperature of BLT prepared by the purchased precursor solution (1#), the annealing temperature of BNT fabricated by the prepared precursor solution (2#) is relatively low, suggesting that the chemical reaction activity of the prepared precursor solution (2#) is higher than that of the purchased precursor solution (1#)

BNT films annealed at above 650 ^oC exhibit sharp peaks with high intensity. Additionally, with increase of Nd^{3+} substitution, peak intensity decreases, and full widths at half maximum (FWHM) increases, which agrees with Xiang and Wu *et al.*[3,13] It was proposed that Nd^{3+} substitution may suppress the growth of BiT grains, results in decrease of crystalline, therefore with increase of Nd^{3+} concentration, XRD peak intensity decreases. It should be noted that, in most BNT films, (117) dominates XRD patterns, demonstrating the random orientation of the BNT films.

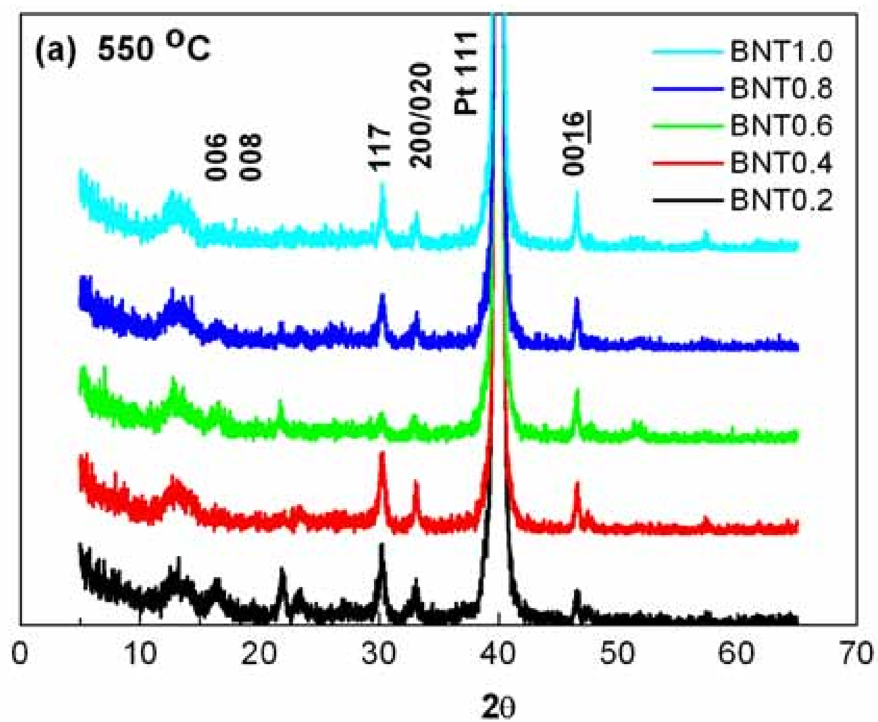
(a) 550 ^{O}C
006
008
117
200/020
Pt 111
0016
BNT1.0
BNT0.8
BNT0.6
BNT0.4
BNT0.2
0
10
20
30
40
50
60
70
2θ

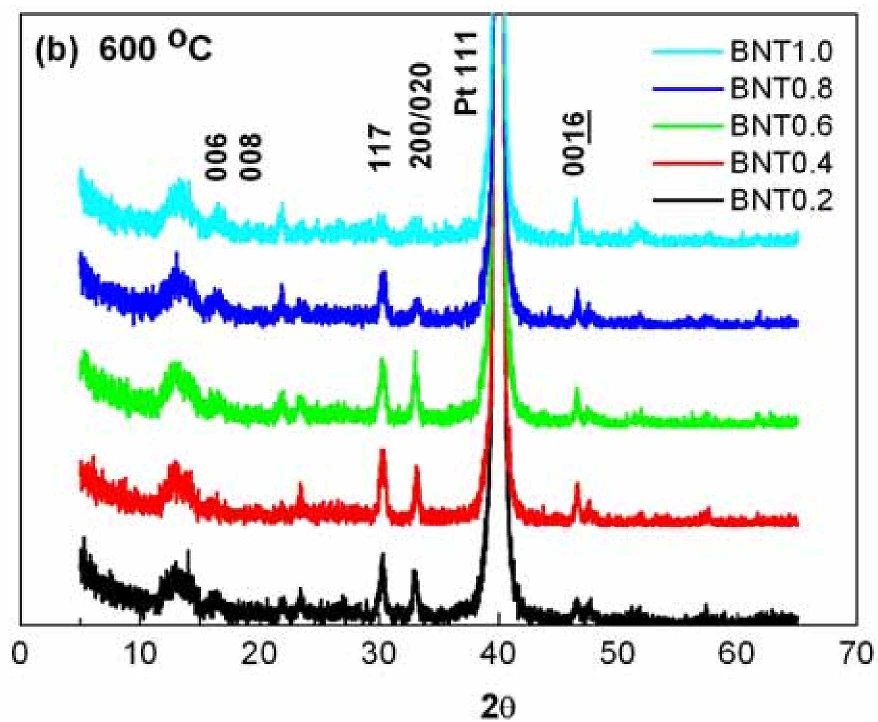
(b) 600 ^{O}C
006
008
117
200/020
Pt 111
0016
BNT1.0
BNT0.8
BNT0.6
BNT0.4
BNT0.2
0
10
20
30
40
50
60
70
2θ

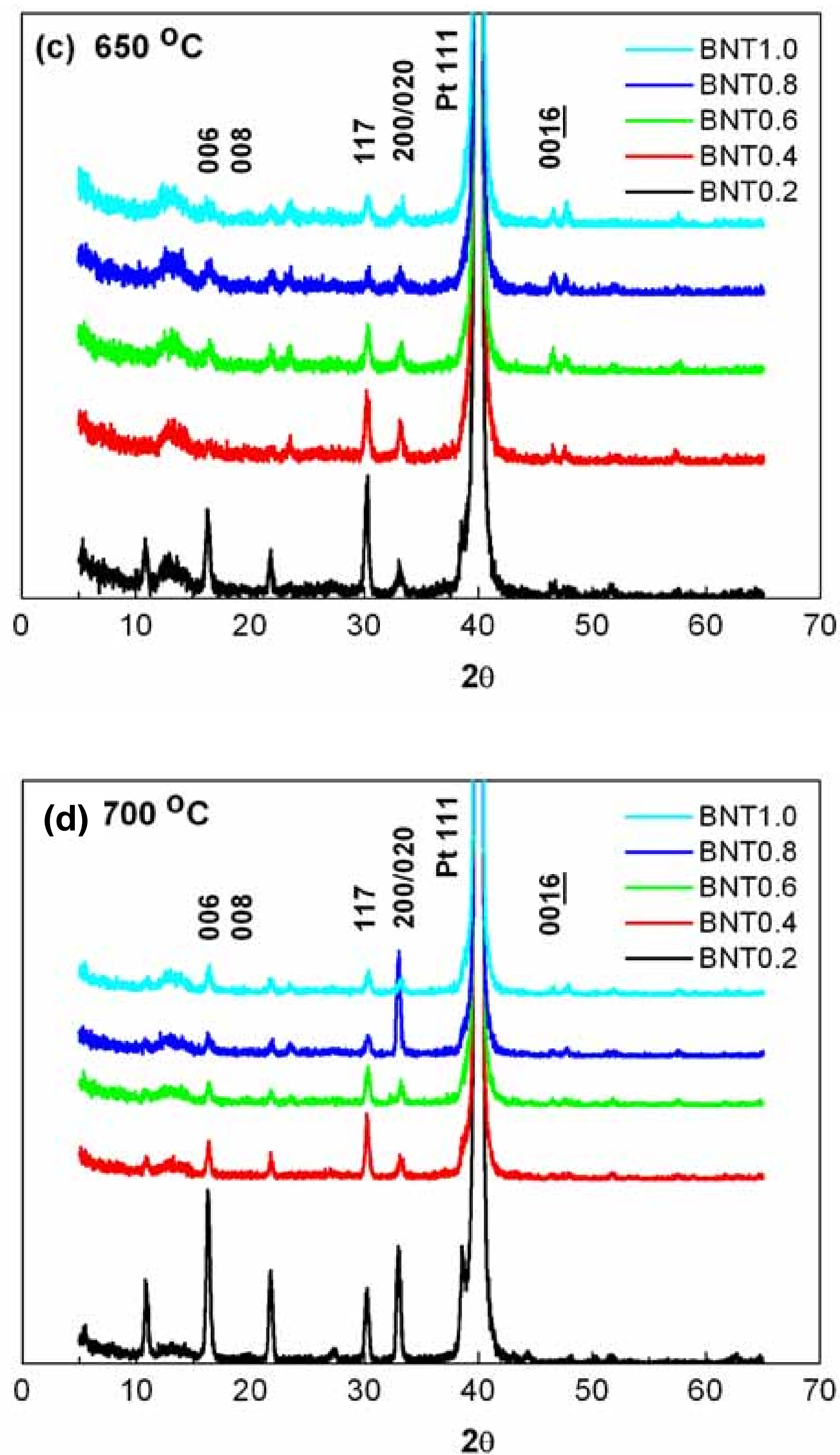

Fig. 4-2 XRD patterns of BNTx (x=0.2, 0.4, 0.6, 0.8, and 1.0) annealed at 550 °C (a), 600 °C (b), 650 °C (c), and 700 °C (d).

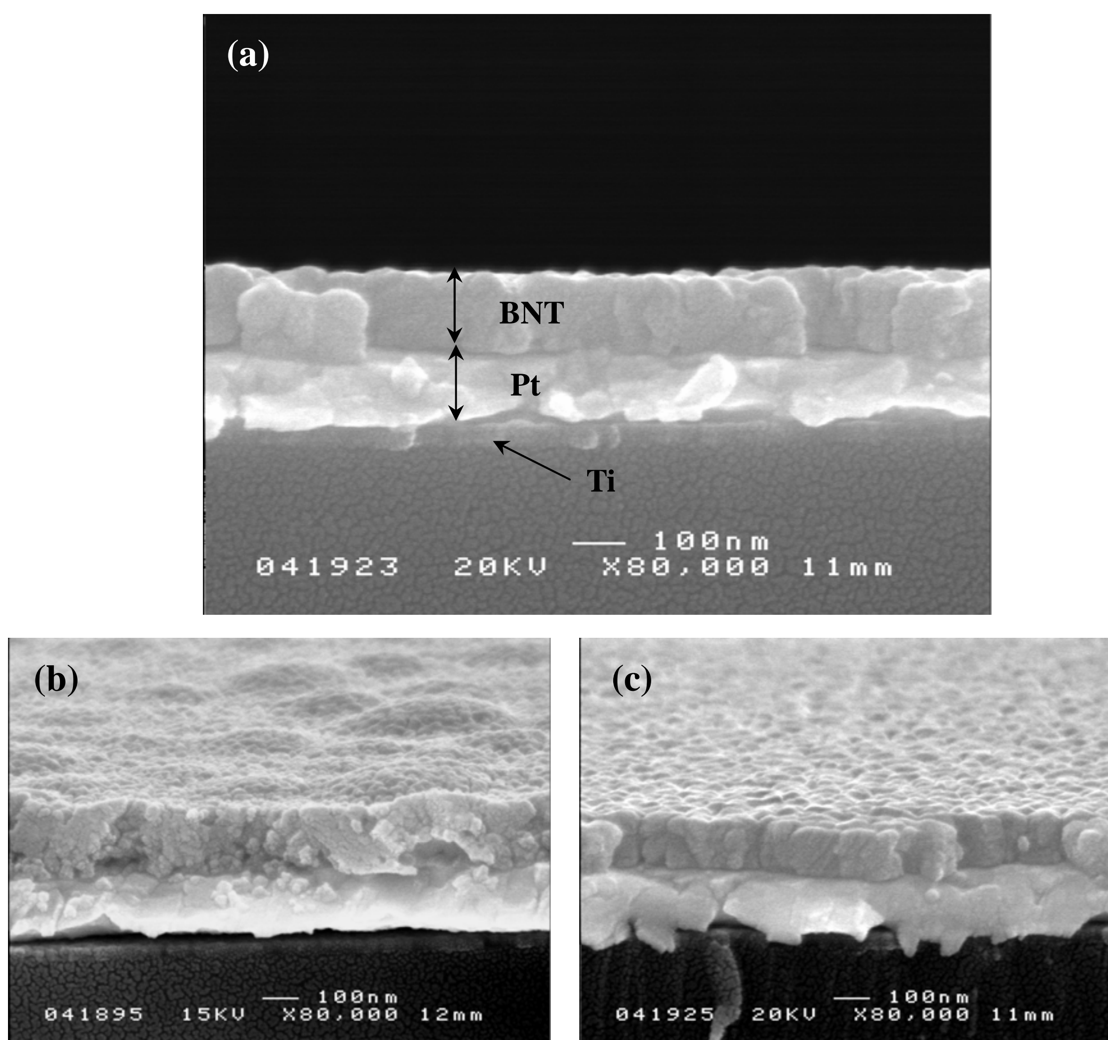

Fig. 4-3 SEM images of BNT film cross section of BNT0.2-600 (a), BNT0.2-550 (b), BNT0.2-600 (c).

Figure 4-3 shows the typical SEM image of BNT films. Thickness of BNT films is estimated as 125 nm from the cross section of BNT thin films, and a typical SEM image is shown in Fig. 4-3(a). Figure 4-3(b,c) show that the films consist of rodlike grain, and with the increase of annealing temperature, the grain size increases extensively. Moreover, it should be noted that the prepared BNT exhibits a dense structure.

4.3.2 Ferroelectric characteristics

4.3.2.1 Remnant polarization and coercive field

Figure 4-4 shows the saturation properties of remnant polarization (P_r) and coercive field (E_c) as a function of the maximum voltage for all the films. It was found that annealing temperature play an important role on remnant polarization (P_r) for all

the films with various concentration of Nd. For the films with the same compositions, remnant polarization (P_r) increases continuously with annealing temperature. As mentioned above, high annealing temperature results in large grain size, which contributes to increase of remnant polarization (P_r). With the increase of Nd substitution, the value of remnant polarization (P_r) decreases. For the BNT0.8 and BNT1.0, the value of remnant polarization (P_r) is as low as 4-6 $\mu C/cm^2$. In all the compositions, BNT0.4 and BNT0.6 exhibit high remnant polarization (P_r), suggesting that these two compositions are optimal at current work.

Figure 4-5 shows the dependence of remnant polarization (P_r) at applied voltage of 5V on the Nd concentration at various annealing temperatures. It is found that for the films fabricated at the same annealing temperature, Pr exhibit an initial increase, and then decrease for further substitution.

In the report of Watanabe *et al.*[7], the similar result that remnant polarization (P_r) increases with initial substitution of Nd, and decreases with further substitution. It has been attributed to the mechanism that Nd is selectively substituted for the bismuth in the perovskite layer at low concentration; however, Nd is also incorporated into bismuth sites in the $(Bi_2O_2)^{2+}$ layer with further increase of Nd. Moreover, Xiang *et al.* [13] proposed that BNT undergoes a tendency from pseudo-orthorhombic symmetry with Nd substitute. It is expected that interior polarization, came from structure distortion of BNT, increases with Nd substitute. In a conclusion, substitution of Nd play a role on the remnant polarization (P_r) of BiT-based ferroelectrics by incorporate into BiT lattice and change the distortion of lattice.

Therefore, in current work, the change of polarization with Nd concentration and annealing temperature could be related with grain growth and crystal structure. For the films with the same composition, with increase of annealing temperature, larger grain size is obtained, resulting in higher polarization. For the films annealed at the same temperature, decrease of grain size due to Nd substitution, which agrees with XRD results, as shown in Fig. 4-2, contributes to decrease of polarization. In a word, substitution of Nd results in an increase of interior polarization due to its influence on crystal structure, and a decrease of polarization due to the suppression of grain growth. These two effects are in competition. For the BNT0.2, BNT0.4 and BNT0.6, the effect of increase interior polarization of Nd plays a dominant role, therefore, with increase of Nd concentration, remnant polarization (P_r) increases. For the BNT0.8 and BNT1.0, the effect of suppression of grain growth by Nd substitution is the dominant one, therefore, remnant polarization (P_r) decreases with Nd concentration.

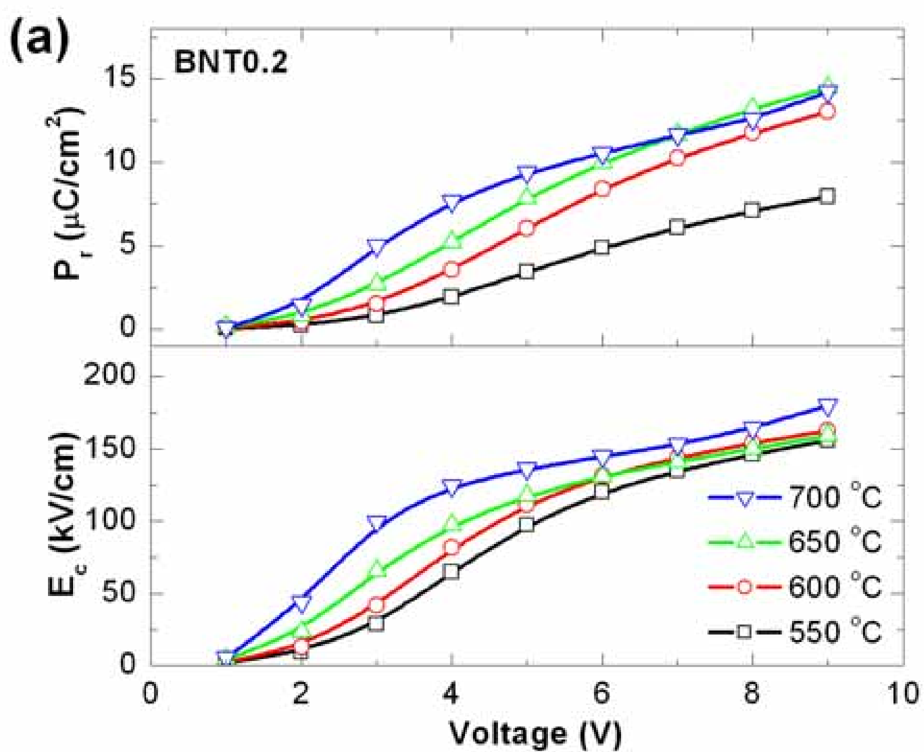
(a)
BNT0.2
P_r ($\mu C/cm^2$)
E_c (kV/cm)
700 °C
650 °C
600 °C
550 °C
Voltage (V)

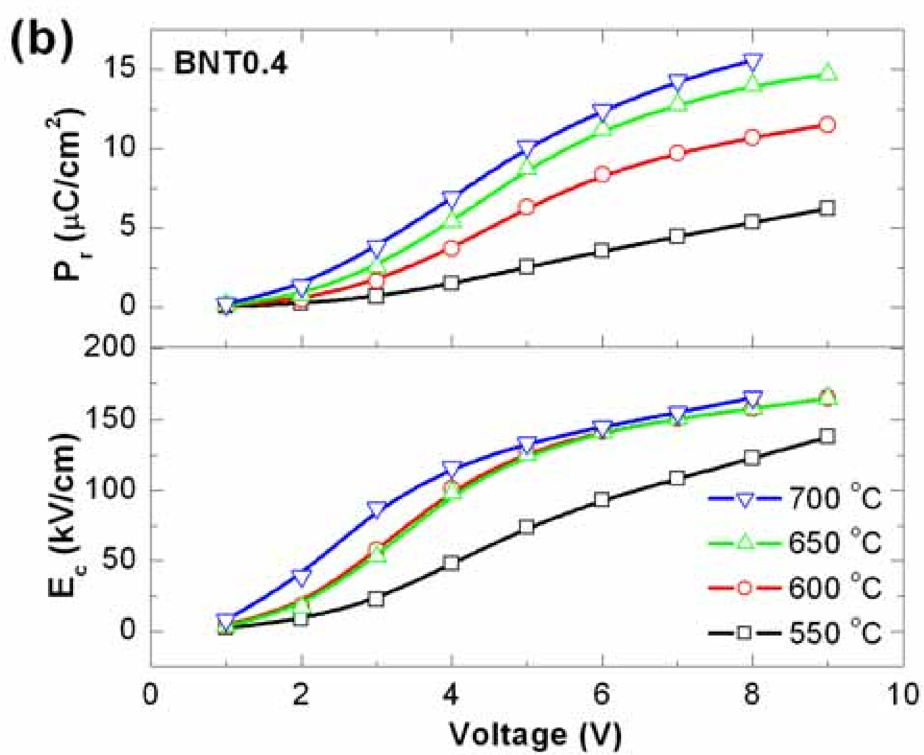
(b)
BNT0.4
P_r ($\mu C/cm^2$)
E_c (kV/cm)
700 °C
650 °C
600 °C
550 °C
Voltage (V)

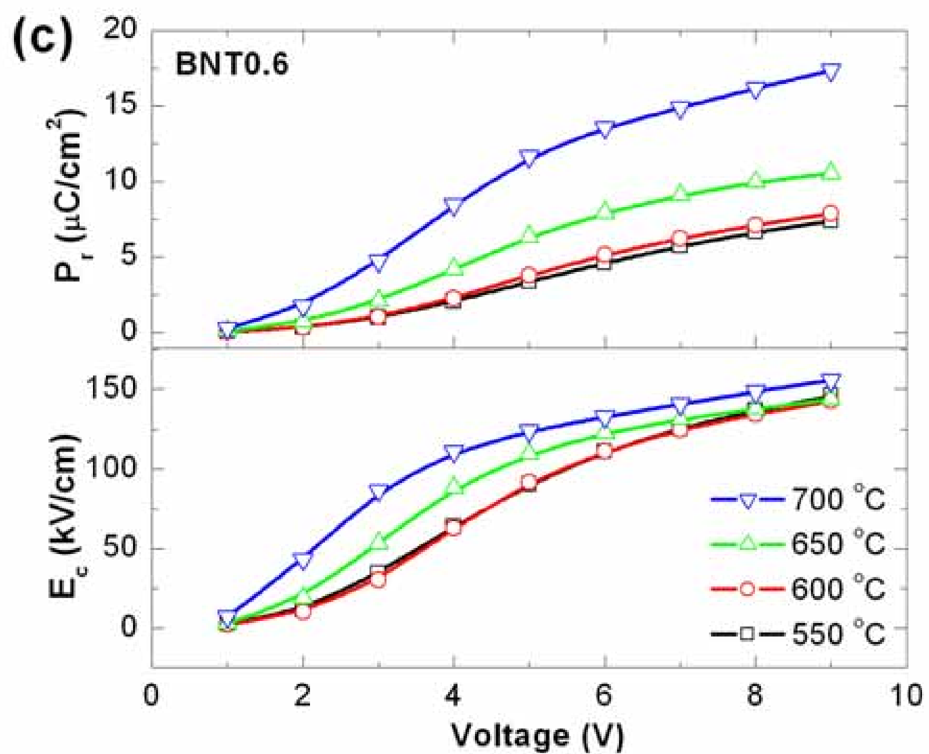
(c)
BNT0.6
P_r ($\mu C/cm^2$)
E_c (kV/cm)
700 °C
650 °C
600 °C
550 °C
Voltage (V)

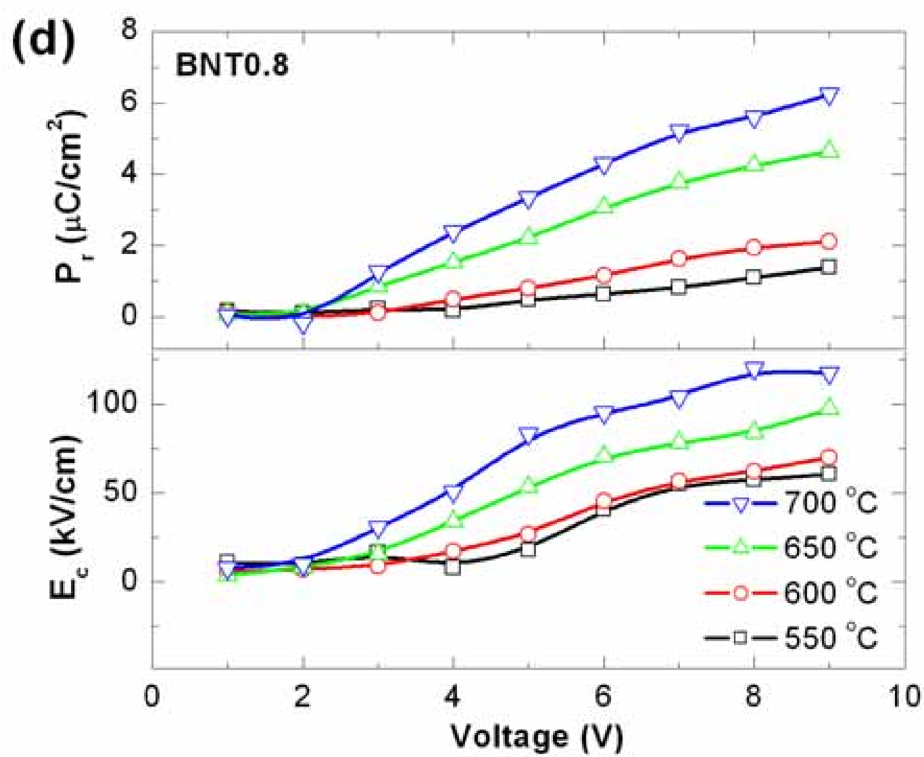
(d)
BNT0.8
P_r ($\mu C/cm^2$)
E_c (kV/cm)
700 °C
650 °C
600 °C
550 °C
Voltage (V)

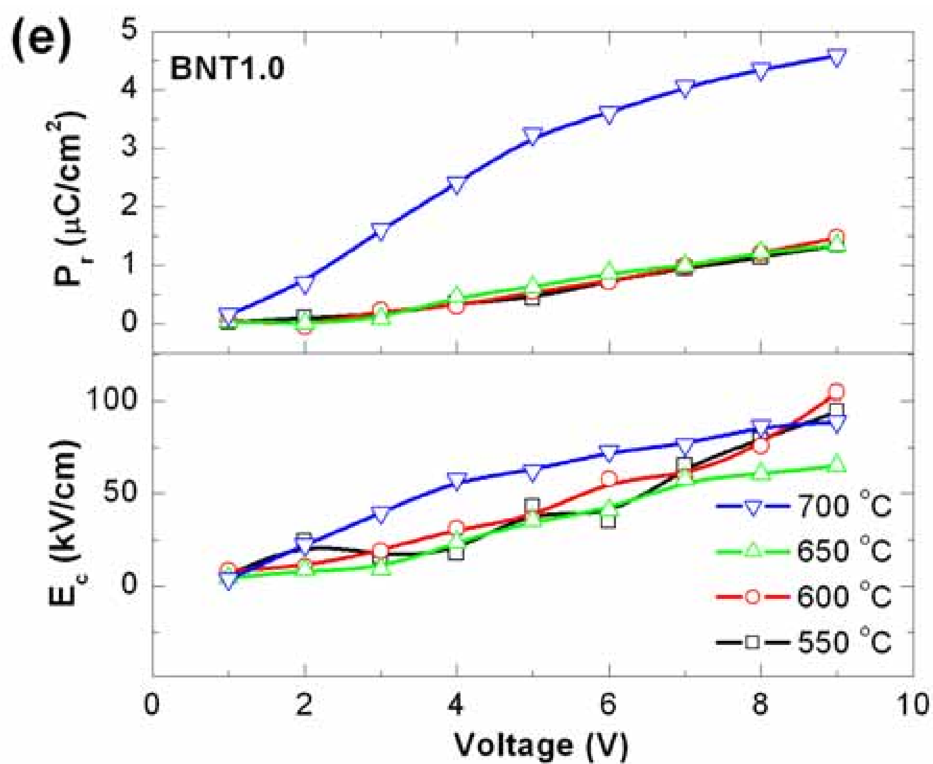

Fig. 4-4 Dependence of remnant polarization (P_r) and coercive field (E_c) of BNTx films (a) BNT0.2, (b) BNT0.4, (c) BNT0.6, (d) BNT0.8, and (e) BNT1.0 on the applied voltage.

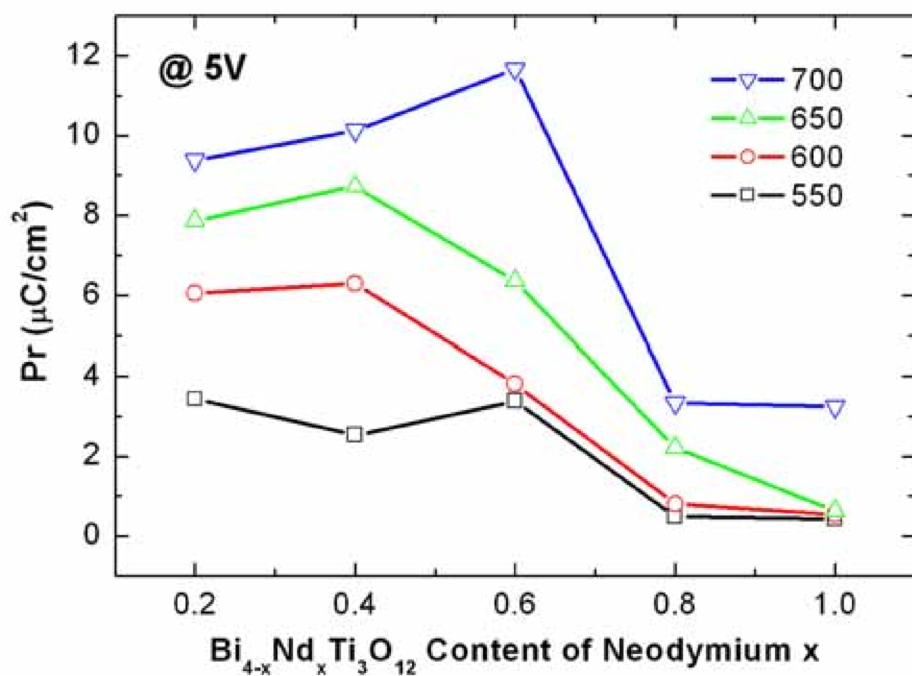

Fig. 4-5 Dependence of P_r on Nd concentration.

4.3.2.2 Fatigue characteristics

$Bi_{4-x}Nd_xTi_3O_{12}$ has been extensively reported as a kind of fatigue-free ferroelectrics.[6-8,14] However, a few of works have also reported that a decrease of polarization was found in this kind of ferroelectric thin films. Therefore, fatigue behavior of $Bi_{4-x}Nd_xTi_3O_{12}$ may be not only related with composition but also the preparation processing. In this part, the fatigue behavior of $Bi_{4-x}Nd_xTi_3O_{12}$ (x=0.2, 0.4, 0.6 and 0.8) has been studied.

Figure 4-6 shows the remnant polarization dependence on switching cycles for BNT0.2, BNT0.4, BNT0.6 and BNT0.8 annealed at various temperatures, such as 550 °C, 600 °C, 650 °C and 700 °C. A marked increase of polarization from 1 to 10^6 switching cycles is found in BNT0.2-700 and BNT0.4-700, which has been reported as a wake-up behavior in bismuth layer ferroelectric films.[15-17] For the composition of $Bi_{3.8}Nd_{0.2}Ti_3O_{12}$, all the films annealed at various temperatures exhibit an increase of polarization from 1 to 10^6 cycles, and BNT0.2-700 shows the largest increase. As shown in Fig. 4-6(a), It is interesting to find that the higher the increase annealing temperature, the pronounced the increase of polarization in BNT0.2 films.

Moreover, it is clear that annealing temperature play an important role on the fatigue behavior for the lowest substitution (BNT0.2), whereas, with the increase of Nd substitution, this effect of annealing temperature on fatigue behavior becomes slighter. For BNT0.6, all the films exhibit nearly the same fatigue behavior, suggesting that the effect of annealing temperature on fatigue behavior is little for BNT0.6.

In conclusion, not only the composition but also the annealing temperature plays an important role on the fatigue behavior of BNTx ferroelectric thin films. In the following part, how the annealing temperature and composition affect the fatigue behavior would be discussed in detail.

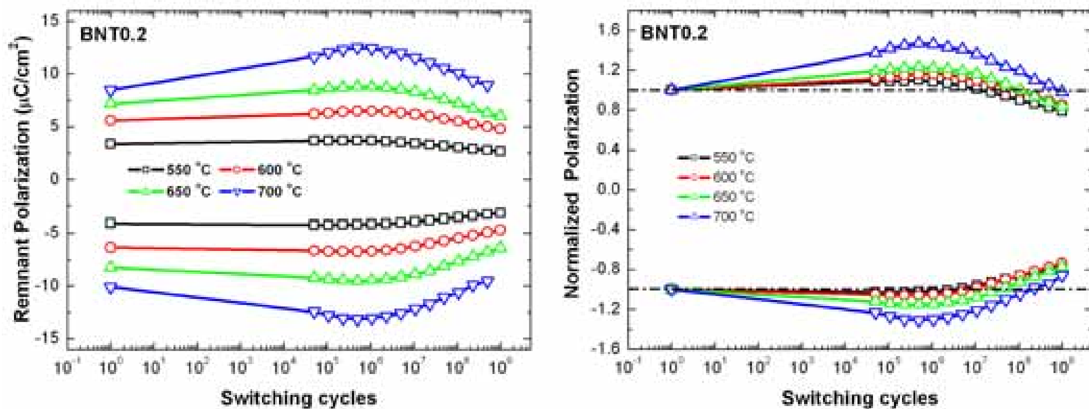

(a)

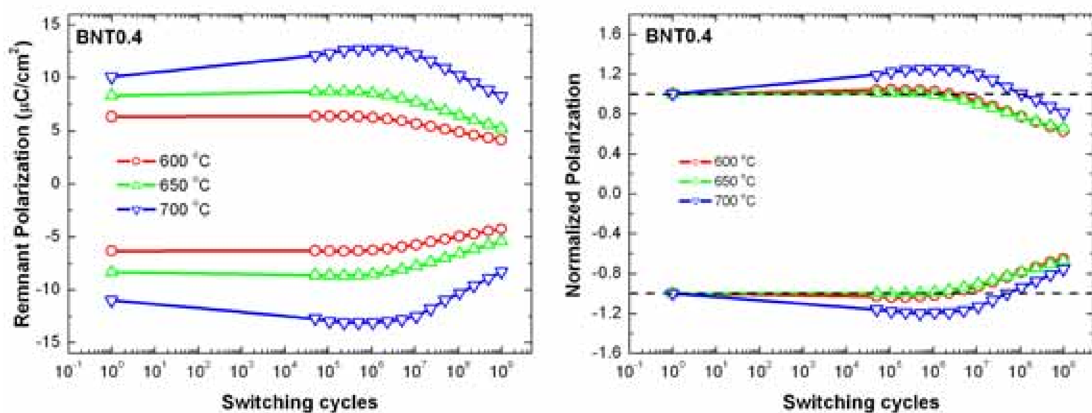

(b)

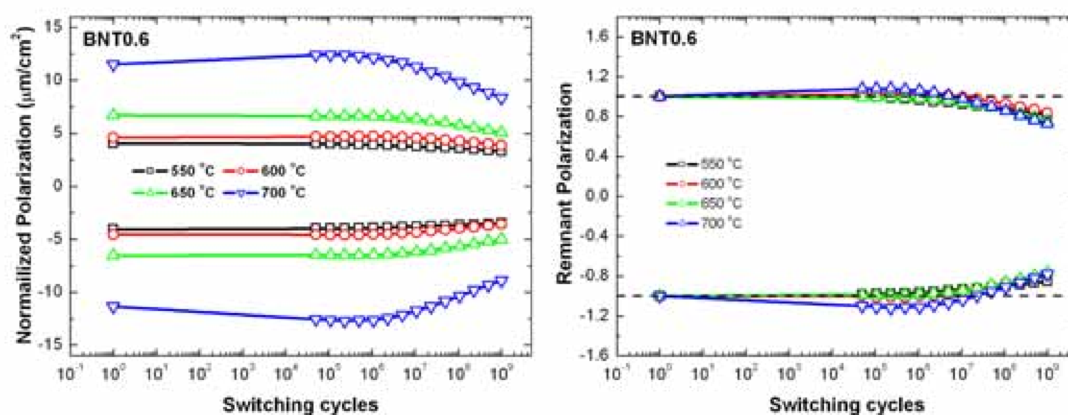

(c)

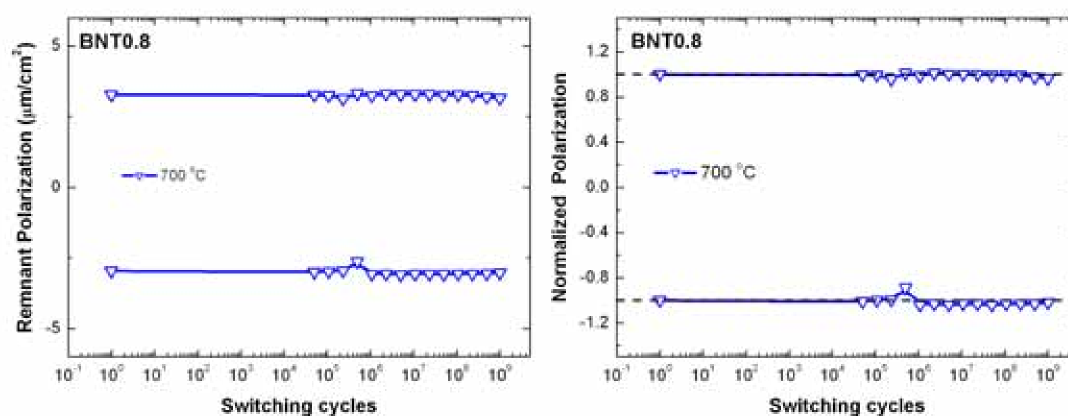

(d)

Fig. 4-6 Dependence of remnant polarization and normalized polarization on switching cycles of BNT0.2 (a), BNT0.4 (b), BNT0.6 (c), BNT0.8 (d).

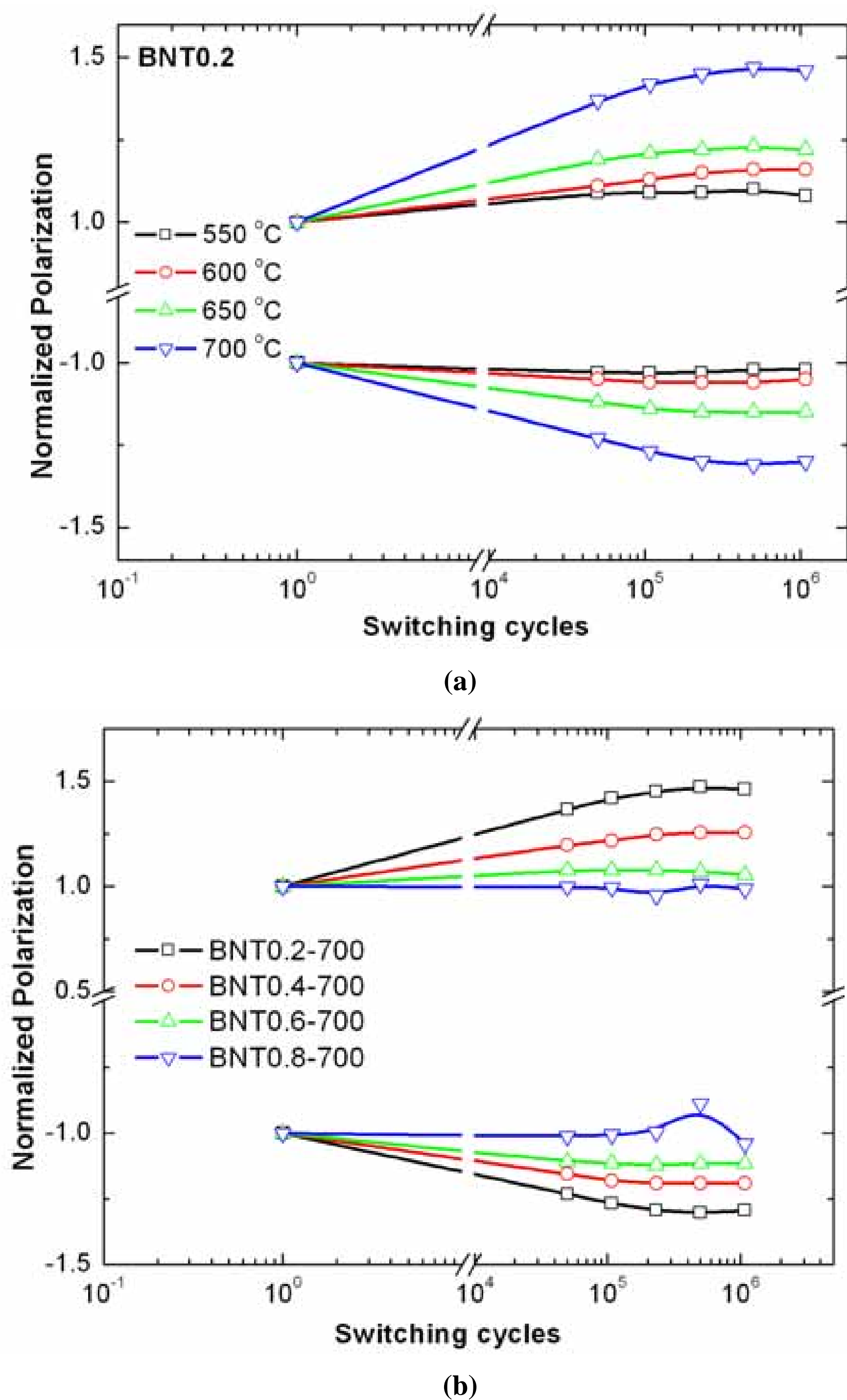

Fig. 4-7 Dependence of normalized polarization on switching cycles from 1-10^6 (a) BNT0.2-T (T=550, 600, 650 and 700 ^{o}C); (b) BNTx-700 (x=0.2, 0.4, 0.6, and 0.8)

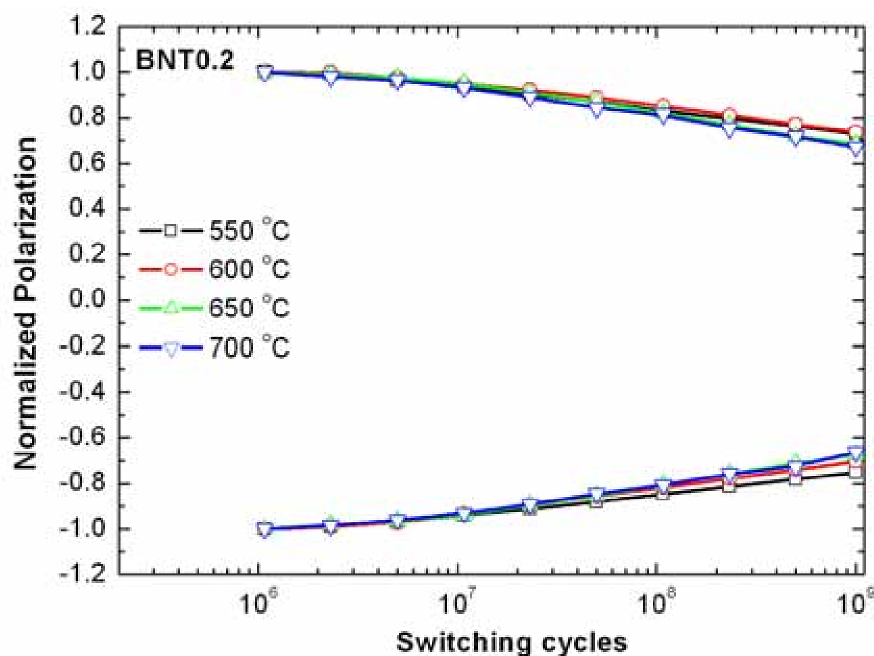

(a)

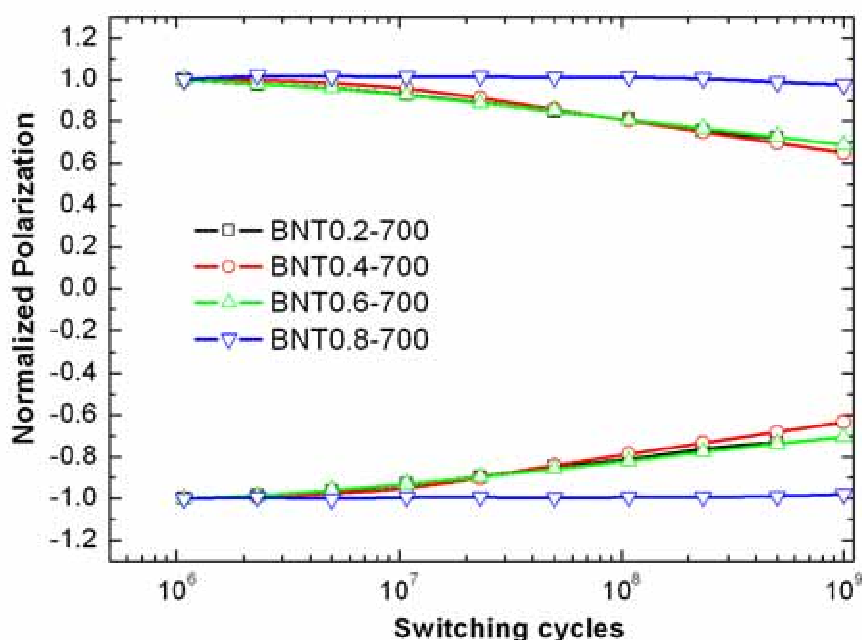

(b)

Fig. 4-8 Dependence of normalized polarization on switching cycles during 10^6-10^9 (a) BNT0.2-T (T=550, 600, 650 and 700 °C); (b) BNTx-700 (x=0.2, 0.4, 0.6, and 0.8)

For the BNT0.2-T (T=550, 600, 650, and 700 °C) and BNTx-700 (x=0.2, 0.4, 0.6, and 0.8), the dependence of the normalized increase of polarization from 1-10^6 cycles is shown in Fig. 4-7. It shows that with the increase of substitution, the increase of

polarization becomes weaker. Moreover, the increase of polarization becomes more pronounced at high annealing temperature. It suggests that this increase of polarization depends on the composition and annealing temperature.

For the BNT0.2, BNT0.4 and BNT0.6, a decrease of polarization could be found from 10^6-10^9 cycles, as shown in Fig. 4-6(a-c). To compare this decrease for all the composition, the dependence of this normalized polarization decrease on switching cycles during 10^6-10^9 is shown in Fig. 4-8. It should be noted that BNT0.2-700, BNT0.4-700 and BNT0.6-700 exhibit a nearly same decrease from 10^6 to 10^9 cycles which is about 35%. BNT0.2 shows almost the same decrease of polarization from 10^6-10^9 cycles regardless of annealing temperature. It demonstrates that the decrease of polarization from 10^6-10^9 cycles does not closely relate to the composition and annealing temperature of BNT films.

From the analysis above, it is clear that the fatigue behavior of BNT films consist of two parts: (1) an increase of polarization in 1-10^6 cycles (2) a decrease of polarization in 10^6-10^9 cycles. Additionally, the increase of polarization from 1-10^6 cycles shows some relationship with the composition and annealing temperature of films, whereas, the decrease of polarization exhibits relatively weak relationship with the composition and annealing temperature of films in 10^6-10^9 cycles. Therefore, it is proposed that the mechanisms of the increase of polarization in 1-10^6 cycles and the decrease of polarization in 10^6-10^9 cycles are different.

The increase of polarization from 1 to 10^6 cycles was attributed to the releasing of the pinning domain in bismuth layered ferroelectric thin film.[3,17] So far the origin of the decrease of polarization from 10^6 to 10^9 cycles is still ambiguous.

4.4 CONCLUSIONS

$Bi_{4-x}Nd_xTi_3O_{12}$ ferroelectric films were fabricated by chemical solution deposition method. The precursor solutions were also prepared in laboratory by using bismuth nitrate $Bi(NO_3)_3 \cdot 5H_2O$, n-tetrabutyl titanate $(C_4H_9O)_4Ti$ and neodymium nitrate $Nd(NO_3)_3 \cdot 5H_2O$. Several compositions such as $Bi_{3.8}Nd_{0.2}Ti_3O_{12}$, $Bi_{3.6}Nd_{0.4}Ti_3O_{12}$, $Bi_{3.4}La_{0.6}Ti_3O_{12}$, $Bi_{3.2}Nd_{0.8}Ti_3O_{12}$, and $Bi_{3.0}Nd_{1.0}Ti_3O_{12}$ were prepared at annealing temperatures of 550 ^oC, 600 ^oC, 650 ^oC, and 700 ^oC. XRD patterns show that all the prepared films exhibit a single phase, and SEM micrographs show that the thickness of fabricated films is about 130 nm.

Ferroelectric measurements including hysteresis loop and fatigue property were carried out on $Bi_{4-x}Nd_xTi_3O_{12}$ ferroelectric films. Due to the large grain size, the films

fabricated at higher annealing temperature exhibit higher polarization. Moreover, substitution of Nd suppresses the grain growth of $Bi_{4-x}Nd_xTi_3O_{12}$, which results in the low polarization of $Bi_{4-x}Nd_xTi_3O_{12}$ films with high concentration of Nd. The fatigue behavior of $Bi_{4-x}Nd_xTi_3O_{12}$ ferroelectric films could be divided into two parts: 1) an increase of polarization in 1-10^6 cycles; 2) a decrease of polarization in 10^6-10^9 cycles. With the increase of Nd substitution, the fatigue resistance increases, and a fatigue-free behavior is found in $Bi_{3.2}Nd_{0.8}Ti_3O_{12}$ films. Based on the analysis, the mechanisms of the increase of polarization in 1-10^6 cycles and the decrease of polarization were found to be different.

REFERENCES

[1] J. F. Scott, and C. A. Paz de Araujo, *Science*, **246**, 1400(1989).

[2] B. H. Park, B. S. Kang, S. D. Bu, T. W. Noh, J. Lee and W. Jo, *Nature*, (London) **401**, 682 (1999).

[3] D. Wu, A. Li, T. Zhu, Z. Li, Z. Liu, and N. Ming, *J. Mater. Res.*, **16**, 1325 (2001).

[4] H. N. Lee, D. Hesse, N. Zakharow, and U. Gösele, *Science*, **296**, 2006 (2002).

[5] T. Kojima, T. Sakai, T. Watanabe, H. Funakubo, K. Saito, and M. Osada, *Appl. Phys. Lett.*, **80**, 2746 (2002).

[6] D. Wu, A. Li, and N. Ming, *J.Appl. Phys.*, **95**, 4275 (2004).

[7] T. Watanabe, H. Funakubo, M. Osada, H. Uchida and I. Okada, *J. Appl. Phys.*, **98**, 024110 (2005).

[8] C. J. Lu, Y. Qiao, Y. J. Qi, X. Q. Chen, and J. S. Zhu, *Appl. Phys. Lett.*, **87**, 222901 (2005).

[9] Y. Noguchi, M. Miyayama, *Appl. Phys. Lett.*, **78**, 1903 (2001).

[10] H. Irie, H. Saito, S. Ohkoshi, and K. Hashimoto, *Adv. Mater.*, **17**, 491 (2005).

[11] H. N. Al-shaareef, B. A. Tuttle, W. L. Warren, T. J. Headley, D. Dimos, J. A. Voige, and R. D. Nasby, *J. Appl. Phys.*, **79**, 1013 (1996).

[12] D. Dimos, H. N. Al-Shareef, W. L. Warren, and B. A. Tuttle, *J. Appl. Phys.*, **80**, 1682 (1994).

[13] P. H. Xiang, Y. Kinemuchi, K. Watari, *Mater. Lett.*, **60**, 2837 (2006).

[14] X. S. Gao, J. M. Xue, and J. Wang, *J. Appl. Phys.*, **98** (2005) 104106.

[15] D. Wu, A. Li, T. Zhu, Z. Liu and N. Ming, *J. Appl. Phys.*, **88** (2000) 5941.

[16] D. Wu, A. Li, T. Zhu, Z. Liu and N. Ming, *J. Appl. Phys.*, **76** (2000) 2208.

[17] D. Dimos, H. N. Al-Shareef, W. L. Warren, and B. A. Tuttle, *J. Appl. Phys.*, **80** (2000) 1682.

.

Chapter 5

Ferroelectric Behavior of $Bi_{4-x}La_xTi_3O_{12}$ Thin Films

In this chapter, $Bi_{4-x}La_xTi_3O_{12}$ (BLT) (x=0.2, 0.4, 0.6 and 0.8) was fabricated by chemical solution deposition (CSD). The behavior of dielectric permittivity (ε), remnant polarization (P_r), and coercive field (E_c) as a function of switching cycles was studied. A decrease of dielectric permittivity (ε) with increase of switching cycles was firstly found in BLT films, demonstrating the existence of a growing dielectric layer during fatigue process. The decrease of dielectric permittivity (ε) of $Bi_{3.8}La_{0.2}Ti_3O_{12}$ due to switch cycling is much more pronounced than that of $Bi_{3.2}La_{0.8}Ti_3O_{12}$. $Bi_{4-x}La_xTi_3O_{12}$ with low concentration of lanthanum (x=0.2 and 0.4) exhibits an increase of polarization with electric field cycling up to 10^6 switching cycles and a remarkable increase of coercive field (E_c) with electric field cycling up to 10^9 cycles. However, these behaviors have not been found in $Bi_{4-x}La_xTi_3O_{12}$ with high concentration of lanthanum (x=0.6 and 0.8), which is attributed to a suppression effect of lanthanum on forming pre-existing defect. With an increase of lanthanum concentration, fatigue resistance increases. $Bi_{3.2}La_{0.8}Ti_3O_{12}$ capacitor exhibits a nearly unchangeable polarization with electric field cycling (±5V, 400 kV/cm) up to 10^9 switching cycles at 50 kHz. It is proposed that the fatigue behavior of BLT films correlates to a redistribution of pre-existing defect from interior BLT to electrode, which results in weakening of domain pinning and forming a dielectric layer between BLT and the electrode.

5.1 INTRODUCTION

Ferroelectric thin films have attracted great attention for application in nonvolatile ferroelectric random access memories (NVFeRAM) integrated with existing Si complimentary metaloxide-semiconductor (CMOS) transistor circuitry.[1,2] Several material systems, such as $Pb(Zr_xTi_{1-x})O_3$(PZT), $SrBi_2Ta_2O_9$ (SBT) and $Bi_4Ti_3O_{12}$ (BiT), have been considered as promising candidates in NVFeRAM,. Considering the long-term reliability of such a device, polarization fatigue is one of the most important factors for the NVFeRAM application of ferroelectric thin films. Fatigue is a decrease in switchable polarization with electric field cycling in ferroelectrics. PZT configured with platinum (Pt) electrodes exhibits severe polarization fatigue, and one solution is to

fabricate PZT thin film on the conducting oxide electrodes, involving (La,Sr)CoO_3 (LSCO),[3] $YBa_2Cu_3O_x$ (YBCO) [4] and RuO_2 [5]. However, it results in high leakage current as well as being complex preparation process.[6,7] Therefore, fatigue-free ferroelectric materials have an advantage over PZT-based ferroelectrics with metal electrodes such as Pt electrode. As a kind of primary fatigue-free ferroelectric material, layered perovskite ferroelectric shows essentially no polarization fatigue with electric field cycling.[1,2] Moreover, an increase of polarization at the initial period of cycling has been reported in fatigue-free ferroelectric thin films,[8,9] which has not been well explained. This kind of materials consist of fluorite-like $[Bi_2O_2]^{2+}$ and perovskite-like $[A_{n-1}B_nO_{3n+1}]^{2-}$ layers, where n=2, 3, 4, and 5.[10,11] So far, several models have been proposed to explain the fatigue-free characteristics in bismuth layered ferroelectric, such as domain wall pinning and unpinning,[12,13] stability of oxygen of perovskite layer,[14] and space charges compensated by a self-regulating $[Bi_2O_2]^{2+}$ layer[1]. However, the primary mechanism of the fatigue-free properties of bismuth-layer ferroelectrics is still ambiguous, and as important parameters in ferroelectric thin film, the coercive field and especially dielectric permittivity (ε) have seldom been considered in studying the fatigue mechanism of bismuth-layer ferroelectric thin film. The main object of this work is to propose the fatigue mechanism in bismuth-layer ferroelectric in accordance with the dependence of polarization, the coercive field and dielectric permittivity (ε) on switching cycles. Moreover, the dependence of substitution concentration on the fatigue behavior in bismuth-layered ferroelectric film is the second subject of this work. Because of the possible influence of La concentration on defect concentration in bismuth-layer materials, $Bi_{4-x}La_xTi_3O_{12}$ (BLT) was selected, and lanthanum (La) were doped to modify the fatigue behavior. The lanthanum dependent fatigue behavior including polarization and coercive field was investigated. Moreover, variation of dielectric permittivity during fatigue process was found. Finally, the origin of fatigue behavior in BiT-based ferroelectric was proposed.

5.2 EXPERIMENT

Thin films were fabricated by the metal organic solution deposition (MOSD) technique. Bismuth nitrate $Bi(NO_3)_3{\cdot}5H_2O$, n-tetrabutyl titanate $(C_4H_9O)_4Ti$ and lanthanum nitrate $La(NO_3)_3{\cdot}6H_2O$ were selected as starting materials. The details of the precursor solution preparation were similar to Wu *et al*.[15] After filtering, the precursor solution was spin-coated on a substrate with a structure of Pt(200nm)/TiO_2(50nm)/SiO_2(500nm)/Si fabricated from Panasonic company. Spinning

was carried out at a speed of 3000rpm for 30 s. The deposited film was dried on a hot plate at 260 °C for 10 min and then annealed using a heating program in a Rapid Thermal Annealing (RTA) furnace at air or O_2 atmosphere. The heat treatment process

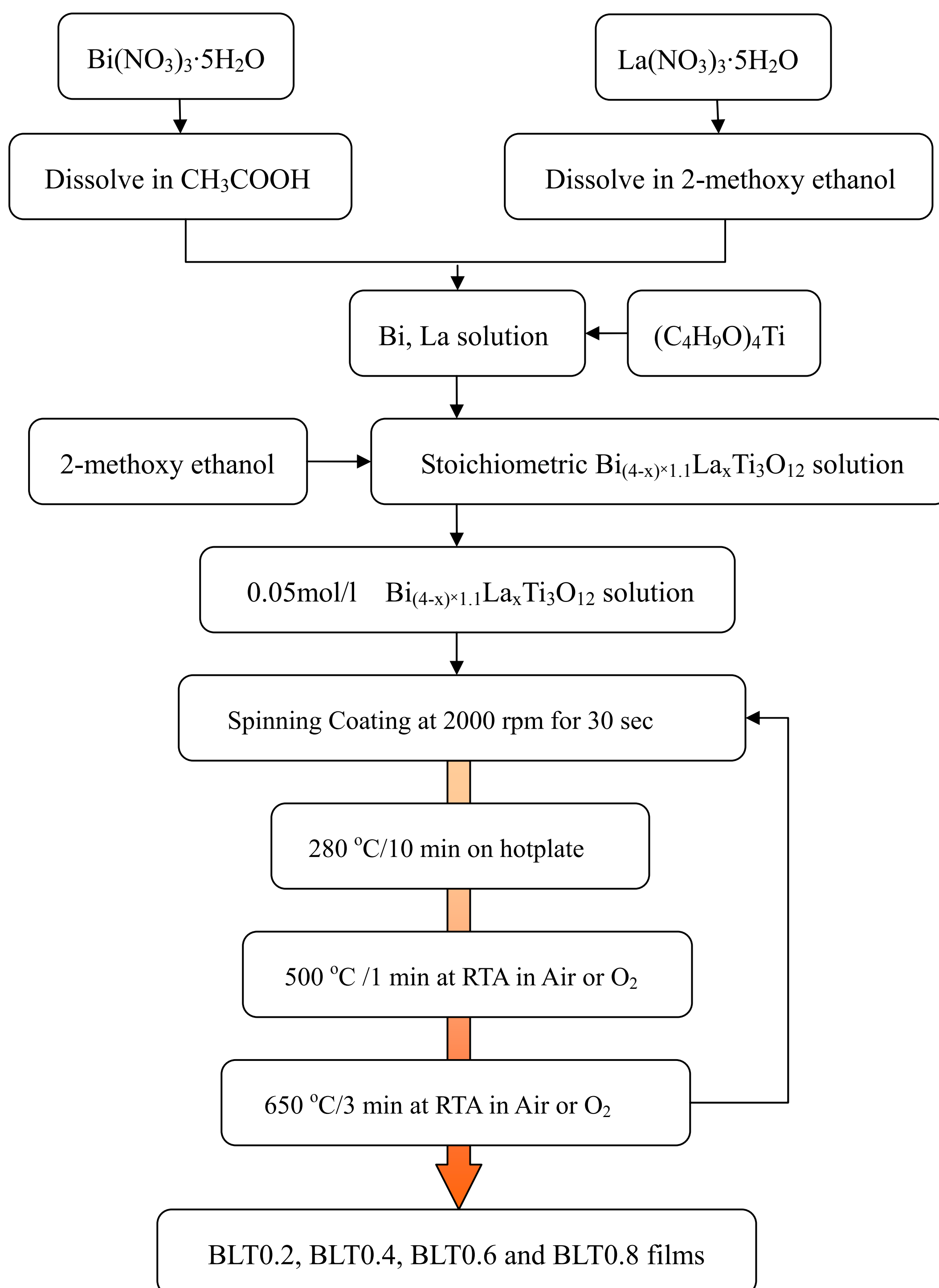

Fig. 5-1 Fabrication flow chart for BLTx ferroelectric films.

consisted of two parts: one was increasing the temperature to 500 ^{o}C at a rate of 100 ^{o}C/sec, and the other is keeping the temperature at 500 ^{o}C for 60 s, and then jumping to 650 ^{o}C for 180 s. Four compositions, $Bi_{3.8}La_{0.2}Ti_3O_{12}$, $Bi_{3.6}La_{0.4}Ti_3O_{12}$, $Bi_{3.4}La_{0.6}Ti_3O_{12}$, $Bi_{3.2}La_{0.8}Ti_3O_{12}$ were prepared, which is abbreviated as BLT0.2, BLT0.4, BLT0.6 and BLT0.8, respectively. The fabrication process is shown in Fig. 5-1. For ferroelectric measurement, a Pt top electrode in the form of 100 μm dots and 200 nm thickness was deposited using a shadow mask at room temperature. Fatigue measurements were carried out at room temperature using TF analyzer 2000 (aixACCT) at 50 kHz up to 10^9 cycles. Capacitance measurements were carried out at room temperature using *LCR* meter (HP 4194A)

5.3 RESULTS

5.3.1 Crystalline phase and morphology

As shown in Fig. 5-2, X-ray diffraction (XRD) patterns show that all samples exhibit a well-crystallized phase, and no secondary phase is found. All the peaks are indexed according to standard powder diffraction data of $Bi_4Ti_3O_{12}$ (PDF#73-2181). As reported by Wu *et al.*,[15] the coincidence of peak position with those of $Bi_4Ti_3O_{12}$ powders suggests that La substitution does not change the lattice symmetry of $Bi_4Ti_3O_{12}$. As mentioned in chapter 4, substitution plays a role on grain growth. Moreover, it was reported that substitution of La exhibits influence on the grain orientation, which can be seen from the change of peak intensities relative to the (117) peak. The intensity ratio $\frac{I(006)}{I(006)+I(117)}$ (here, *I* stands for peak intensity) is used to estimate the degree of (00*l*) plane orientation. The values of the $\frac{I(006)}{I(006)+I(117)}$ are shown in Tab. 5-1. The value of BLT0.6 is largest, suggesting that relatively more grain volumes with (00*l*) plane exist in BLT0.6 films, which agrees with previous report.

Thickness of BLT films were about 125nm from scanning electron microscopy (SEM) image of BLT/substrate cross section view, as shown in Fig. 5-3.

Tab. 5-1 Degree of (00*l*) plane orientation.

	BLT0.2	*BLT0.4*	*BLT0.6*	*BLT0.8*
$\frac{I(006)}{I(006)+I(117)}$	0.45	0.54	0.75	0.34

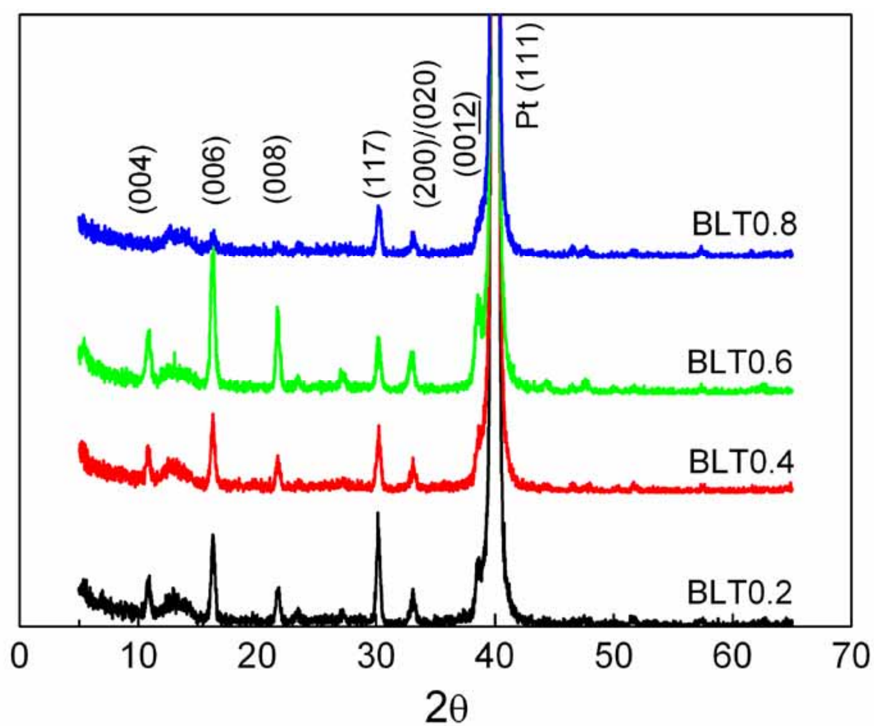

Fig. 5-2 XRD patterns for BLTx (x=0.2, 0.4, 0.6, 0.8, and 1.0) annealed at 650 °C.

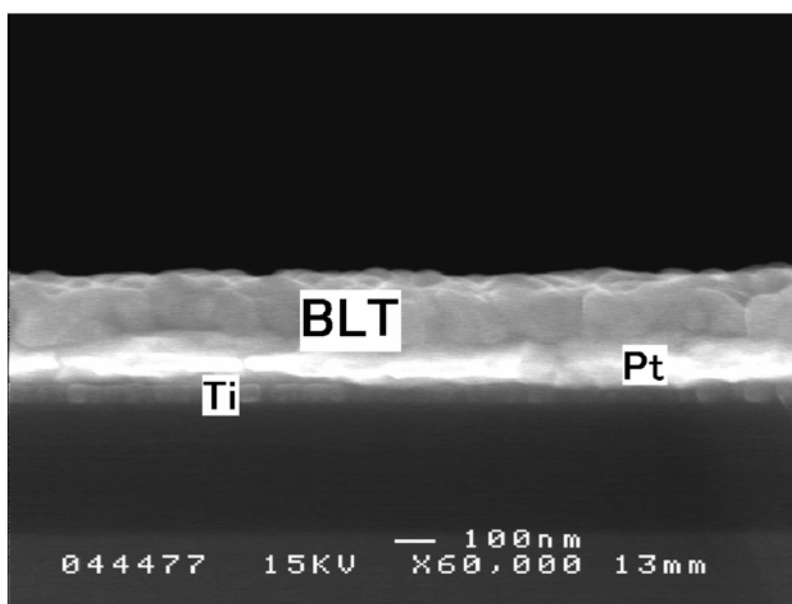

Fig. 5-3 SEM image of cross section of BLT film.

5.3.2 Ferroelectric characteristics

5.3.2.1 Remnant polarization and coercive field

The applied voltage dependence of remnant polarization (P_r) and coercive field (E_c) is shown in Fig. 5-4, which agrees with Wu *et al.*[15] Even though saturated P_r and E_c vary with La concentration, all compositions exhibit nearly saturated P_r and E_c at an applied voltage of 5V (about electric field of 400 kV/cm). Similar to neodymium (Nd)-substituted BiT,[16] P_r of the BLT ferroelectric films increase with at a low concentration of Nd or La substitution, while decrease markedly at higher concentration. Similar with substitution Nd in chapter 4, La substitution results in an increase of interior polarization due to its influence on crystal structure, and a decrease of polarization due to suppression of grain growth, and these two factors are in competition. Coercive field is independent on La substitution, and all films show similar coercive fields at the same applied voltage.

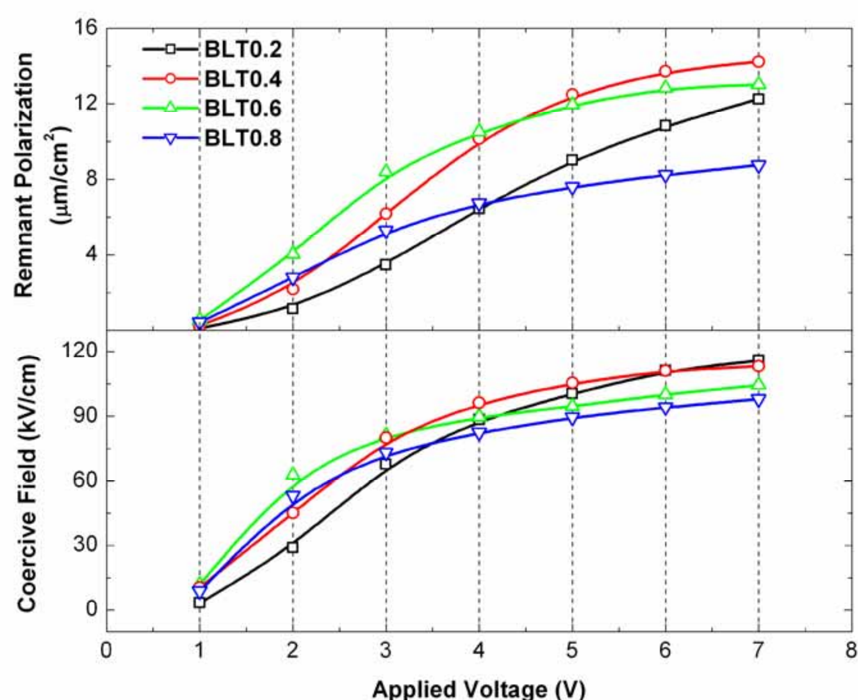

Fig. 5-4 Remnant Polarization (P_r) and coercive field (E_c) of Pt//BLT//Pt as a function of maximum applied voltage.

5.3.2.2 Fatigue characteristic

Figure 5-5 shows P_r variation of BLT films with electric field cycling at 5V and 50 kHz up to 10^9 switching cycles. As shown in Fig. 5-5, BLT0.8 exhibits fatigue-free behavior and BLT0.6 exhibits a little polarization fatigue, while significant P_r decrease

of 15% is observed in BLT0.4 after 10^9 switching cycles. This suggests that polarization suppression decreases with an increase of La concentration in BiT ferroelectric. Therefore, fatigue-free behavior is found in BiT doped with high concentration La. In other words, La substitution improves the fatigue resistance of BiT ferroelectrics, and the more La that is doped into BiT, the better the fatigue properties of BiT ferroelectrics becomes. Even though there are extensive reports on substitute effects, such as La^{3+}, In^{3+}, Zr^{4+} and N^{3-}, on ferroelectric properties of BiT ferroelectric film,[15,17-19] to our knowledge, investigation on substitute concentration dependence of fatigue behavior is rare.

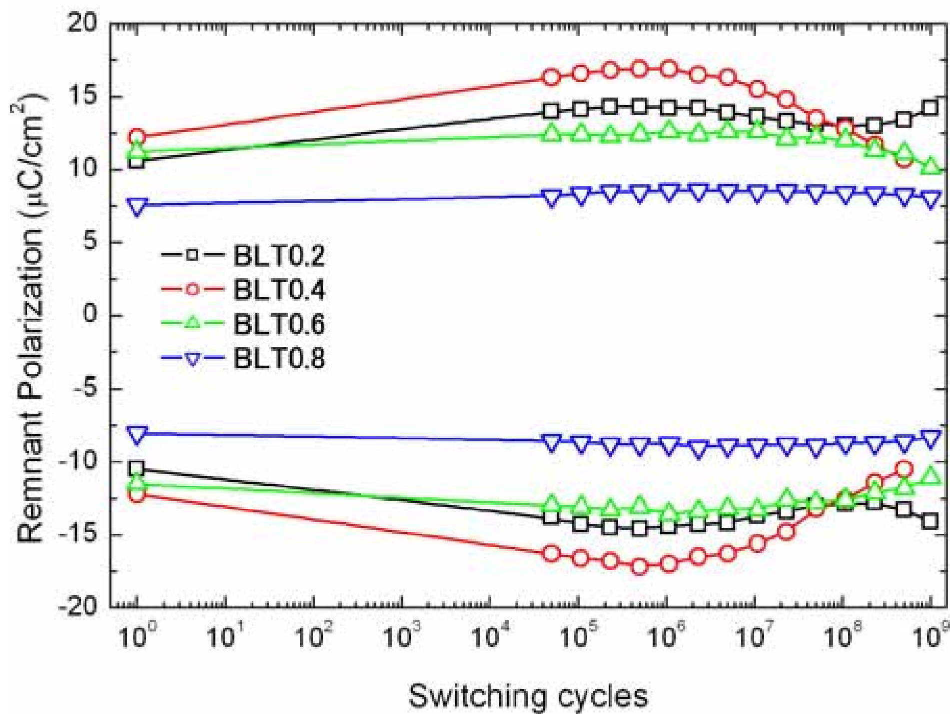

Fig. 5-5 Fatigue behavior of Pt//BLT//Pt capacitors with a fatigue voltage of 5V (about 400 kV/cm) at 50 kHz up to 10^9 cycles.

Moreover, a marked increase of P_r with initial switching cycles to 10^6 was found in BLT0.2 and BLT0.4. The increase of polarization with increase of switching cycles has been previously reported for $Pb(Zr_xTi_{1-x})O_3$ (PZT) and $SrBi_2Ta_2O_9$ (SBT) ferroelectric film. [8,9] It is proposed to be due to the unlocking of domains that were initially pinned during fabrication. However, the reason that pinned domains could be released by switching cycles has not been discussed in detail. To identify the change between initial films and fatigued films, the polarization-electric field (P-E) hysteresis loops of BLT films before and after switch 10^6 cycles were plotted, as shown in Fig. 5-6. More

saturated P-E loops are obtained in BLT0.2 and BLT0.4 after 10^6 switching cycles, which agrees with the estimation that the pinned domains are released. However, BLT0.6 and BLT0.8 exhibit nearly the same P-E loops up to 10^6 switching cycles, demonstrating that the releasing effect of pinned domains is weaker than those in BLT0.2 and BLT0.4. We believe that it could be attributed to the effect of La substitution on the concentration of defects, such as oxygen vacancies and bismuth vacancies in BLT ferroelectric films.[20,21]

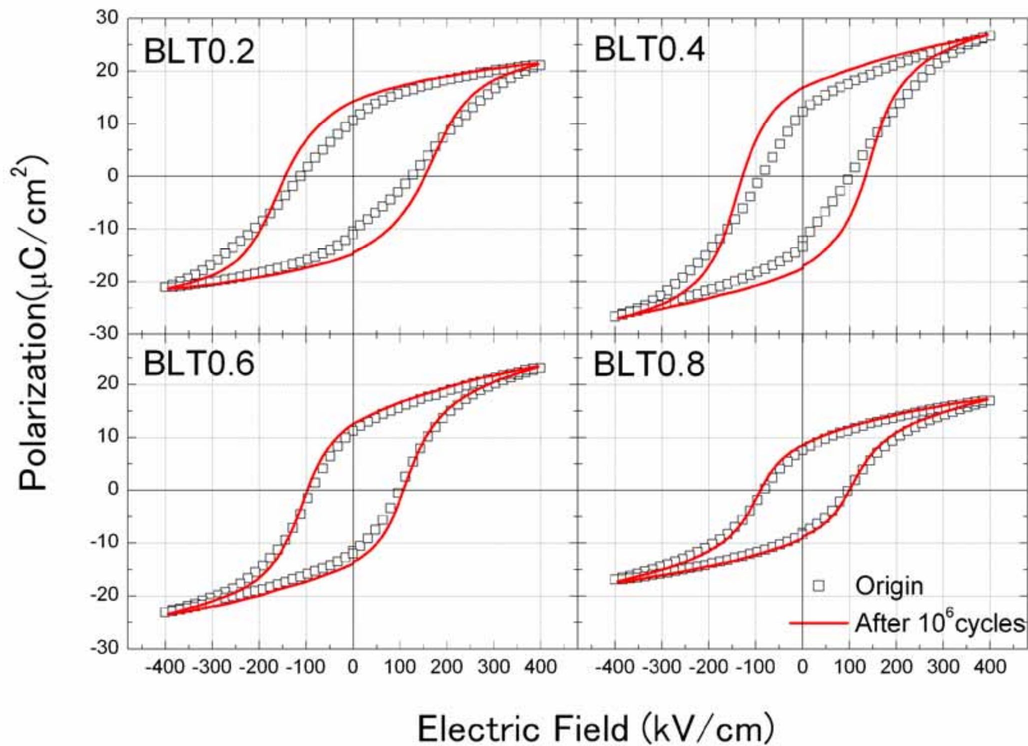

Fig. 5-6 P-E hysteresis loop of Pt//BLT//Pt before and after 10^6 switching cycles (at 5V).

As another important parameter, E_c was also investigated in the current work. It is found that E_c varies with electric field cycling too, and Fig. 5-7 shows the switching cycle dependence of E_c. As shown in Fig. 5-7, BLT0.2 and BLT0.4 exhibit higher E_c than those of BLT0.6 and BLT0.8, and E_c of BLT0.2 increases with increase of switching cycles, while E_c of BLT0.6 and BLT0.8 show only a little change. It is proposed that the variation of E_c with increase of switching cycles could be explained by a dielectric layer mode,[22,23] which was often employed to discuss the thickness dependence of E_c and the dielectric permittivity (ε) in $Ba(Sr_xTiO_{1-x})_3$ and PZT films with metal electrode.

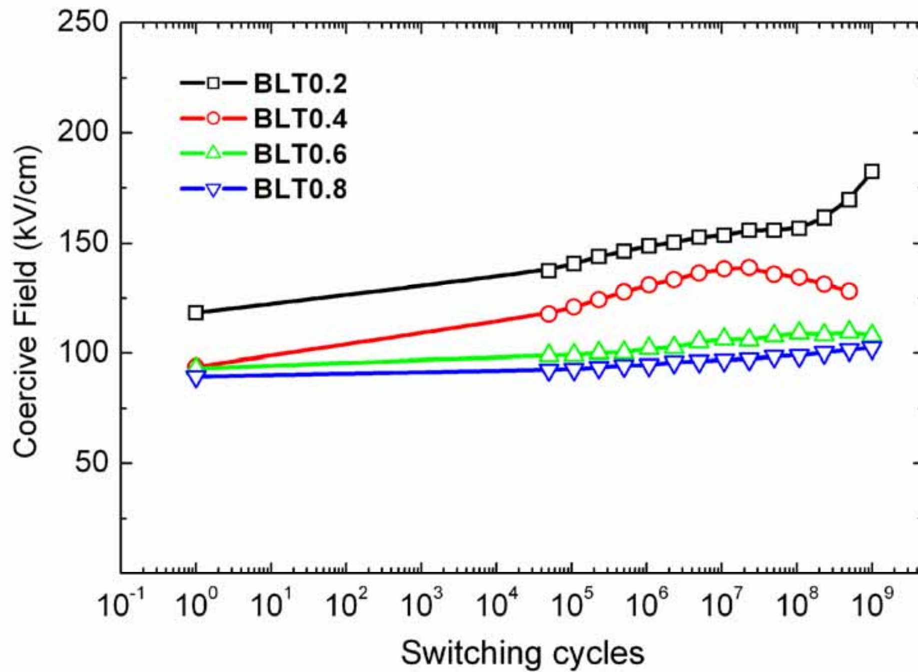

Fig. 5-7 Coercive Field (E_c) of Pt//BLT//Pt capacitors as a function of switching cycles.

Previous works have reported that the existence of a low-dielectric layer always accompanies with the variation of dielectric permittivity (ε).[22] Even though, some researchers proposed the existence of an interface layers in BiT-based ferroelectric films,[24, 25] potential relationship between this interface and fatigue characteristics were rarely discussed so far. To our knowledge, current work is the first time to investigate the dependence of ε on switching cycles in BiT-based ferroelectric films. The Dielectric measurement was carried out on BLT films before fatigue and after fatigue process. Figure 5-8 (a, b) shows the capacitance of BLT0.2 and BLT0.8 before fatigue and after 10^6, 10^7, 10^8 or 10^9 cycling. It is found the more switching cycles, the lower the dielectric permittivity (ε) became. It shows a strong evidence of an interface layer in BLT ferroelectric films.

Moreover, the dependence of normalized permittivity on switch cycles is shown in Fig. 5-9, exhibiting that a pronounced decease of permittivity (ε) was found in BLT0.2 due to fatigue process, while a slight decrease of dielectric permittivity (ε) was found in BLT0.8 films. It is proposed that the thickness of this interface increases with increase of switching cycles, which is attributed to the migration of the defect, such as oxygen vacancies in BLT films s, and the details of this mechanism will be discussed in the following chapter.

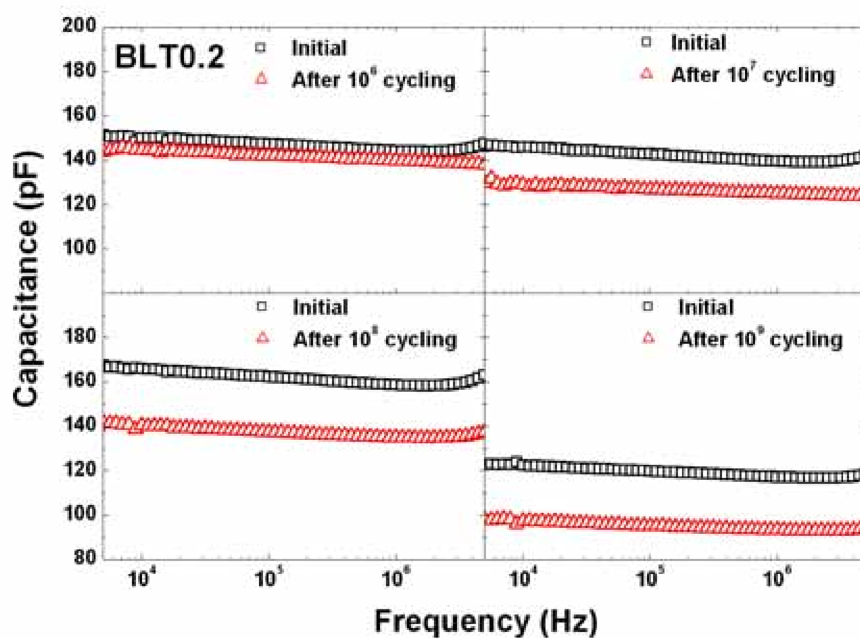

(a)

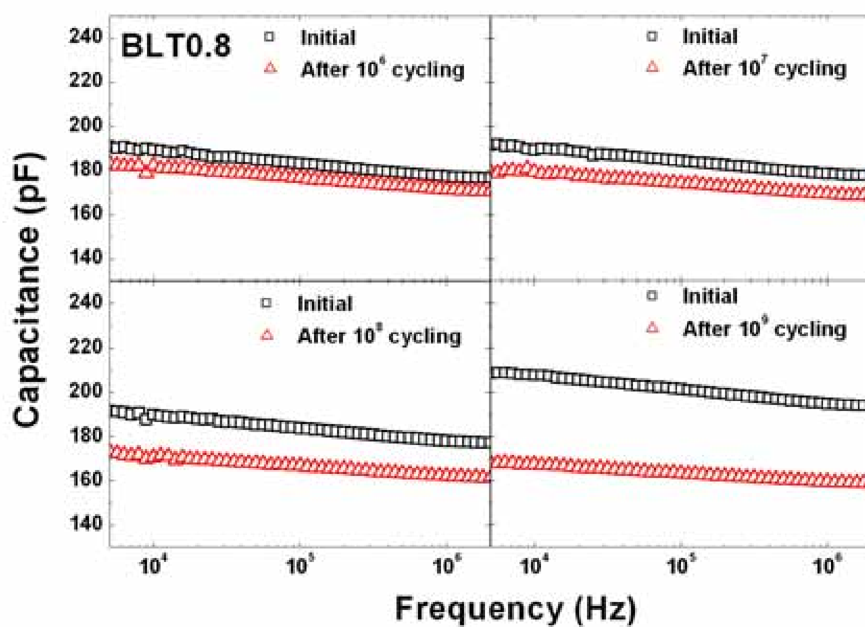

(b)

Fig. 5-8 Capacity of Pt//BLT0.2//Pt (a) and Pt//BLT0.8//Pt (b) capacitors as a function of switching cycles.

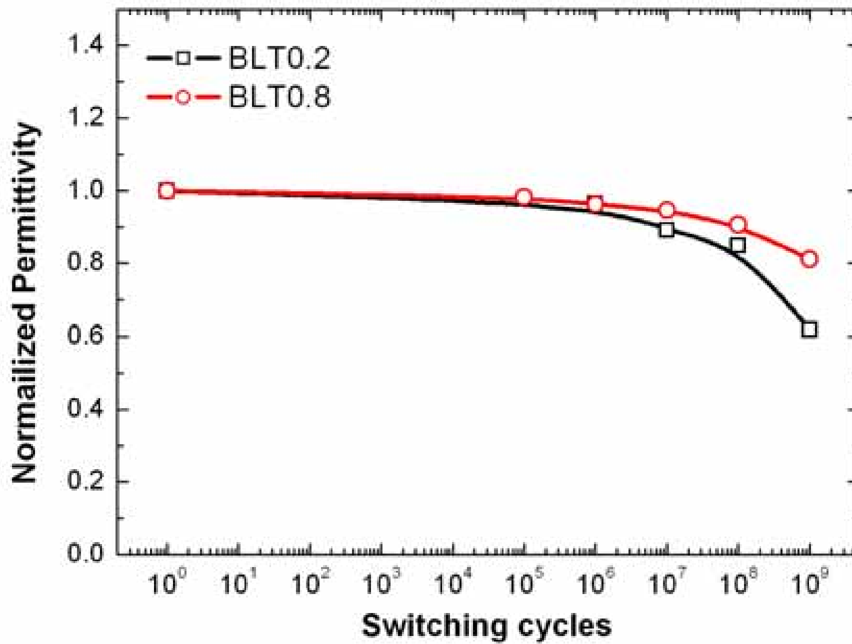

Fig. 5-9 Dependence of normalized permittivity of BLT0.2 and BLT0.8 on switching cycles.

5.4 DISCUSSION

Recently, the fatigue behavior of ferroelectrics has been attributed to space charge as well as oxygen vacancies in many research reports. Scott *et al.*[26] reported a reduction of oxygen near the electrode after fatigue, demonstrating that fatigue behavior correlates to the increase of oxygen vacancy. Investigation on PZT/RuO_x showed that fatigue properties were improved with an increase of oxygen content in RuO_x electrode,[27] indicating that the increase of fatigue resistance came from the decrease of oxygen vacancies. It has also been suggested that domain pinning by oxygen vacancies contributes to the polarization fatigue behavior in ferroelectric such as PZT.[9,13] These results show the important role of oxygen vacancies on fatigue behavior of ferroelectric thin films. In chapter 3, we have confirmed the existence of oxygen vacancies in BLT films.[20,21]

In the current work, behaviors of polarization, coercive field (E_c) and dielectric permittivity (ε) in the process of fatigue have been discussed. As expected, La substitution plays an important role on oxygen vacancies concentration in BLT films. We believe that variations of polarization, coercive field (E_c) and dielectric permittivity (ε) with switching cycles are attributed to the redistribution of the oxygen vacancies due to external electric field cycling in BLT films.

As mentioned above, BLT0.2 and BLT0.4 exhibit an increase of polarization with

increase of switching cycles up to 10^6 cycles, while this behavior is absent in BLT0.6 and BLT0.8. It is expected that an increase of La substitution results in reducing concentration of oxygen vacancies. He *et al.* [28] suggested that a strong domain-pinning happens only if a significant number of oxygen vacancies accumulate at the domain wall. Compared to BLT0.6 and BLT0.8, there are more pre-existing oxygen defects in BLT0.2 and BLT0.4, therefore, domain pinning by oxygen vacancies becomes strong. However, an external electric field cycling may result in migrating of oxygen vacancies from the interior film to the electrode,[29] and form a dielectric layer between the electrode and the interior BLT film, which has been observed by Jin *et al.*[30] at (Ba,Sr)TiO_s/Pt interface. It is proposed here that releasing of the pinned domain due to the migrating of oxygen vacancies contributes to the increase of polarization with increase of switching cycles up to 10^6, as shown in Fig. 5-5, 5-6. However, further migration of oxygen vacancies from the interior film to the electrode formed a dielectric layer which may weaken the external field.[30] Consequently, it contributes electric field applied to interior BLT film decrease. Therefore, polarization of BLT0.2 and BLT0.4 decrease after 10^6 cycling. It should be noted that the shape of the P-E hysteresis loop of BLT0.2 becomes rounded with electric field cycling from 10^8 to 10^9 cycles, suggesting that leakage degradation happens. For BLT0.6 and BLT0.8, low concentration of pre-existing defects results in weak domain pinning, therefore, the influence of pinning-domain releasing and weakening external field due to formation of dielectric layer could be weak. In a conclusion, BLT0.6 and BLT0.8 exhibit stable polarization after 10^9 cycling.

Beside polarization, variation of the coercive field (E_c) with cycling could be also explained by the above mechanism. A marked increase of E_c with switching cycle is found in BLT0.2 and BLT0.4. There are many reports on increasing of E_c due to the decrease of thickness,[22,23,25] suggesting the importance of the dielectric layer when the thickness is small. In current results, the increase of E_c in BLT0.2 and BLT0.4 is attributed to the growth of the dielectric layer due to the extensive space charge accumulation. On the other hand, E_c with a stable value up to 10^9 cycling is found in BLT0.6 and BLT0.8, demonstrating that formation of the dielectric layer is weak due to the low concentration of pre-existing defects.

5.5 CONCLUSIONS

$Bi_{4-x}La_xTi_3O_{12}$ ferroelectric films are fabricated by chemical solution deposition process, and the precursor solution was also prepared in laboratory. The effect of substitute lanthanum (La) on fatigue behavior of $Bi_4Ti_3O_{12}$ has been investigated. It is found that fatigue resistance increases with the substitution concentration of La. In the $Bi_{4-x}La_xTi_3O_{12}$ (BLT) with a low concentration of La, an increase of polarization up to 10^6 switching cycles is found, which is absent in BLT with a high concentration of La. Variation of BLT fatigue behavior is proposed to be related to the suppression effect of La on pre-existing defects, such as oxygen vacancies in BiT ferroelectrics. A decrease of dielectric permittivity with increase of switching cycles shows strong evidence of a growing dielectric layer during fatigue process. By combining domain pinning unpinning model and dielectric layer model, a new mechanism of the fatigue characteristics of $Bi_{4-x}La_xTi_3O_{12}$ films has been proposed.

REFERENCES

[1] C. A. Araujo, J. D. Cuchiaro, L. D. Mcmillan, M. S. Scott and J. F. Scott, *Nature*, **374**, 627 (1995).

[2] B. H. Park, B. S. Kang, S. D. Bu, T. W. Noh, J. Lee and W. Jo, *Nature*, **401,** 682 (1999).

[3] J. Lee and R. Ramesh, *J. Appl. Phys.*, **68**, 484 (1996).

[4] V. G. Keramidas, D. K. Fork, J. Lee, and A. Safari, *Appl. Phys. Lett.*, **61**, 1537 (1992).

[5] S. D. Bernstein, T. Y. Wong, Y. Kisler, and R. W. Tustison, *J. Mater. Res.*, **8**, 12 (1993).

[6] P. C. Fazan, *Integ. Ferroelect.*, 4, 247 (1994).

[7] W. Kinney, *Integ. Ferroelect.*, 4, 131 (1994).

[8] D. Wu, A. Li, H. Ling, T. Yu, Z. Liu and N. Ming, *Appl. Phys. Lett.*, **76**, 2208 (2000).

[9] D. Dimos, H. N. Al-shareef, W. L. Warren, and B. A. Tuttle, *J. Appl. Phys.*, **80**, 1682 (1996).

[10] B. Aurivillius, *Ark. Kemi.*, **1,** 463 (1949).

[11] B. Frit, J. P. Mercurio, *J. Alloys Compds.*, **188,** 27 (1992).

[12] J. Chen, M. P. Harmer, and D. M. Smyth, *J. Appl. Phys.*, **68**, 5783 (1990).

[13] H. N. Al-shaareef, B. A. Tuttle, W. L. Warren, T. J. Headley, D. Dimos, J. A. Voige, and R. D. Nasby, *J. Appl. Phys.*, **79**, 1013 (1996).

[14] Z. G. Zhang, J. S. Liu, Y. N. Wang, J. S. Zhu, F. Yan, X. B. Chen, and H. M. Shen, *Appl. Phys. Lett.*, **73**, 788 (1998).

[15] D. Wu, A. Li, T. Zhu, Z. Li, Z. Liu, and N. Ming, *J. Mater. Res.*, **16**, 1325 (2001).

[16] T. Watanabe, H. Funakubo, M. Osada, H. Uchida and I. Okada, *J. Appl. Phys.*, **98**, 024110 (2005).

[17] S. T. Zhang, Y. F. Chen, J. Wang, G. X. Cheng, Z. G. Liu, and N. B. Ming, *Appl. Phys. Lett.*, **84**, 3660 (2004).

[18] Y. C. Chang and D. H. Kuo, *Appl. Phys. Lett.*, **89**, 072903 (2006).

[19] H. Irie, H. Saito, S. Ohkoshi, and K. Hashimoto, *Adv. Mater.*, **17**, 491 (2005).

[20] N. Zhong and T. Shiosaki, *J. Appl. Phys.*, **100,** 034107 (2006).

[21] N. Zhong, S. Okamura, K. Uchiyama, and T. Shiosaki, *App. Phys. Lett.*, **87**, 252901 (2005).

[22] P. K. Larsen, G. J. M. Dormans, D. J. Taylor, and P. J. van Veldhoven, J. *Appl. Phys.*, **76**, 2405 (1994).

[23] C. Zhou, and D. M. Newns, *J. Appl. Phys.*, **82**, 3081 (1997).

[24] K. T. Kim, S. H. Song, and C. Kim, *J. Vac. Sci. Technol.*, A **22**, 1315 (2004).

[25] X. S. Gao and J. Wang, *J. Appl. Phys.*, **99** 074103 (2006).

[26] J. F. Scott, C. A. Paz de Araujo, B. N. Melnick, L. D. McMillan, and R. Zuleeg, *J. Appl. Phys.*, **70**, 382 (1991).

[27] C. W. Law, K. Y. Tong, J. H. Li, K. Li and M. C. Poon, *Thin Solid Films*, **354**, 162 (1999).

[28] L. He and D. Vanderbilt, *Phys. Rev.*, B **68**, 134103 (2003).

[29] A. K. Tagantsev, M. Landivar, E. Colla, and N. Setter, *J. Appl. Phys.*, **78**, 2623 (1995).

[30] H. Z. Jin, J. Zhu, P. Ehrhart, F. Fitsilis, C. L. Jia, S. Regnery, K. Urban, and R. Waser, *Thin Solid Films*, **429**, 282 (2003).

Chapter 6

Proposed Model for Fatigue Behavior in $Bi_{4-x}R_xTi_3O_{12}$

Based on the results in chapters 2-5, a model of fatigue behavior in $Bi_{4-x}R_xTi_3O_{12}$ (R=Nd or La) is proposed. In this chapter, the details of this model are discussed. To confirm this model, the effects of annealing atmosphere, fatigue frequency, etc. were been studied.

6.1 LOW-DIELECTRIC LAYER MODEL

A strong dependence of dielectric permittivity and coercive field on the thickness of ferroelectric thin films has been reported in many ferroelectric thin films, such as $(Ba,Sr)TiO_3$ (BST),[1-3] $Pb(Zr,Ti)O_3$ (PZT), [4] and $KNbO_3$,[5] Generally, this phenomenon of the decrease of dielectric permittivity and increase of coercive field with decreasing film thickness can be attributed to the creation of a low-dielectric layer at the electrode/film interface. It is suspected that a thin low-dielectric layer is formed between the ferroelectric and the electrode during the top-electrode deposition. Figure 6-1 shows the schematic illustration of the low-dielectric layer model.

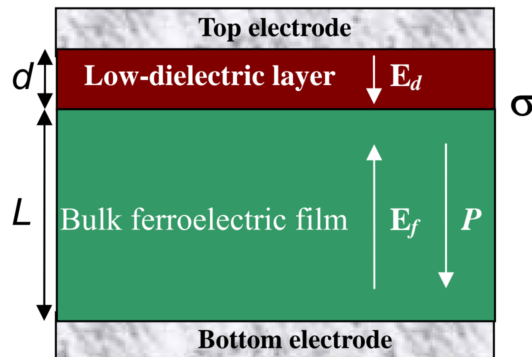

Fig. 6-1 Schematic illustration of low-dielectric layer model (the thickness of the low-dielectric layer and bulk ferroelectric film are *d* and *L*, $d<<L$).

The relation between the applied field E and the field applied to by the bulk ferroelectric film E_f could be described as:[6-8]

$$E_f = E - \frac{d}{\varepsilon_d L} P \quad (6\text{-}1)$$

where L, d, ε_d, and P are the thickness of the bulk ferroelectric film, the thickness of the low-dielectric layer, the dielectric permittivity of the low-dielectric layer, and the polarization of the bulk ferroelectric film, respectively.

Jin *et al.* [9] reported direct observation of a defect layer in BST films, as shown in Fig. 6-2. As indicated by the white line in Fig. 6-2, the separation of the two 'bb' lines near the interface is larger than the separation of the rows close to the bulk BST films. This result indicates the existence of a low-dielectric layer at the interface between bulk film and electrode.

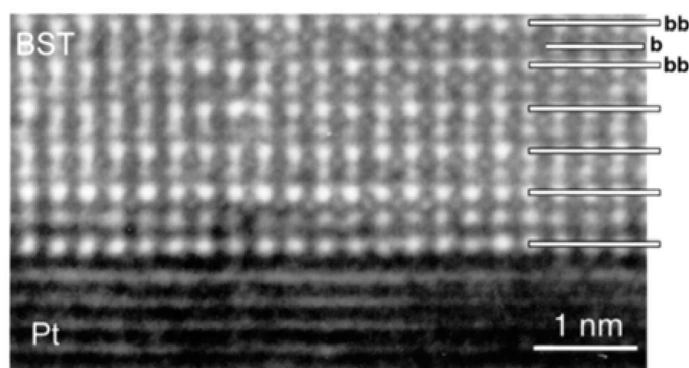

Fig. 6-2 High-resolution TEM lattic image of the BST/Pt interface.[9]

6.2 DOMAIN PINNING AND UNPINNING MODEL

Recently, ferroelectric thin films have been explored for use in nonvolatile ferroelectric random access memory (NvFeRAM), however, severe polarization fatigue during electric field cycling was found in the otherwise promising ferroelectric $Pb(Zr,Ti)O_3$ (PZT), particularly with metal electrodes such as Pt. Therefore, investigations to find the fatigue-free ferroelectric materials have been extensive. So far, the reported fatigue-free ferroelectrics always belong to the Aurivillius family, whose general formula is $(Bi_2O_2)^{2+}(A_{n-1}B_nO_{3n+1})^{2-}$ (where n=2, 3, 4, and 5). To explain the fatigue-free behavior of these bismuth layer ferroelectrics, a domain pinning and unpinning model was proposed.

Dimos *et al.* [10] and Warrant *et al.* [11,12] suggested that the domain boundaries constitute strong electrostatic potential wells. If charges become trapped at such a boundary, it tends to pin the boundary, thereby reducing the switchable polarization, as shown in Fig. 6-3. The fatigue-free behavior of ferroelectrics such as $Bi_4Ti_3O_{12}$-based (BiT) and $SrBi_2Ta_2O_9$ (SBT) is attributed to the self-recovery mechanism. Compared to PZT, the domain wall pinning effect in BiT and SBT is weak, and the cycling field can

be expected to unpin the domain walls. Moreover, the unpinning of domain wall by the cycling field must occur at least as rapidly as the domain wall pinning. The weak domain wall pinning in BiT and SBT was postulated to result from the following factors: 1) the smaller magnitude of ferroelectric polarization which results in weaker trapping of individual charges and/or lower trapped charge density at the domain boundary. 2) a relatively low oxygen vacancy concentration in the perovskite sublattice.

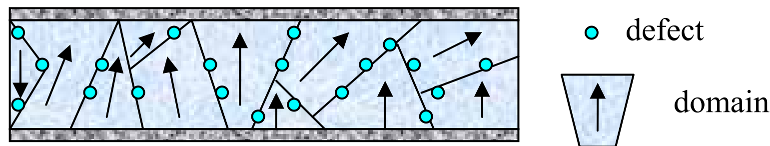

Fig. 6-3 Schematic drawing of domain pinning.

6.3 FATIGUE BEHAVIOR IN CURRENT WORK

As shown in Fig. 6-4, the fatigue process of $Bi_{4-x}R_xTi_3O_{12}$ (R=La or Nd, x=0.2, 0.4, 0.6, and 0.8) consists of two parts: 1) an increase of polarization from 1 to 10^6 cycles; and 2) a decrease of polarization from 10^6 to 10^9 cycles.

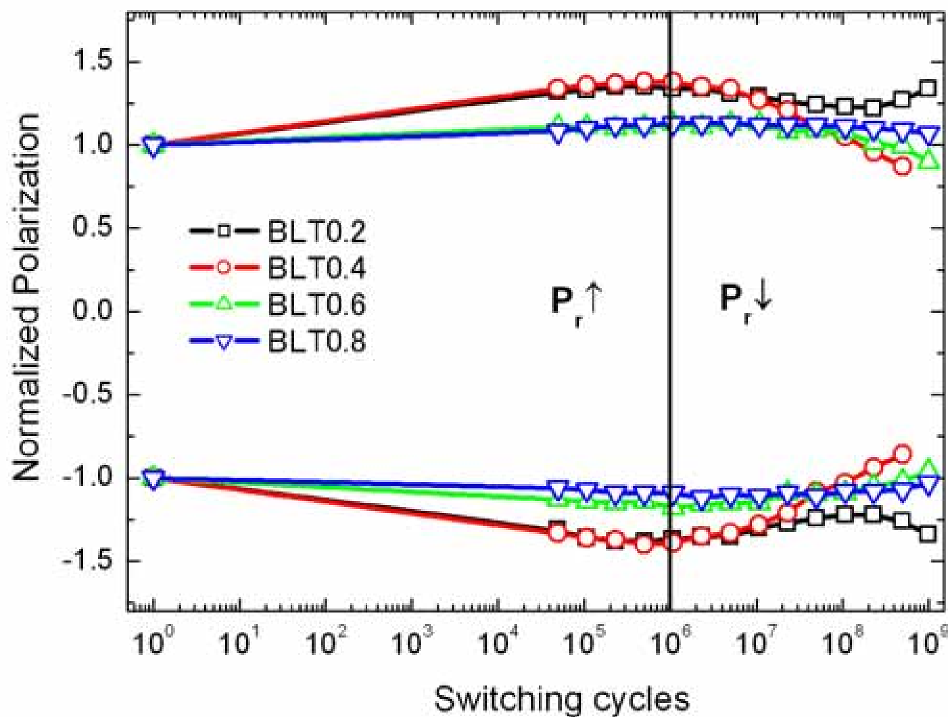

Fig. 6-4 Dependence of normalized polarization on switching cycles.

The analysis of the fatigue behavior of $Bi_{4-x}Nd_xTi_3O_{12}$ reported in chapter 4 further shows that the mechanisms which contribute to these two processes (1-10^6 and 10^6-10^9) are different. Therefore, it is necessary to combine several models to explain the fatigue phenomenon of $Bi_{4-x}R_xTi_3O_{12}$ ferroelectric thin films. It should be noted that most proposed fatigue mechanisms address defect concentration. Therefore, the proposed model begins with defects.

As is well known, oxygen vacancy is the major defect in perovskite ferroelectric containing titanate.[13-16] The oxygen vacancy is formed during the process of annealing due to the evaporation of bismuth, as shown in Eq. 6-2:

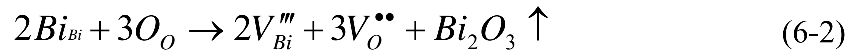

$$2Bi_{Bi} + 3O_O \rightarrow 2V_{Bi}''' + 3V_O^{\bullet\bullet} + Bi_2O_3 \uparrow \quad (6\text{-}2)$$

It is clear that high annealing temperature results in a high concentration of the defect. Moreover, with an increase of substitute La or Nd, the concentration of the defect decreases due to the suppression effect of the substitution on the evaporation of bismuth.

6.3.1 The dependence of polarization on cycles

6.3.1.1 An increase of polarization (1-10^6 cycles)

The domain pinning and unpinning effect is not only one of the most accepted mechanisms for the fatigue-free phenomenon, but also one of the few models that could explain the increase of polarization during the initial period of the switching cycles. However, the origin of domain unpinning is still ambiguous. It is reasonable to believe that the domain unpinning is caused by the decrease of the defect amount trapped in the domain walls.

In the current work, it was found that the increase of polarization from 1-10^6 cycles relates to the annealing temperature and the concentration of the substitute. These results are summarized as follows:

1) The films prepared at higher annealing temperatures exhibit a large increase of polarization during 1-10^6 switching cycles.
2) With an increase of substitution concentration, the increase of polarization during 1-10^6 switching cycles becomes weaker.
3) The increase of polarization during 1-10^6 switching cycles is absent in $Bi_{3.2}R_{0.8}Ti_3O_{12}$ films (R=La or Nd)

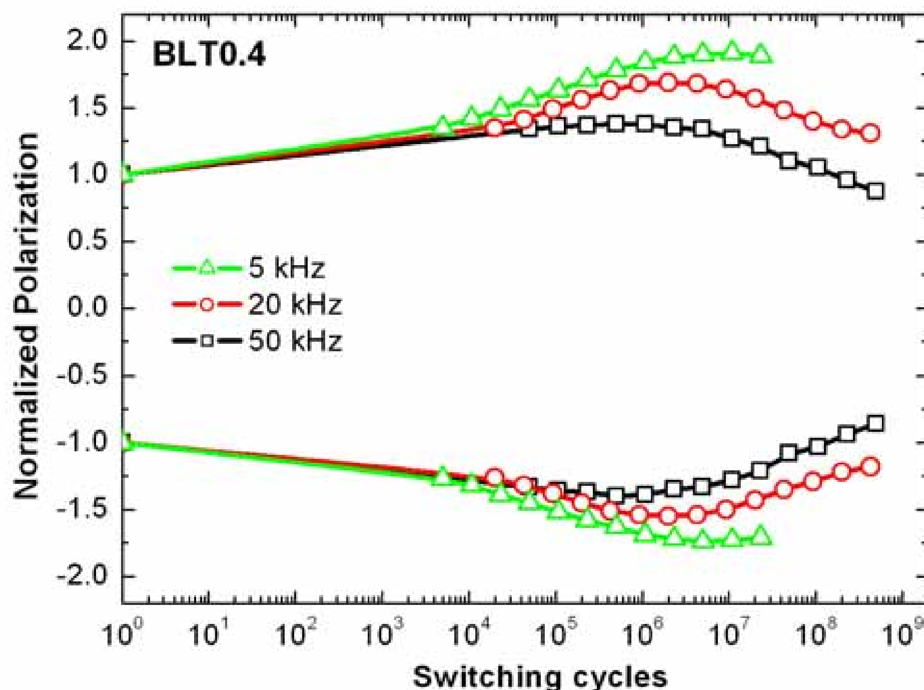

Fig. 6-5 Dependence of normalized polarization on cycles of BLT0.4 at 5 kHz, 20 kHz and 50 kHz.

Moreover, the dependence of polarization on cycles of BLT0.4 at different fatigue frequencies is shown in Fig. 6-5. It is interesting to find that the increase of polarization during 1-10^6 cycles varies with fatigue frequency. Three fatigue frequencies, 5 kHz, 20 kHz, and 50 kHz, are selected to analyze frequency effect. With the increase of fatigue frequency, the increase of polarization during 1-10^6 cycles becomes smaller.

6.3.1.2 A decrease of polarization (10^6-10^9 cycles)

A decrease of polarization during 10^6-10^9 cycles was found in most films. However, it was not seen in $Bi_{3.2}R_{0.8}Ti_3O_{12}$ films (R=La or Nd). Moreover, this decrease shows a weak relationship with annealing temperature, composition, and fatigue frequency for $Bi_{4-x}R_xTi_3O_{12}$ films.

6.3.2 The dependence of dielectric permittivity and tangent loss on cycles

Even though the low-dielectric layer model may relate to the switching behavior of ferroelectric films, [17] detailed work has not been reported. Due to the relatively low dielectric permittivity of this interface layer, it is expected that the dielectric permittivity of the ferroelectric capacity is lower than that of the ferroelectric bulk films. Therefore, study on the dependence of dielectric permittivity and tangent loss on cycles is

desirable.

6.3.2.1 Measurement process

Dielectric permittivity and tangent loss were measured by an impedance analyzer (HP4194A). Figure 6-6 shows how the dielectric permittivity and tangent loss measurements were carried out. The measurements were made at the initial condition, after fatigue 10^6 cycles, after fatigue 10^7 cycles, after 10^8 cycles, and after 10^9 cycles. It should be noted that for one sample, all these measurements were carried out on the same top electrode to eliminate the effect from the size of the top electrode.

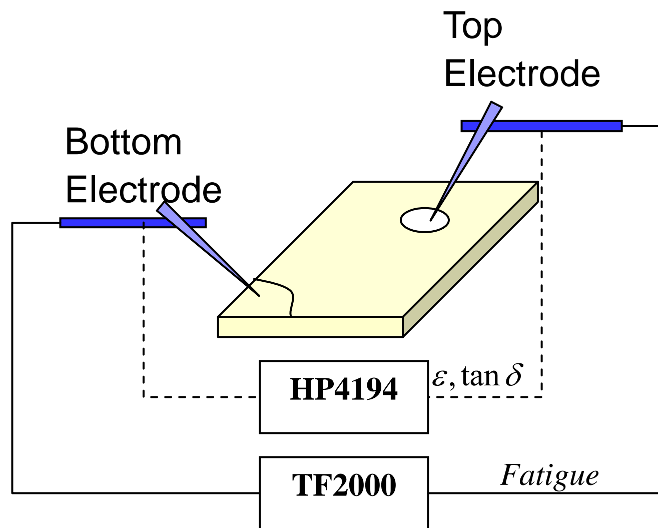

Fig.6-6 Schematic illustration of the measurement on the fatigued $Bi_{4-x}R_xTi_3O_{12}$ films.

6.3.2.2 Influence of composition on dielectric properties

Capacitance and tangent loss of $Bi_{3.8}La_{0.2}Ti_3O_{12}$ (BLT0.2) and $Bi_{3.2}La_{0.8}Ti_3O_{12}$ (BLT0.8) were measured at initial film and film fatigued 10^9 cycles, as shown in Fig. 6-7. A decrease of capacitance occurs in both $Bi_{3.8}La_{0.2}Ti_3O_{12}$ and $Bi_{3.2}La_{0.8}Ti_3O_{12}$ films after 10^9 cycles, whereas, change of tangent loss was small. Even though the decrease of dielectric permittivity after 10^9 cycles was found in BLT0.8, nearly no change of polarization was found, as shown in Fig. 6-4. It demonstrates that the decrease of dielectric permittivity is not caused by the change of polarization. Therefore, the decrease of dielectric permittivity relates to the switching cycles. Normalized dielectric permittivity is plotted as switching cycles, shown in Fig. 6-8.

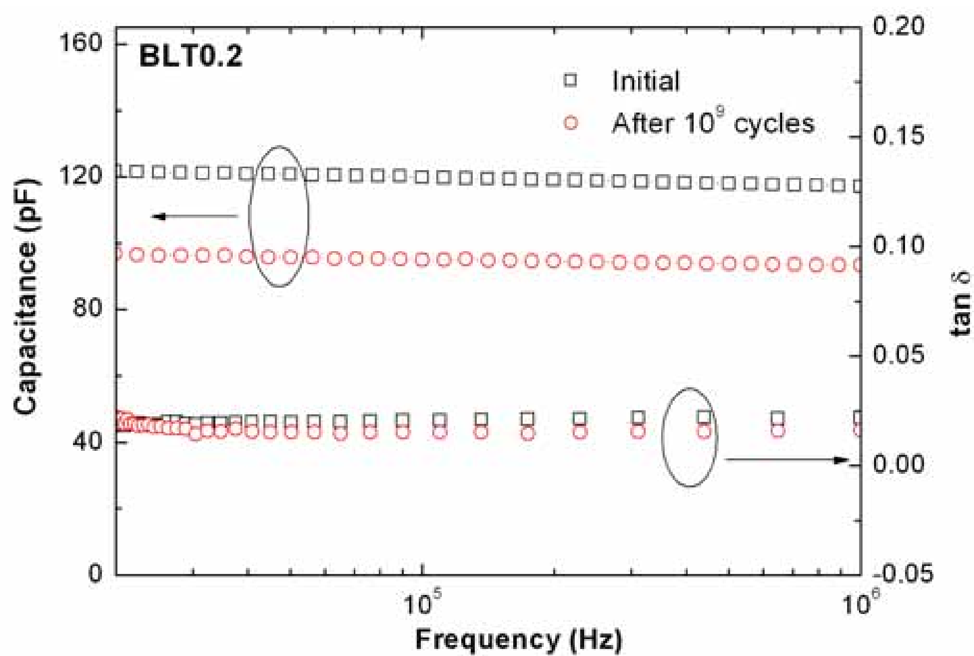

(a)

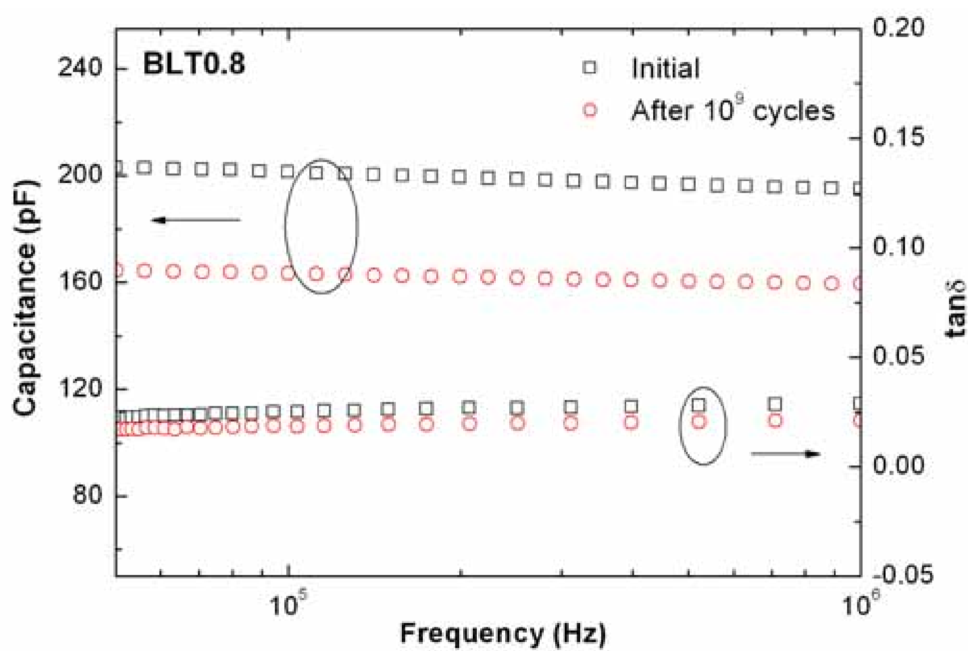

(b)

Fig. 6-7 Capacitance and tanδ of initial and after 10^9 cycles for BLT0.2 (a) and BLT0.8 (b) films.

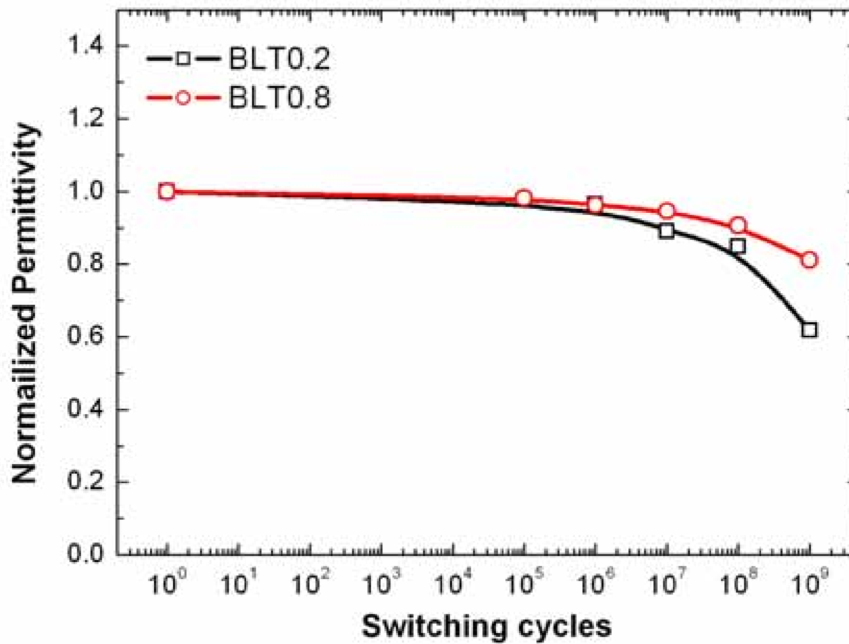

Fig. 6-8 Dependence of normalized dielectric permittivity (ε) of BLTx on cycles.

The effect of switching cycles on dielectric permittivity is summarized as follows:

1) Both BLT0.2 and BLT0.8 exhibit a continuous decrease of dielectric permittivity with increase of cycles.
2) After 10^9 cycles, a decrease of dielectric permittivity as large as 40% is observed in BLT0.2, whereas, it is about 20% for BLT0.8.
3) At the same fatigue condition, BLT0.2 shows a larger decrease of dielectric permittivity than BLT0.8

6.3.2.3 Influence of fatigue frequency on dielectric properties

So far, some relationships between the defects and fatigue behavior in BiT-based ferroelectric thin films were found. If the fatigue behavior is attributed to the dynamic process of defect, it is expected that a change of fatigue frequency would result in different fatigue behaviors. Moreover, the fatigue behavior is also dependent on the cycling frequency.

Figure 6-9 shows the variations of dielectric permittivity of BLT0.8 with cycles at fatigue frequencies of 20 kHz and 50 kHz. It is found that a lower fatigue frequency results in a larger decrease of dielectric permittivity.

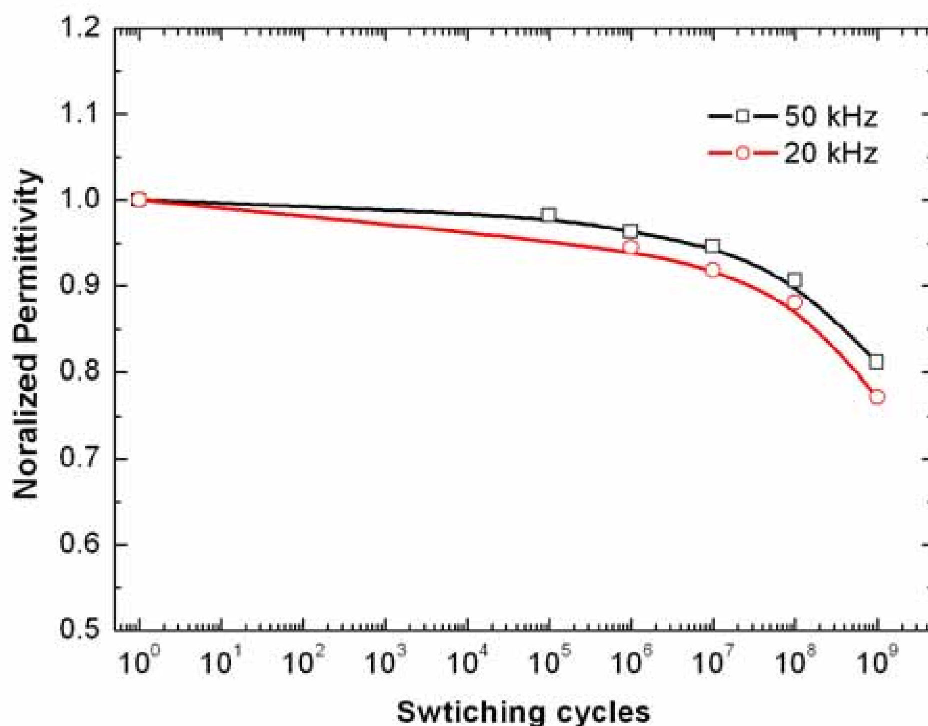

Fig. 6-9 Dependence of dielectric permittivity (ε) of BLT0.8 on switching cycles at 50 kHz and 20 kHz fatigue frequency.

6.3.3 Fatigue and dielectric behavior of films prepared at O_2 atmosphere

To confirm the relationship between the fatigue behavior and defects in BiT-based films, $Bi_{3.8}La_{0.2}Ti_3O_{12}$ films were prepared using the same technical process, except the RTA annealing process was preformed in an O_2 atmosphere, abbreviated as BLT0.2-O_2 hereafter. The polarization and dielectric permittivity after various cycles were measured.

6.3.3.1 X-ray diffraction (XRD)

Because of the anisotropic properties of BiT-based ferroelectrics,[18,19] it is expected that the fatigue behavior would be influenced by the orientation of the prepared films. The orientation of $Bi_{3.8}La_{0.2}Ti_3O_{12}$ films fabricated in O_2 atmosphere was investigated using XRD, shown in Fig. 6-10. Except a slight decrease of peak intensity, BLT0.2-O_2 shows patterns similar to BLT0.2. (117) peak dominates the XRD patterns, demonstrating that BLT0.2-O_2 has random orientation. This result is the same as BLT0.2 prepared in air. Therefore, the influence of orientation on fatigue behavior could be neglected.

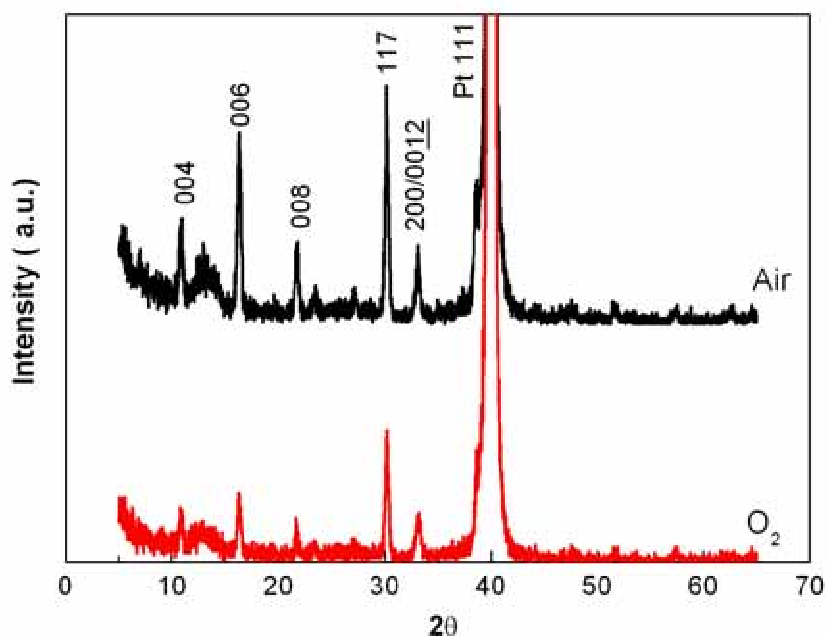

Fig. 6-10 XRD patterns of BLT0.2 fabricated in air and O_2 atmosphere.

6.3.3.2 The dependence of polarization on cycles

Fatigue measurements were carried out on both BLT0.2-Air and BLT0.2-O_2, and the dependence of normalized polarization on cycles is shown in Fig. 6-11. The influence of O_2 annealing on fatigue behavior is summarized as follows:

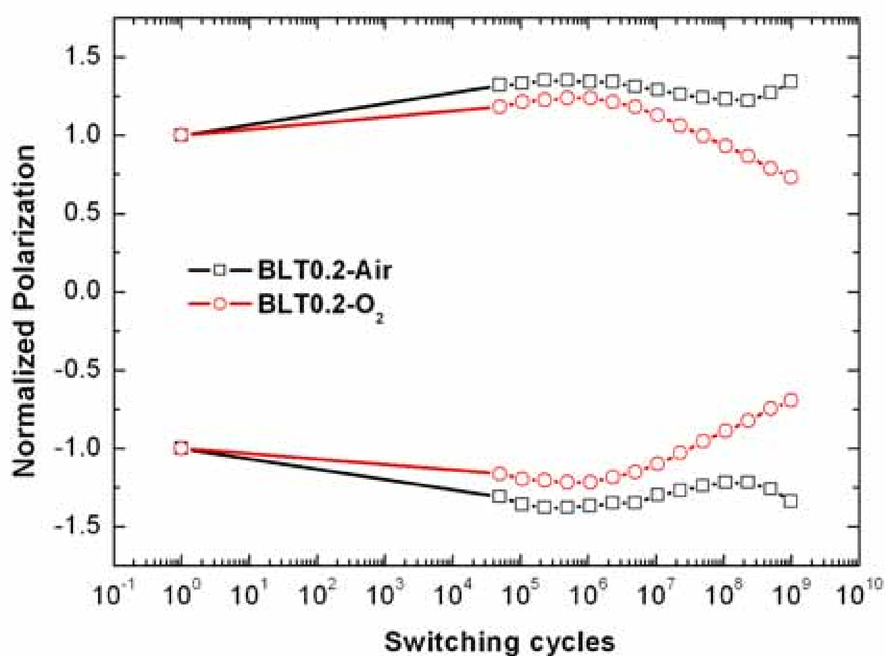

Fig. 6-11 Dependence of normalized polarization on cycles (BLT0.2- Air and BLT0.2- O_2).

1) During 1-10^6 cycles, BLT0.2-O_2 shows a relatively weaker increase of polarization than that of BLT0.2-Air.
2) As mentioned in chapter 5, shape of the P-E hysteresis loop of BLT0.2-Air becomes rounded with electric field cycling from 10^8 to 10^9 cycles, suggesting that leakage degradation occurs. However, this leakage degradation is suppressed by the O_2 annealing process, due to the decrease of polarization during 10^8-10^9 cycles.
3) BLT0.2-O_2 exhibits similar fatigue behavior to that of BLT0.4-Air.

6.4 A NEW MODEL FOR FATIGUE BEHAVIOR OF $Bi_{4-X}R_XTi_3O_{12}$ FERROELECTRIC FILMS: DEFECT-REDISTRIBUTION MODEL

Recently, the fatigue behavior of ferroelectrics has been attributed to space charge as well as oxygen vacancies in many research reports. Scott *et al.* [20] reported a reduction of oxygen near the electrode after fatigue, demonstrating that fatigue behavior correlates to oxygen vacancy. Investigation of PZT/RuO_x showed that fatigue properties were improved with an increase of oxygen content in the RuO_x electrode,[21] indicating that the increase of fatigue resistance came from the decrease of oxygen vacancies. It has also been suggested that domain pinning by oxygen vacancies contributes to the polarization fatigue behavior in ferroelectrics such as PZT.[22,23] These results show the important role of oxygen vacancies on fatigue behavior of ferroelectric thin film. Most recently, the existence of oxygen vacancies in BLT films has been confirmed.[24,25]

6.4.1 Introduction of defect-redistribution model

On the basis of the results in the present work, a model is proposed to explain the fatigue behavior of $Bi_{4-x}R_xTi_3O_{12}$ (R=La or Nd) (BRT) ferroelectric films. It seems that the redistribution of the pre-existing defects such as oxygen vacancy in BRT (R=La or Nd) (BRT) contributes to the fatigue behavior; therefore this model is called a defect-redistribution model.

As shown in Fig.6-12, an initial film contains a region near electrode (called trappable layer) and a region far from the electrode (called safe layer). It is assumed that the charged defects could move according to applied switching field during fatigue. The defects in the trappable layer might be trapped during this movement. On the other hand, the defect in the safe layer can not be trapped. After extensive defect trapping from trappable layer, a low-dielectric layer is formed near electrode.

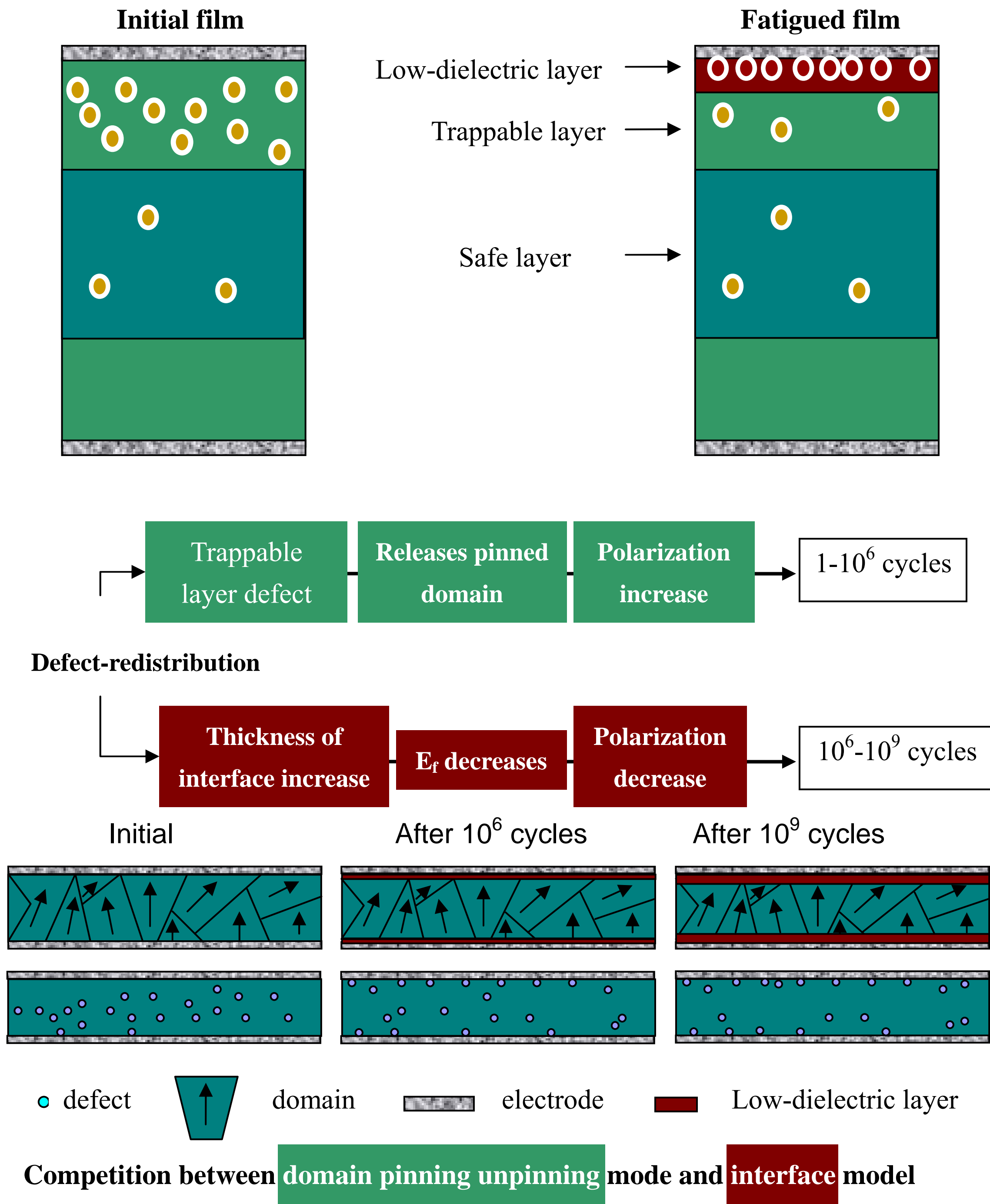

Fig. 6-12 Schematic illustration of defect-redistribution model

Detail of defect-redistribution model is introduced as follows:

1) In the BRT ferroelectric films, there are some pre-existing defects, such as oxygen vacancies and bismuth vacancies, and the presence of these defects results in the pinning domain effect. Because of the applied switching field in

the fatigue process, these charged defects, especially at the trappable layer, are easily trapped in the interface between the bulk film and the electrode due to the strong electrostatic potential wells. Therefore, the concentration of the defects in the trappable layer decreases with increase of switching cycles. During the initial fatigue period from 1 to 10^6 cycles, the fatigue behavior BRT ferroelectric films is dominated by the release of pinned domains because the concentration of defects in the trappable layer decreases. It is proposed here that releasing of the pinned domain due to the migrating of defects, such as oxygen vacancies, contributes to the increase of polarization with increase of switching cycles up to 10^6.

2) On the basis of the low-dielectric layer model, a low-dielectric interface exists between bulk film and electrode. Due to the increase of the trapped defects in the interface with increase of switching cycles, this low-dielectric interface layer grows during the fatigue process. With the increase of the low-dielectric interface layer thickness, the field applied on the bulk film decreases.[26] Therefore, polarization decreases after 10^6 cycles.

6.4.2 Explanation of the results by defect-redistribution model

The schematic illustration of the defect-redistribution model is shown in Fig. 6-12. Defect-redistribution model accounts for the results found in the current research: such as, the influence of La and Nd concentration and the fatigue measurement frequency on fatigue behavior, the dielectric variation of fatigued BRT ferroelectric films, the change of coercive field of fatigue BRT films etc. The model accounts for the results found in the current research. Below is a detailed explanation of the model.

6.4.2.1 The dependence of fatigue behavior on La and Nd concentration

In BRT ferroelectric films with low concentration of R, an increase of polarization is found during 1-10^6 cycles and a decrease of polarization is found during 10^6-10^9 cycles. However, BRT films with high concentration of R exhibit a stable polarization during the whole fatigue process.

As is well-known, oxygen vacancy is the major defect in perovskite ferroelectric with titanium. Previous works showed that concentration of oxygen vacancies could be controlled by substitution due to the suppression effect of substitutes, such as La and Nd, on the evaporation of bismuth in BRT films, shown in Eq. 6-2. With the increase of the substitute La and Nd, it is expected that the concentration of oxygen vacancies

decreases. He *et al.* [27] suggested that strong domain-pinning happens only if a significant number of oxygen vacancies accumulate at the domain wall. In the defect-redistribution model, if the concentration of defects is too low to realize a pinning domain and form low-dielectric interface layer, a stable polarization could be obtained during the fatigue process.

As shown in Fig. 4-7, increase Nd concentration causes the increase of polarization to become slighter during 1-10^6 cycles. A high concentration of substitute Nd results in a low concentration of pre-existing defects in BNT films. Therefore, less pinned domain is expected in the BNT films with a high concentration of substitute Nd. In the defect-redistribution model, the increase of polarization during 1-10^6 cycles is attributed to the releasing of the pinned domain. If the pre-existing pinned domain is less, a weaker increase of polarization is reasonable.

6.4.2.2 The dependence of fatigue behavior on annealing temperature

For the BNT films with the same concentration of Nd, the films annealed at higher temperature show larger increase of polarization during 1-10^6 cycles, as shown in Fig. 4-7(a). Similar to the analysis above, a higher annealing temperature results in higher concentration of defects, and more pre-existing pinned domain is expected. Due to more pre-existing pinned domains in BNT films annealed at higher temperature, a responding strong increase of polarization is found.

6.4.2.3 The dependence of dielectric permittivity on switching cycles

In all the BRT ferroelectric films, a continuous decrease of dielectric permittivity with increase of switching cycles is found, as shown in Fig. 6-8, 6-9. Correspondingly, the growth of a low-dielectric layer means that the layer becomes thicker. Therefore, the dielectric permittivity decreases with the increase of $\frac{d_i}{d_0}$ (d_i : thickness of low-dielectric layer; d_0: thickness of measured BRT capacitors), which agrees with Tagantsev *et al.*. [8] Because BLT0.8 has a lower concentration of defects, such as oxygen vacancies, than BLT0.2, the influence of the growing dielectric layer due to defects redistribution on dielectric permittivity is weaker; therefore, a slight decrease of dielectric permittivity (ε) is found in BLT0.8, compared with a decrease of dielectric permittivity in BLT0.2, which agrees with the results shown in Fig. 6-8.

6.4.2.4 The influence of fatigue measurement frequency on polarization and dielectric variation

As shown in Fig. 6-5 and 6-9, fatigue frequency also plays a role on polarization variation and dielectric variation with increase of switching cycles. The increase of polarization during 1-10^6 cycles becomes pronounced with the decrease of fatigue frequency. Moreover, the decrease of dielectric permittivity becomes obvious with the decrease of fatigue frequency.

Since the redistribution of defects is a dynamic process, it is expected that a lower fatigue frequency results in more trapped defects by the interface. Therefore, more pinned domains are released, and growth of the low-dielectric interface layer is enhanced.

6.4.3 Estimation of growth of low-dielectric layer

Based on the above discussion, a principal capacitor of BRT layer is in series with capacitor of the interfacial layer, shown in Fig. 6-13.

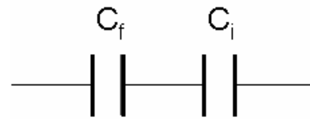

Fig. 6-13. Equivalent circuit of the Pt//BRT//Pt films (C_f and C_i are the capacitance of bulk BRT film and low-dielectric layer)

The relationship of the Pt//BRT//Pt capacitances of each capacitor can be written as:

$$\frac{1}{C_a} = \frac{1}{C_i} + \frac{1}{C_f} \qquad (6\text{-}3)$$

where C_a is the measured capacitance, C_i is the capacitance of the interface, and C_f is the capacitance of the bulk BRT film. Eq.6-3 could be changed into Eq.6-4 by the assumption of $\varepsilon_f >> \varepsilon_i$ and $d_f >> d_i$:[28]

$$\frac{d_a}{\varepsilon_a} \approx \frac{d_i}{\varepsilon_i} + \frac{d_0}{\varepsilon_f}, \qquad (6\text{-}4)$$

Where, d_a and d_i are the thickness of the measured film and the thickness of interface, respectively, ε_a, ε_i, and ε_f are the dielectric permittivity of measured film, interface (dielectric layer), and the BRT bulk layer, respectively. It is expected

that d_a, ε_i, and ε_f are unchanged during the fatigue process. Therefore, the decrease of ε_a, as shown in Fig. 6-7 and 6-8, is attributed to the increase of d_i. We would like to estimate the increase of d_i during the fatigue process, according to previous reported results such as $\frac{d_i}{\varepsilon_i}$ and ε_f *etc.* $\frac{d_i}{\varepsilon_i}$ of deposited films was reported as 0.081 nm at 100 kHz in Pt//$Ba_{0.5}Sr_{0.5}TiO_3$//$La_{0.67}Sr_{0.33}MnO_3$,[29] 0.077 nm in Pt//$Ba_{0.5}Sr_{0.5}TiO_3$//Pt,[30] and 0.0885 nm at 10 kHz in Pt//$Bi_{3.15}Nd_{0.85}Ti_3O_{12}$//Pt.[31] According to all these previous results, $\frac{d_i}{\varepsilon_i}$ of deposited on Pt//BRT//Pt was assumed to be 0.085 nm at 10 kHz. In the current work, dielectric permittivity at 10 kHz of fatigued BLT films was summarized in Tab. 6-1.

Table 6-1 Dielectric permittivity of BLT films (ε_a) in current work at 10 kHz.

	As-deposited	*10^6 cycling*	*10^7 cycling*	*10^8 cycling*	*10^9 cycling*
BLT0.2	182.4	176.0	161.4	154.5	112.7
BLT0.8	229.3	221	217.4	206.0	184.7

According to Eq. 6-4, ε_f of BLT0.2 and BLT0.8 was calculated to be 207.6 and 271.1, respectively. Then, $\frac{d_i}{\varepsilon_i}$ of fatigued Pt//BLT//Pt was estimated, as shown in Tab. 6-2.

Table. 6-2 Summary of the $\frac{d_i}{\varepsilon_i}$ of fatigued Pt//BLT//Pt on assuming that $\frac{d_i}{\varepsilon_i}$ of deposited Pt//BLT//Pt was 0.085 nm at 10 kHz.

Equivalent thickness	*composition*	*As-Deposited*	*10^6 cycling*	*10^7 cycling*	*10^8 cycling*	*10^9 cycling*
$\frac{d_i}{\varepsilon_i}$ (nm)	BLT0.2	0.085	0.109	0.172	0.207	0.507
	BLT0.8	0.085	0.105	0.114	0.146	0.216

As expected, an increase of $\frac{d_i}{\varepsilon_i}$ with increase of switching cycles is found, demonstrating an increase of d_i during the fatigue process. Assuming ε_i is about

10,[29] the dielectric layer increases from 1 nm to 5 nm for BLT0.2 and 1 nm to 2 nm for BLT0.8.

6.4.4 Estimation of polarization of bulk BLT film

As indicated by the defect-redistribution model, with an increase of low-dielectric layer thickness, a decrease of polarization is expected due to the decrease of the electric field applied to the bulk BLT film. Next is the estimation of the variation of the electric field applied to the bulk BLT film during the fatigue process on the basis of the growth of the low-dielectric layer obtained in above part.

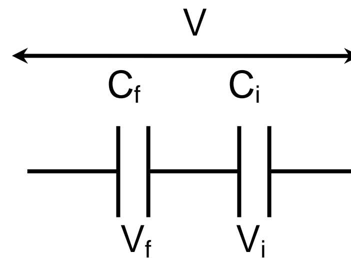

Fig. 6-14 Equivalent circuit of the Pt//BRT//Pt films (V_f and V_i are the voltage applied to bulk BRT and low-dielectric layer).

The relationship of the V, V_f, V_i can be written as:

$$V = V_f + V_i \tag{6-5}$$

$$C_i V_i = C_f V_f \tag{6-6}$$

$$C_i = \frac{\varepsilon_0 \varepsilon_i d_i}{A_i} \tag{6-7}$$

$$C_f = \frac{\varepsilon_0 \varepsilon_f d_f}{A_f} \tag{6-8}$$

where C_i and C_f are the capacitance of the low-dielectric layer and bulk BRT film, respectively; ε_0, ε_i, and ε_f are the permittivity of free space (8.854×10^{-14} F/cm), relative permittivity of the low-dielectric layer, and relative permittivity of the bulk BLT film, respectively; d_i and d_f are the thicknesses of the low-dielectric layer and the bulk BLT layer, respectively; and A_i and A_f are the acreage of the low-dielectric layer and bulk BLT layer.

From Eq.6-5~8, the relationship between V, V_f, V_i can be written as:

$$V_f = \frac{V}{\frac{\varepsilon_f}{\varepsilon_i} \times \frac{d_i}{d_f} + 1} \quad (6\text{-}9)$$

Enter the previous results in the previous part, the ratio of V_f/V could be estimated for the fatigued BLT ferroelectric films. Those results are summarized in Tab.6-3.

Tab. 6-3 Summary of the $\frac{V_f}{V}$ of fatigued Pt//BLT//Pt on assuming that $\frac{d_i}{\varepsilon_i}$ of deposited Pt//BLT//Pt was 0.085 nm at 10 kHz.

	As-Deposited	*10^6 cycling*	*10^7 cycling*	*10^8 cycling*	*10^9 cycling*
BLT0.2	0.876	0.846	0.777	0.744	0.542
BLT0.8	0.844	0.814	0.801	0.759	0.681

Since the applied voltage of fatigue measurement is 5V for all BLT films, the V_f could be estimated from Tab.6-3. On the basis of Fig.5-4, the estimated and experimental results for the dependence of remnant polarization on switching cycles are plotted in Fig.6-15. It should be noted that since the effect of the low-dielectric layer on the fatigue behavior is dominant during 10^6-10^9 switching cycles, it is appropriate to compare the estimated and experimental results during this fatigue period. Moreover, the estimated remnant polarizations were obtained considering the increase of remnant polarization during 1-10^6 switching cycles.

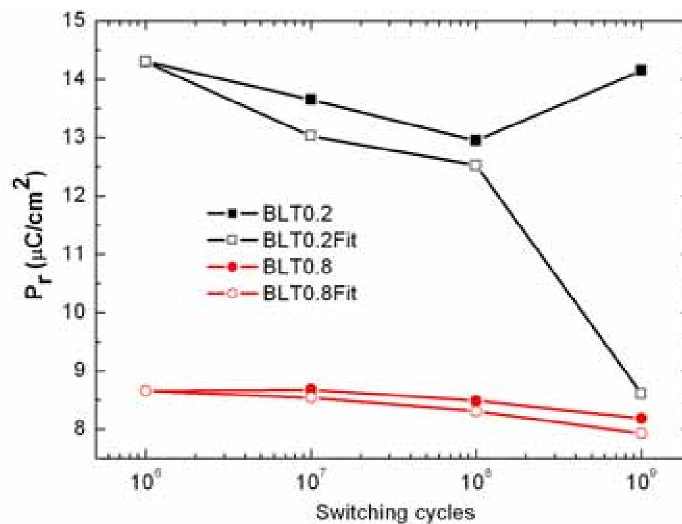

Fig.6-15 Dependence of remnant polarization on switching cycles (estimated and experimental results).

Figure 6-15 shows a decrease of remnant polarization (P_r) with increase of switching cycles in estimated results. These estimated results agree well with experimental results, except P_r after 10^9 switching cycles.

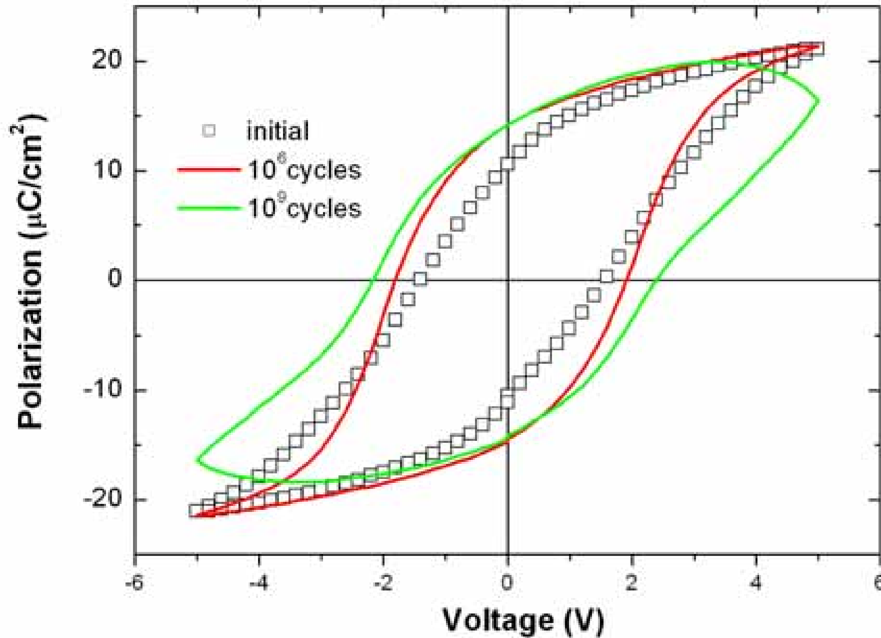

Fig.6-16 P-E hysteresis loop of Pt//BLT0.2//Pt (at 5V).

As mentioned in Chapter 5, the increase of P_r during 10^8-10^9 switching cycles is attributed to the increase of leakage due to the rounded P-E loop of BLT0.2 film after fatigued for 10^9 cycles, as shown in Fig.6-16. Since the P_r is estimated on the basis of the low-dielectric layer growth, the influence of leakage has not been considered. Therefore, the difference between the experimental results and the estimated results of P_r for BLT0.2 film fatigued for 10^9 switching cycle is reasonable.

As shown in Fig.6-15, the estimated results agree well with the experimental results, suggesting that growth of the low-dielectric layer during the fatigue process.

6.5 CONCLUSIONS

A model for the fatigue behavior of $Bi_{4-x}R_xTi_3O_{12}$ (R=La and Nd) ferroelectric films is proposed, which is called the defect-redistribution model. The fatigue behavior of BRT ferroelectric films closely relates to the distribution of pre-existing defects such as oxygen vacancy and bismuth vacancy etc. In the whole fatigue process, the increase of polarization due to the releasing of pinned domains and the decrease of polarization due

to growth of the low-dielectric interface layer are in competition. On the basis of proposed defect-redistribution model, the growth of low-dielectric layer has been estimated for the first time. Moreover, remnant polarization (P_r) has also been estimated for films fatigued at various switching cycles. The estimated results exhibit good agreement with the experimental results, suggesting the appropriateness of proposed defect-redistribution model.

REFERENCES

[1] J. C. Shin, J. H. Park, C. S. Hwang, and H. J. Kim, *J. Appl. Phys.*, **86**, 506 (1999).

[2] W. J. Lee, H. G. Kim, and S. G. Yoon, *J. Appl. Phys.*, **80**, 5891 (1996).

[3] C. B. Parker, J. P. Maria, and A. I. Kingon, *Appl. Phys. Lett.*, **80**, 340 (2002).

[4] P. K. Larsen, G. J. Dormans, D. J. Taylor, and P. J. van Veldhoven, *J. Appl. Phys.*, **76**, 2405 (1994).

[5] J. F. Scott, C. A. Paz de Araujo, and L. D. Mcmillan, *Ferroelectrics*, **140**, 219 (1993).

[6] S. L. Miller, R. D. Nasby, J. R. Schwandk, M. S. Rogers, and P. V. Dressendorfer, *J. Appl. Phys.*, **68**, 6463 (1990).

[7] C. J. Brennan, *Ferroelectrics*, **132**, 245 (1992).

[8] A. K. Tagantsev. M. Landivar, E. Colla, and N. Setter, *J. Appl. Phys.*, **78**, 2623 (1995).

[9] H. Z. Jin, J. Zhu, P. Ehrhart, F. Fitsilis, C. L. Jia, S. Regnery, K. Urban, R. Waser, *J. Appl. Phys.*, **92**, 4594 (2002).

[10] D. Dimos, W. L. Warren, M. B. Sinclair, B. A. Tuttel, and R. W. Schwartz, *J. Appl. Phys.*, **76**, 4305 (1994).

[11] W. L. Warren, D. Dimos, B. A. Tuttle, R. D. Nasby, and G. E. Pike, A*ppl. Phys. Lett.*, **65**, 1018 (1994).

[12] W. L. Warren, D. Dimos, B. A. Tuttle, G. E. Pike, R. W. Schwartz, P. J. Clew, and D. C Mcintyre, *J. Appl. Phys.*, **77**, 6695 (1995).

[13] A. E. Paladino, *J. Am. Ceram. Soc.*, **65**, 426 (1982).

[14] A. Fouskova and L. E. Cross, *J. Appl. Phys.*, **41**, 2834 (1970).

[15] K. Morii, H. Kawano, I. Fujii, T. Matusi, and Y. Nakayama, *J. Appl. Phys.*, **78**, 1914 (1995).

[16] B. S. Kang, S. K. Choi, and C. H. Park, *J. Appl. Phys.*, **94**, 1904 (2003).

[17] T. Mihara, H. Watanabe, H. Yoshimori, C. A. Paz de Araujo, B.Mlnick, and L. D. McMillan, *Integ. Ferroelect.*, **1**, 269 (1992).

[18] P. H. Xiang, Y. Kinemuchi, and K. Watari, *J. Mater. Res.*, **21**, 1830 (2006).

[19] S. E. Cummins, L. E. Cross, *J. Appl. Phys.*, **39**, 2268 (1968).

[20] J. F. Scott, C. A. Paz de Araujo, B. N. Melnick, L. D. McMillan, and R. Zuleeg, *J. Appl. Phys.*, **70**, 382 (1991).

[21] C. W. Law, K. Y. Tong, J. H. Li, K. Li and M. C. Poon, *Thin Solid Films*, **354**, 162 (1999).

[22] D. Dimos, H. N. Al-shareef, W. L. Warren, and B. A. Tuttle, *J. Appl. Phys.*, **80**, 1682 (1996).

[23] H. N. Al-shaareef, B. A. Tuttle, W. L. Warren, T. J. Headley, D. Dimos, J. A. Voige, and R. D. Nasby, *J. Appl. Phys.*, **79**, 1013 (1996).

[24] N. Zhong and T. Shiosaki, *J. Appl. Phys.*, **100,** 034107 (2006).

[25] N. Zhong, S. Okamura, K. Uchiyama, and T. Shiosaki, *App. Phys. Lett.*, **87**, 252901 (2005).

[26] H. Z. Jin, J. Zhu, P. Ehrhart, F. Fitsilis, C. L. Jia, S. Regnery, K. Urban, and R. Waser, *Thin Solid Films*, **429**, 282 (2003).

[27] L. He and D. Vanderbilt, *Phys. Rev.*, B **68**, 134103 (2003).

[28] K. Natori, D. Otani, and M. Sano, *Appl. Phys. Lett.*, **73**, 632 (1998).

[29] Miao, Y. Wang, H. Y. Tian, X. Y. Zhou, H. L. W. Chan, C. L. Choy, L. X. Cao, and B. R. Zhao, *J. Phys. D: Appl. Phys.*, **39**, 2565 (2006).

[30] B. Y. Lee, C. S. Hwang, *Appl. Phys. Lett.*, **77**, 124 (2000).

[31] X. S. Gao and J. Wang, *J. Appl. Phys.*, **99**, 074103 (2006).

Chapter 7

Major Conclusions and Suggestions for Future Work

In the present dissertation, polarization fatigue behavior of $Bi_{4-x}R_xTi_3O_{12}$ (BRT) (R=La and Nd) ferroelectric thin films has been studied to explain the origin of the fatigue phenomenon of bismuth layer ferroelectric films. According to the proposed mechanisms, such as domain pinning and unpinning effect, stability of the oxygen of perovskite layer and space charges compensated by a self-regulating $[Bi_2O_2]^{2+}$ layer, defects are involved. Therefore, it is expected that change of defect concentration may contribute to change of the fatigue behavior of BRT ferroelectrics. Considering the influence of substitutes, La and Nd were selected to control the defect concentration in BRT ferroelectric thin films.

7.1 MAJOR CONCLUSIONS

1) The existence and type of defects in $Bi_{3.25}La_{0.75}Ti_3O_{12}$ ferroelectric thin films were investigated using dielectric relaxation. The details of the dielectric properties and ac conductivity in the temperature range of 25-600 ^oC are reported for the first time. In addition to a dielectric peak at 483 ^oC attributed to the para-ferroelectric phase transition, three dielectric relaxations were found at ～250 ^oC,～400 ^oC, and ～500 ^oC, respectively. The relaxation behaviors of models at ～400 ^oC and ～500 ^oC are in according with Arrhenius law and Vögel-Fulcher law, respectively, suggesting different mechanisms of these two modes. It is proposed that the relaxation at ～250 ^oC is related to both oxygen vacancies and bismuth vacancies; the relaxation at ～400 ^oC is attributed to single-ionized oxygen vacancies $V_O^{\bullet}$, and the relaxation at ～500 ^oC is attributed to space change which came from double-ionized oxygen vacancies $V_O^{\bullet\bullet}$. In a word, there are several types of defects in BiT-based ferroelectric thin films, and it is the first time to clarify in detail the type and existence of these defects in $Bi_{3.25}La_{0.75}Ti_3O_{12}$ thin films by dielectric relaxation.

2) Ferroelectric measurements, especially polarization fatigue, were carried out on $Bi_{4-x}R_xTi_3O_{12}$ (BRT) (R=La and Nd) ferroelectric thin films. It was found that the fatigue behavior of BRT films depends on not only the composition but also the annealing temperature. With an increase of substitute concentration, the fatigue

resistance of BRT films increases. A fatigue-free behavior was found in $Bi_{3.2}La_{0.8}Ti_3O_{12}$ and $Bi_{3.2}Nd_{0.8}Ti_3O_2$ ferroelectric thin films. The fatigue process (1-10^9 cycles) consists of two parts: 1) an increase of polarization during 1-10^6 cycles and 2) a decrease of polarization during 10^6-10^9 cycles. Moreover, the increase of polarization (1-10^6 cycles) closely relates to composition and annealing temperature, while little relationship was found for the decrease of polarization (10^6-10^9 cycles). This demonstrates that the mechanisms of the increase of polarization (1-10^6 cycles) and the decrease of polarization (10^6-10^9 cycles) are different.

3) Based on the fatigue results, a model of fatigue behavior in BRT ferroelectric films is proposed. To confirm this model, the effect of annealing atmosphere and fatigue frequency etc. was studied. The model shows that the fatigue behavior of BRT films closely relates to the distribution of pre-existing defects such as oxygen vacancy and bismuth vacancy. The fatigue process is a re-distribution process of the pre-existing defects from the bulk BRT films to the interface between the bulk film and the electrode. At the initial fatigue period (1-10^6 cycles), the decrease of defect concentration in the bulk film dominates the fatigue behavior. During the fatigue process of 10^6-10^9 cycles, the major factor is an increase of the interface thickness between the bulk film and the electrode, which is attributed to extensive migration of defects from the bulk film to the interfac. In the whole fatigue process, the increase of polarization due to the releasing of pinned domain and the decrease of polarization due to growth of the low-dielectric interface layer are in competition. According to the defect-redistribution model, growth of the low-dielectric layer and remnant polarization for the films fatigued at various switching cycles can be estimated. Good agreement is found between the estimated results and the experimental results, suggesting that the proposed defect-redistribution model is appropriate to explain the fatigue behavior of BRT ferroelectric thin films.

In conclusion, with the increase of substitute La or Nd, the fatigue properties of BRT ferroelectric thin films are improved. However, a decrease of polarization is also found with an increase of substitute concentration. For the application of nonvolatile ferroelectric random access memories (NvFeRAM), high polarization and excellent fatigue properties are both required; therefore $Bi_{3.4}Nd_{0.6}Ti_3O_{12}$ and $Bi_{3.4}La_{0.6}Ti_3O_{12}$ are promising candidates.

7.2 SUGGESTIONS FOR FUTURE WORK

In the current work, $Bi_{3.4}Nd_{0.6}Ti_3O_{12}$ and $Bi_{3.4}La_{0.6}Ti_3O_{12}$ are considered as promising candidates for application to nonvolatile ferroelectric random access memories (NvFeRAM). To further improve the ferroelectric properties, such as polarization and fatigue resistance, the processing condition should be optimized. According to the fatigue mechanism proposed here, the lower concentration of pre-existing defects, the better fatigue behavior will be, therefore, annealing in oxygen atmosphere is expected to reduce the concentration of pre-existing oxygen vacancies in BRT ferroelectric thin films. Moreover, the concentration of additional bismuth should be optimized to obtain high value of polarization. These both need to be verified.

To examine the correctness of the present proposed model, microstructure characterization methods, such as transmission electron microscopy (TEM), secondary ion spectrometer (SIMS) should be applied. Due to the high concentration of defects at the interface, different lattices are expected to be found in the bulk film and in the interface region, respectively. TEM measurement could be carried out on films fatigued at various cycles to observe the change of interface thickness.

Since the fatigue behavior of BRT ferroelectric thin films is attributed to a dynamics process of the pre-existing defects, heat treatment is expected to recover BRT films, such as recovery of suppression dielectric permittivity.

ACKNOWLEDGMENTS

The word described in this dissertation could not have been accomplished without the collaboration of many other people, to whom I wish to express my greatest gratitude.

First of all, I sincerely thank my academic supervisor Prof. Tadashi Shiosaki, Graduate School of Materials Science, Nara Institute of Science and Technology, for his extensive guidance, patience, encouragement and support through the course of this work. Without his help, I could not have had the opportunity to work in his research group in the fascinating field of ferroelectric materials and devices. Thank so much for your kindness and help in all aspects of daily life.

I would like to thank Assoc. Prof. Kiyoshi Uchiyama for his professional advice and technical help. Help of assistance professor Hiroaki Takeda is greatly acknowledged for his great patience in giving advice in not only my research work but also daily life. I thank to Assist. Prof. Takashi Nishida for his valuable guidance for the measurement system in the laboratory.

I would like to offer sincere thanks to Prof. Takashi Fuyuki and Prof. Hiroshi Daimon for their valuable and insightful comments.

I express my gratitude to all the students in the Information Device Science group now, and the students who have graduated in the last three years. It has been a pleasant and fruitful experience for me to work with them, and thanks for making a good and friendly research environment. I also thank Prof. Rodney Durnham for his great help of correcting the English of this dissertation.

I would like to thank the Ministry of Education, Culture, Sports, Science and Technology (Monbukagakusho: MEXT) of the Japanese government for the full financial support (Monbusho Scholarship) over the past two and a half years. I acknowledge the financial support of the NAIST Presidential Special Fund.

Finally, I owe a lot to my family for their endless encouragement. Without their support, I could not have had a chance to come to Japan for a Ph.D degree. My husband Pinghua Xiang has been always supporting me during the whole study life. I am thankful for all the things he has given to me.

List of publications

Main publications

1) C-axis-oriented $Bi_{3.25}La_{0.75}Ti_3O_{12}$ ferroelectric thin film fabricated by chemical solution deposition
N. Zhong and T. Shiosaki, ***Mater. Lett.*** *61 (2007) pp.*2935-2938.

2) Dielectric behavior of $Bi_{3.25}La_{0.75}Ti_3O_{12}$ Ferroelectric Film
N. Zhong and T. Shiosaki, ***J. Appl. Phys.*** *100 (2006) pp.*034107-1~7.

3) Single-ionized-oxygen-vacancy-related dielectric relaxation in $Bi_{3.25}La_{0.75}Ti_3O_{12}$ ferroelectric film
N. Zhong, S. Okamura, K. Uchiyama, and T. Shiosaki, ***Appl. Phys. Lett.*** *87 (2005) pp.*252901-1~3.

Other publications

1) Dielectric and Vibrational Properties of La^{3+} Substituted Relaxor $(Na_{1/2}Bi_{1/2})TiO_3$ Ceramics
N. Zhong, A. Hushur, G. Shabbir and S. Kojima, ***J. Kore. Phys. Soc.*** *46 (2005) pp.*134-137.

2) Effect of rare earth additives on the microstructure and dielectric properties of $0.67Pb(Mg_{1/3}Nb_{2/3})O_3$-$0.33PbTiO_3$ Ceramics
Ni Zhong, Pinghua Xiang, Dazhi Sun, Xian-lin Dong, ***Mater. Sci. Eng. B,*** 116 (2005) *pp.*140-145.

3) Calcium substituting B-site in relaxor ferroelectrics with perovskite structure probed by chemical ordering
Ni Zhong, Wen-long Yao, Ping-hua Xiang, Chu-de Feng and Seiji Kojima, ***Solid State Commun.*** 134/6 (2005) *pp.*425-429.

4) Electric properties of $Pb(Mg_{1/3}Nb_{2/3})O_3$-$PbTiO_3$ Ceramics Modified with WO_3
Ni Zhong, Xianlin Dong, Dazhi Sun, Pinghua Xiang, Hui Du, ***Mater. Res. Bull.*** *39 (2004) pp.*175-184.

5) The Effect of substitute WO_3 on Relaxation Behavior of $Pb(Mg_{1/3}Nb_{2/3})O_3$-$PbTiO_3$ Ceramics
Ni Zhong, Xianlin Dong, Dazhi Sun, Hui Du, Hong Yang, ***Matrer. Sci. Eng. B**, 106 (2004) pp.*263-268.

6) Investigation on Pyroelectric Effect of Multi-component PMN-PT Ferroelectric Ceramics
Ni Zhong, Dazhi Sun, Hui Du, Hong Yang, Xianlin Dong, ***Mater. Sci. Forum.*** *March 2003 Functionally Graded Materials VII [0-87849-915-6] pp.*431-434.

7) Single-Calcination Synthesis Mechanism of Pure-Perovskite $Pb(Ni_{1/3}Nb_{2/3})O_3$-$PbTiO_3$ Using a Coating Method
Ping-Hua Xiang, **Ni Zhong**, Xian-Lin Dong, *et.al,* ***J. Am. Ceram.Soc.****88 (2005) pp.239-242*

8) Sintering Behavior Mechanical and Electrical Properties of Lead Zirconate Titanate/NiO Composites from Coated Powders
Pinghua Xiang, Xianlin Dong, Chude Feng, **Ni Zhong**, Jinkun Guo, ***Ceram. Int.*** *30 (2004) pp. 765-772*

9) Fabrication and Dielectric Properties of Lanthanum-Modified Lead Zirconate Titanate Using Coprecipitation Powder Coating
PingHua Xiang, **Ni Zhong**, Xian-Lin Dong *et.al,* ***Mater. Lett.*** *58 (2004) pp.2675-2678*

10) Dielectric Breakdown Properties of Zr-Rich Lead Zirconate Titanate Ceramics
Hong Yang, Xianlin Dong, **Ni Zhong**, Yonglin Wang, ***Jpn. J. Appl. Phys*** *43 (2004) pp.7579-7582*

11) Single-calcination synthesis of pyrochlore-free $Pb(Ni_{1/3}Nb_{2/3})O_3$-$PbTiO_3$ using a coating method
Pinghua Xiang, **Ni Zhong**, Xianlin Dong, ***Solid State Commun****.127 (2003) pp.699-701*

Proceedings

1. **Ni Zhong**, and Tadashi Shiosaki, "Dielectric characteristic of fatigued $Bi_{4-x}La_xTi_3O_{12}$ ferroelectric films", The 16th International Symposium on the Application of Ferroelectrics, 27-31 May., 2007, Nara, Japan.
2. **Ni Zhong**, and Tadashi Shiosaki,, "(001)-oriented $Bi_{3.25}La_{0.75}Ti_3O_{12}$ ferroelectric thin film ", The 23th Meeting on Ferroelectric Materials and Their Applications, 24-27 May, 2006, Kyoto, Japan.
3. **Ni Zhong,** A. Hushur, G. Shabbir and S. Kojima, "Dielectric and Vibrational Properties of La^{3+} Substituted Relaxor $(Na_{1/2}Bi_{1/2})TiO_3$ Ceramics" 5th Korea-Japan Conference on Ferroelectricity, 18-21 August, 2004 Seoul, South Korea,